Development of an optical fibre multiplexed Bragg grating strain measurement system

By

James Edward Andrew Kemp

A thesis submitted to the City University for the degree of Doctor of Philosophy in Electrical, Electronic and Information Engineering

Measurement and Instrumentation Centre
Department of Electrical, Electronic and Information Engineering
City University
Northampton Square
London EC1V 0HB

September 1998

Table of contents

LIST OF TABLES

LIST OF FIGURES

ACKNOWLEDGEMENTS

I wish to express my genuine thanks to Professor Ken Grattan and Professor Andy Palmer for their help, support and supervision throughout my research.

I would also like to thank, (in no special order): Roger Valsler, Dr Ning, Ferdinand Carty, Romin Ashoori and Mr S. Xioa for their excellent technical assistance.

I am particularly indebted to Dr Xian Jiang, many thanks.

Finally, I would like to thank my family and my wife, Joanna, without whose continuous support and encouragement, this work would not have been possible.

When I'm rich and famous I'll remember you!

DECLARATION

I grant power to the University Librarian to allow this thesis to be copied in whole or in part without further reference to the author. This permission covers single copies made for study purposes, subject to normal conditions of acknowledgement.

Abstract

Strain sensing continues to be an area of research interest due to its importance in a variety of fields including civil, mechanical and aerospace engineering. This has intensified with the advent of the concept of 'smart structures', i.e. structures that possess both the means to detect changes in their environment and the ability to respond to those changes. Strain measurement techniques using optical fibre based sensors have attracted a great deal of interest due to the advantages afforded by the nature of the fibres themselves in such measurement systems.

This thesis represents a body of work concerning the design, development and analysis of an optical fibre based strain sensor system, utilizing Bragg gratings as the prime sensing elements.

Wavelength demodulation is examined and a wavelength shift detection scheme utilizing a Wollaston prism interferometer is presented having been considered as a means to achieve wavelength demodulation in sensor systems. However, further analysis suggested an alternative was needed and the final wavelength demodulation scheme chosen, based on the Michelson interferometer, is analysed in this context.

A time-domain based demultiplexing system is presented where the signals from individual Bragg gratings are separated electronically by using a matrix of fast GaAs switches. This system is successfully demonstrated and the capability of addressing a potentially large number of Bragg gratings sensors elements is considered. Results are presented in the form of strain and temperature sensitivity data and an analysis of the results in the frequency domain demonstrates that the crosstalk present in the system is very low.

The results presented are set in the context of work reported in the literature and in the light of results achieved elsewhere.

SYMBOLS AND ABBREVIATIONS

APD	Avalanche photodiode
BPF	Bandpass filter
CCD	Charge coupled device
DSA	Digital Storage Adaptor
EDFA	Erbium doped fibre amplifier
FTS	Fourier transform spectroscopy
FWHM	Full width half maximum
GaAs	Gallium Arsinide
L_c	Coherence length
LED	Light emitting diode
LPG	Long pitch grating
NEP	Noise equivalent power
OPD	Optical path difference
OTDR	Optical time domain reflectrometry
SLD	Super luminescent diode
SNR	Signal to noise ratio
TDM	Time division multiplexing
UV	Ultra violet
WDM	Wavelength division multiplexing

n	Refractive index
n_e	Extraordinary refractive index
n_o	Ordinary refractive index

$\mu\varepsilon$	Microstrain
λ	Wavelength (in nm)
$\Delta\lambda$	Change in wavelength
λ_a	Average wavelength in a dual wavelength beatpattern
λ_B	Bragg wavelength
λ_m	Modulated wavelength in a dual wavelength beatpattern

Chapter 1:

Introduction

1.1 Strain sensing background

The need to measure the effects of external forces acting upon a structure has been present for many years. For large scale civil engineering structures, such as bridges, dams and buildings, the ability to detect excessive strains is matter of safety. The same is true for other areas, such as aerospace engineering where a failure could be potentially fatal.

Understandably, the concept of mechanical, civil and aerospace engineering structures that can detect and react to responses from sensors integrated within the structure itself has generated much research interest. The term 'smart structures' was first coined in research involving the integration of radar antennas with the skins of military aircraft and evolved to involve the whole structure. It has now come to describe the concept of a structure that can automatically sense its internal and external environmental conditions; communicate this information to a processing unit and if necessary adapt the characteristics of the structure in response to this information.

In many ways smart structures mirror biological organisms. Senses, such as touch, sight etc. inform the organism about its environment, the brain decides on a course of action and the muscles carry them out. A comparable engineering solution would involve sensors designed to detect whatever measurands were considered important, a suitable signal processing and decision-making unit, and a series of transducers and actuators to alter the structural parameters.

Obviously, this is a multi-disciplinary research area and one that has yet to offer a system that can compete with even relatively simple biological organisms. However, the potential benefits that could be afforded not just in terms of safety, but also in reliability in general and resultant financial economies through less frequent maintenance; has meant that research is continuing.

A variety of materials for this type of application would be usable, in particular carbon and glass-fiber based composites seem good choices partly due to the ease with which sensing elements can be placed within them. Other materials, such as concrete, can also have sensors embedded within them during fabrication. Simply bonding the sensors to the surface of the structure in question is another option and does have the advantage that it can be done at any time within the lifetime of the structure, though the information

obtained may require a different interpretation.

One of the important technologies for this type of application will be strain sensing. There are number of possible candidates for sensing elements that could be used. Sensors based on piezoelectric, electrostrictive, silicon and fiber optic technologies all offer advantages and disadvantages. However, a lengthy comparison between available sensing technologies is available in the literature (e.g. [19]) and thus beyond the scope of this thesis and is not undertaken here.

The remainder of this thesis will concentrate on fibre-optic sensing (which discussed in general terms in the next Section) and in particular on the use of Bragg gratings - an optical fiber based sensing element that has a number of advantages for this type of application.

1.2 Optic fibre sensors

Until the early 1970s, the main use of fibre optic cables had been for medical endoscopic instruments. Improvements in fibre fabrication techniques meant that the mass production of very loss optical fibres was possible. This combined with improvements in light sources (e.g. single frequency laser-diodes and high bandwidth LEDs) and detectors caused a rapid rise in the use

of optical fibre links for communications. Modern fibres are now so pure that losses may be attributed to fundamental scattering at the molecular level (e.g. Rayleigh scattering). The rapid growth in this field continues as fibre communications are used more frequently and on bigger projects such as trans-Atlantic links.

Conversely, optical sensing methods were well established prior to the 1970s. These methods ranged from simple optical switches based upon breaking a beam, up to quite complex interferometry. The application of optical fibres to sensing first occurred in 1976 when Vali *et al* [56] demonstrated a fibre based Sagnac interferometer and a year later Rogers [44] demonstrated fibre based current sensors. Since these initial experiments, the area of optical fibre based sensors has increased rapidly and includes a wide range of detectable measurands.

Fibre optic sensors are now a well-established technology and have been discussed in detail in review papers and book series (e.g. [11][53] and [19]) wherein details are to be found. In summary, intrinsic fibre optic based sensors (as opposed to extrinsic systems that use optical fibre as a link to conventional optical sensing systems) have a number of advantages over other sensing technologies. The small size of fibre optic cables means that they can realistically be placed almost anywhere without damaging the integrity of the structure itself. They are immune to electromagnetic interference, which

eliminates the need for shielding to minimise electrical noise picked up by electrically active sensors.

Fibre-optic sensors can offer high-sensitivity to a variety of measurands and high bandwidths (several MHz). The inherent strength of the glass means that, they are less prone to fatigue and corrosion than some technologies and can perform in a range of environments including high temperatures.

As mentioned in the previous Section, strain is one of the key measurements for a range of applications and for a fibre-optic based strain-sensing system there are three basic arrangements: the fibre Fabry-Perot interferometer, the polarimetric fibre sensor and the in-fibre Bragg grating.

The fibre Fabry-Perot interferometer consists of two partially reflective elements placed reasonably close together (i.e. less than the coherence length of light source used) (this shown schematically in a later Section as Figure 3_12). The device operates as a standard interferometric device and the phase difference between the two reflected beams must be due to the round trip between the two reflective elements. Anything that changes the length of the optical round trip (such as strain) will effect the phase difference and thus can be detected. The main disadvantage of this device is that it is not easy to multiplex a series of them.

The polarimetric fibre sensor uses high-birefringent fibres as the sensing elements. High-birefringent fibres are capable of propagating two orthogonally polarized modes at different velocities. The phase difference between the two modes, and hence the polarization state of the emerging light, is dependent on the state of strain and temperature of the fibre itself. Thus, by monitoring the polarization state of the emerging light, the strain of the fibre within the sensing region can be determined.

The third choice, Bragg gratings, are intra-core structures that consists of a periodic modulation of refractive index. They are small, sensitive to strain and temperature and offer the possibility to be effectively multiplexed to form a quasi-distributed network. These devices form the focus of this thesis.

Truly distributed optical-fibre sensors have been developed that utilize the entire length of the fibre to determine the effect of measurand at any point. However, most technologies of this type use a scattering effect of the fibre itself (e.g. Raman scattering) that enable temperature measurements to be made much more conveniently than strain. In addition, the accuracy to which the position of local variations in the measurand can be determined is limited, typically a resolution of the order ~1m would be expected.

1.3 Aims and objectives

The major aims and objectives that this thesis will attempt to complete are outlined below:

1. A review of the recent literature and an evaluation of the possibilities for new grating sensor schemes is carried out.

2. An investigation into the techniques of operation of an in-fibre Bragg grating as an optical sensing element for temperature and/or strain measurement has been carried out and an estimation of the sensitivity of a system of potential industrial value will be made experimentally.

3. An examination of the various systems aspects that are required in a sensing instrument based on Bragg gratings will be carried out, including the most appropriate choice of the light source and detector used. In particular, the issues involved in developing an effective scheme for decoding the measurand dependent, wavelength encoded reflections from the Bragg gratings will be investigated.

4. Development of a sensor system capable of demultiplexing a number of Bragg grating sensing elements in series along a single fibre. To be effective, the reflected signal returned from each individual grating should

be separated from the returned signal from the other gratings, with as little negative effect on the sensitivity of the measurements due to the presence of the other gratings as possible. In addition, the system is designed such that the level of crosstalk (crosstalk occurs when a signal from one grating is misinterpreted as having originated from different grating) should obviously be as small as possible.

5. Reporting of results on the performance of the system developed and the potential for its improvement and development, in terms of potentially offering an increased resolution and a higher number of sensors.

1.4 Structure of thesis

The thesis is divided into a series of chapters describing the work done to achieve the aims and objectives shown above. An outline of the various sections of this thesis is given below:

Chapter 1

Section 1.1 introduced the background to strain sensor systems and the types of applications that a successful strain measurement system could have. Section 1.2 introduced the background to fibre-optic sensors and highlighted the advantages a fibre-based system can have over other types of sensor devices, and Sections 1.3 and 1.4 discussed the aims and objectives, and the

thesis structure. Section 1.5 links to the work of the next chapter.

Chapter 2

Chapter 2 will cover the background material particular to the use of Bragg gratings in this way, including essential aspects of fabrication and their essential basic operation. Their operation will be demonstrated through the use of a simple computer model of a Bragg grating sensor in Section 2.3, prior to which Section 2.2 will discuss the basic theory of the two main methods of multiplexing a number of sensors in series (i.e. wavelength domain and time domain). Section 2.4 is a literature review, which enables the work to be placed in the context of recent research in the field. Section 2.5 summarizes the work and leads into the next chapter on wavelength demodulation methods.

Chapter 3

Chapter 3 reviews the work undertaken involving the use of a Wollaston prism which was investigated as a possible method of resolving the wavelength encoded signals that are returned from a Bragg grating. Sections 3.1.1 and 3.1.2 present discussion of the operation of a Wollaston prism and how it can be used as the basis of an optical interferometer. Section 3.2 presents the method used and results of an experimental demonstration of wavelength change determination using a Wollaston prism. Section 3.3 presents a related

section of work whereby a Wollaston prism interferometer is used as an integral part of a displacement measurement sensor. Section 3.4 will discuss the wavelength demodulation scheme actually employed in subsequent work and why the Wollaston interferometer was shown unsuitable for inclusion in the final system.

Chapter 4

An effective multi-sensor system requires numerous sensors to be operated simultaneously. Chapter 4 will present the development, component choice, construction and operation of an optical time-domain based demultiplexing system developed during this project for such operation. Section 4.2 will investigate roles and the choices of the individual component parts of the system, whilst Section 4.3 will show results from the system and enable a comparison of performance against specification to be carried out. The results discussed will lead into a final section of Chapter 4, in preparation for a discussion of the potential of the concept and future work.

Chapter 5

Chapter 5 will include a discussion about the results produced by the system and look at possible avenues for future research work that could be done to enhance performance and flexibility beyond that achieved. Section 5.1 will

look at the problems that may occur if grating sensors with the same Bragg wavelength are used in series. Section 5.2 discusses improvements that could be made to the current system and reflects on the way forward for such research.

1.5 Summary

In Chapter 1, it has been shown that an efficient strain measurement system would have a range of applications and as such is becoming an increasingly important issue. This is not solely due to the interest in the relatively new concept of smart structures but also because of the safety and economic benefits that can result from detecting the effects of excessive strain (such as, for example, small cracks) early.

Optic fibre based sensors represent a possible solution to this problem and a number of configurations have been suggested as sensing elements. Of these, the Bragg grating sensor has the most potential due to its small size, potential sensitivity and ability to be multiplexed. This is the basis for the rest of the thesis, and leads into Chapter 2, in which the background theory of the Bragg grating, including its use as a strain sensor, is examined and a literature review presents some of the work published in this area.

Chapter 2:

Background material

2.1 Background theory of Bragg gratings

As mentioned in Section 1 above, an optical fibre based system for strain measurement would have a wide range of applications. Fibre Bragg gratings are small, potentially quite cheap and sensitive to both temperature and strain and therefore could be an ideal choice for a range applications.

In essence, Bragg gratings consist of a longitudinal, periodic change in refractive index of the core of the fibre, this acts as multiple reflective structure and the interference pattern created by the superposition of these reflections changes the reflection and transmission spectra of the grating itself. By monitoring the reflective spectra of a grating, any changes in the measurand (e.g. strain or temperature) can be detected.

The background theory to Bragg gratings is studied in the following sections. Section 2.1.1 discusses some of the more common grating fabrication

techniques. Section 2.1.2 analyzes the gratings behaviour in terms of strain and temperature effects, in light of the primary application of this research.

2.1.1 Grating Fabrication

In-fibre grating structures were initially made by physically deforming the structure of the fibre itself or by setting up a standing wave within the fibre using a powerful ultraviolet, UV, laser. However, for mass-production most gratings are produced via a side-writing process, wherein the Bragg gratings are produced by placing the fibre in a modulated intensity pattern of a powerful ultraviolet laser. The pattern is produced either holographically (W. W. Morey *et al*, 1989) or with a intensity mask.

The processes are described in several texts (e.g. [19]). In summary, for holographic production, a spatial interference pattern is created by splitting the UV beam into two components that are then recombined. The fibre is placed within the resultant modulated intensity pattern, this is shown below in Figure 2_1.

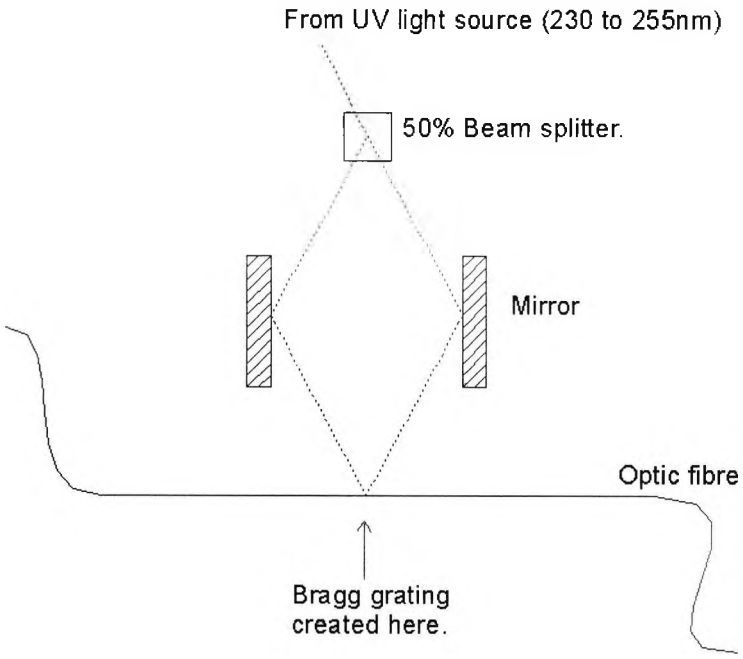

Figure 2_1: One method of forming Bragg gratings holographically.

(After G. Meltz *et al* [39])

The advantage of this method is that the Bragg wavelength of the grating produced can be altered by changing the angle at which the two UV beams recombine, since this will vary the nature of the interference pattern produced. This means that Bragg wavelengths need not be restricted to the wavelength of the writing laser source alone, as was the case with early gratings.

Phase mask, and intensity mask, Bragg grating production both involve using a wide UV beam to illuminate a mask that is placed in front of the fibre. The intensity mask modulates the intensity of the UV light directly. The phase

mask, however, acts as diffraction grating and the $\pm 1^{st}$ order diffracted beams interfere producing an intensity modulation, the period of which is one-half that of the phase mask used. The phase masks can be formed by various processes and are fabricated in such a manner to reduce the 0^{th} order signal as much as possible, whilst maximising the 1^{st} orders (typically as much as 35% of the total power can be transmitted though this first order beams).

2.1.1.1 Photosensitivity of fibres

For either method of producing the intensity pattern is used, the process whereby the UV intensity pattern is converted into a change in refractive index is still not fully understood but the photorefractive effect is thought to be at least partly responsible. This process is outlined below in Figure 2_2. The areas where UV light is incident with the fibre, free electrons are liberated from the fibre, probably via a two photon process (suggested by Lam and Garside [31], who showed that the strength of the grating increases as the square of the power of the writing laser). These free electrons then drift into the other areas of the fibres so that when the UV beam is removed, regions of differing density remain. Low density in the regions from which the electrons have been removed and high density in the regions that have gained extra electrons and it is these regions of varying densities that create the refractive index modulation in the fibre.

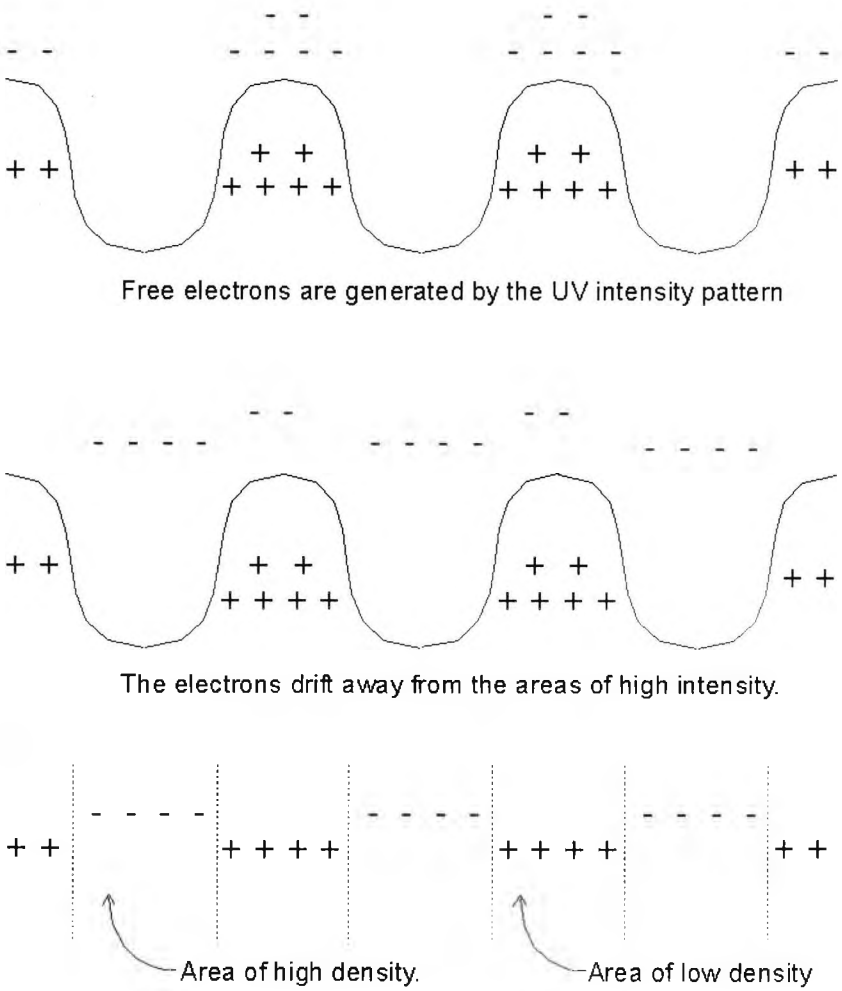

Figure 2_2: Bragg grating formation process.

The photorefractive effect.

The source of these free electrons is likely to be oxygen-deficient germania defects within the fibre. Meltz *et al*, [39] showed that strong refractive index changes were possible using UV light in the range of the defect absorption

peak (240-250nm).

These defects are caused during fibre drawing [24] and by ionizing radiation [18] and a great deal of research has been directed toward eliminating them as far as possible so as reduce the associated absorption of light. However, the issue of photosensitivity has meant that methods of increasing the effect of these defects are needed in order to produce more effective grating structures. Some of these methods of increasing photosensitivity are outlined below.

Hydrogenation or hydrogen loading of optical fibres can create very high photosensitivity in fibres [32]. Hydrogen loading is carried out by diffusing hydrogen molecules into the fibre preform rods at high pressure and temperature. The hydrogen molecules react in the glass at normal Si-O-Ge sites creating oxygen deficiency centres by the formation of an OH species. This method can create fibres that allow permanent changes in the refractive index of the order of 0.1. However, this method does have two disadvantages, firstly the increased photosensitivity is not a permanent effect as the hydrogen will diffuse out of the glass over time. Secondly, the OH species formed does have its own associated absorption characteristics located at 1390 and 1410nm that can introduce unacceptable losses at these wavelengths.

'Flame brushing' is a similar technique for increasing the photosensitivity of the fibre [9]. Hydrogen molecules are introduced to the glass by applying a

hydrogen and oxygen fuelled flame to the region. The hydrogen reacts with the glass in a similar manner to the hydrogen loading case described above. The drawback of this method is that the flame can reach temperatures in excess of 1700°C that can weaken the fibre.

The use of Boron as a codopant in germanosilica fibres has been shown to increase the UV photosensitivity in optical fibres [10]. The boron does not change the number of oxygen deficiencies within the fibre, instead the boron allows photoinduced stress relaxation to occur. This stress relaxation changes the refractive index via the stress-optic effect. Table 2_1 shows a comparison of photosensitivity for a variety of fibres and techniques.

Fibre Type	GeO_2 in fibre core mol %	Reflectivity of 1.5mm Bragg gratings %	Time required to inscribe grating. (min)
Philips, matched cladding	5	17	60
Philips, depressed cladding	4	20	60
Deeside fibre	5	17	60
Corning payout fibre	8	29	90
Hydrogenated standard fibre	4	60	10
High index fibre	20	77	10
Reduced fibre	12	97	5
Boron codoped	17	91	1
Hydrogenated boron codoped fibre	17	87	10sec.

Table 2_1: Comparison of photosensitivity for a variety of fibres and techniques.

(After D. L. Williams *et al*, [59])

2.1.2 Strain \ Temperature effects

As mentioned above, a Bragg grating can be thought of as a multiple reflective structure where each boundary between low and high-density regions of the fibre produces a back reflection, albeit a small one. This is shown in Figure

2_3 below.

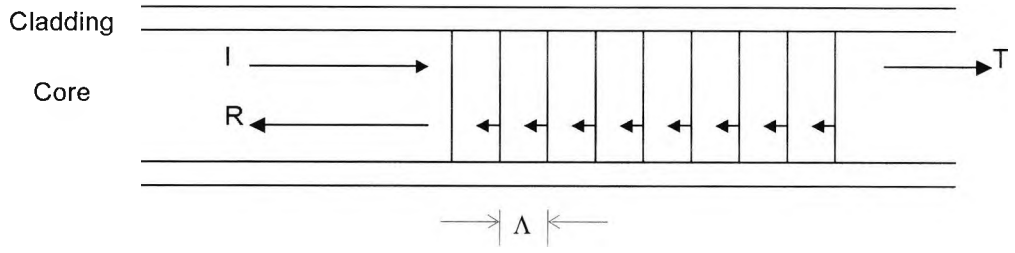

Figure 2_3: Periodic structure of grating. Where I, R and T are the incident, reflected and transmitted rays respectively.

The multiple reflections interfere with each other and it can be seen from the diagram above that only particular wavelengths will constructively interfere in reflection (i.e. the wavelength that matches the optical round trip between successive reflections). The exact wavelength reflected by the Bragg grating is called the Bragg wavelength and the characteristic Bragg grating equation (2_1) given below gives its numerical value

$$\lambda_B = 2n\Lambda \qquad (2\_1)$$

where λ_B is the Bragg wavelength, n is the refractive index and Λ is the grating pitch. λ_B is therefore directly proportional to the optical round trip path length between successive reflections. When illuminated by a broad band source the grating acts as a notch filter in transmission and as a

complementary band pass filter in reflection, as shown in Figure 2_4 below.

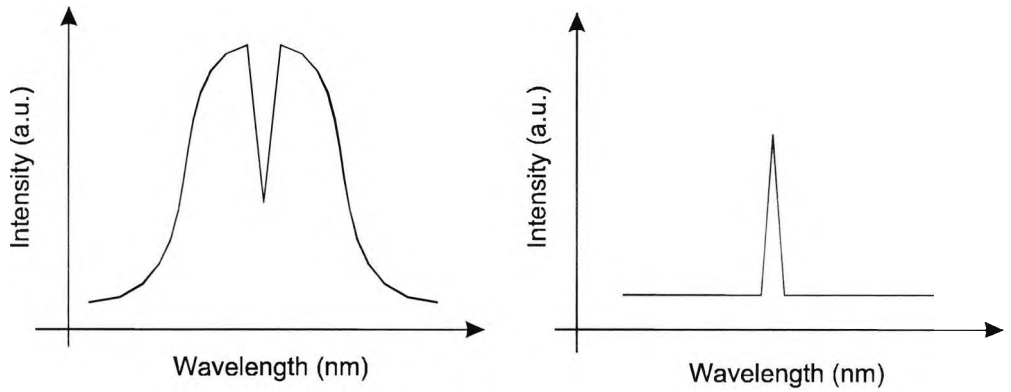

Figure 2_4: Bragg grating spectra in (a) transmission and (b) reflection when illuminated by a broadband source.

The optical characteristics of the reflected portion of light (as shown in Figure (b) above) has an almost Gaussian distribution of wavelengths and can have a very narrow linewidth (of the order of 0.1nm is common). Consequently, the reflections from individual gratings can be quite low power (≈10's of nW), which means that they can be difficult to detect. However, the narrow linewidth makes identifying any changes in the Bragg grating wavelength easier.

From the grating equation (2_1) it is obvious that anything that changes the optical round trip of the grating will change λ_B. Bragg gratings are sensitive to

changes in strain and to changes in temperature due to changes in the physical dimensions of the fibre (thereby changing the period of the grating) or by changes in the average refractive index of the fibre itself. The change in λ_B for a temperature change ΔT or a change in length Δl is given by a Taylor expansion of Equation 2_1 (assuming small changes), which results in Equation 2_2, [63], given below

$$\Delta\lambda_B = 2\left(\Lambda\frac{\partial n}{\partial l} + n\frac{\partial \Lambda}{\partial l}\right)\Delta l + 2\left(\Lambda\frac{\partial n}{\partial T} + n\frac{\partial \Lambda}{\partial T}\right)\Delta T \qquad (2\_2)$$

The first term in the above equation gives the Bragg grating wavelength shift due to a longitudinal strain, ε, and can be rewritten as equation 2_3 given below.

$$\Delta\lambda_B = \lambda_B(1-\rho_e)\varepsilon \qquad (2\_3)$$

The photoelastic coefficient, ρ_e, is given by [63]

$$\rho_e = \frac{n^2}{2}\left(\rho_{12} - v(\rho_{11}+\rho_{12})\right) \qquad (2\_4)$$

Where n is the core refractive index of the fibre, v is Poisson's ratio (v=0.16) and ρ_{12} and ρ_{11} are components of the strain-optic tensor. For a typical fibre

ρ_{12}=0.252, ρ_{11}=0.113. Using these parameters, the expected sensitivity at 1550nm is 1.2pm/με.

The second term in Equation 2_2 represents the effect of changes in temperature on Bragg wavelength and can be rewritten as

$$\Delta\lambda_B = \lambda_B(\alpha+\xi)\Delta T \qquad (2\_5)$$

Where ξ is the thermo-optic coefficient (a typical value would be -8.3×10^{-6} / °C for germania-doped silica-core fibre and would be similar for the fibre used for this work) and is given by:

$$\xi = \left(\frac{1}{n}\right)\left(\frac{\partial n}{\partial T}\right) \qquad (2\_6)$$

and α is the thermal expansion coefficient and is given by

$$\alpha = \left(\frac{1}{\Lambda}\right)\left(\frac{\partial \Lambda}{\partial T}\right) \qquad (2\_7)$$

and is approximately equal to 0.55×10^{-6} / °C for silica. It is clear that the change in refractive index change is by far the more dominant effect. The expected sensitivity at a ~1550nm is approximately 13.7pm / °C.

2.1.3 Bragg grating operation

In essence, using a single Bragg grating as a sensor requires only a relatively simple system. All that is required, in addition to the Bragg grating, is a broadband source, a detector and a method for detecting changes in the returned Bragg wavelength such as a spectrum analyser.

The grating is attached to the material that is to be measured. This can be achieved by bonding the fibre in place onto the surface or, in particular for the case of composite materials, the fibre can be placed within the material itself during its construction. Whichever method is employed, any changes in the strain or temperature of the material will change the centre wavelength of the returned portion of light. This wavelength peak can be monitored and thus the strain of the material can be detected from a knowledge of the parameters involved.

In laboratory conditions, this type of situation must be tested in a repeatable manner to determine the characteristics of the system. This was done in one of two ways in this thesis. Either by attaching the fibre to the underside of a small brass beam. The brass beam is supported at both ends and small weights are placed on top produced a three point bend in the beam and strain in the fibre.

The other method employed stretches the fibre by attaching it to two posts, one of which can be moved with a micrometer to read the fibre elongation directly.

The two main problems with a system of this nature are, firstly, the number of sensors that are used (i.e. more is preferable) and, secondly, the cross-sensitivity of the Bragg grating response to both strain and temperature. Various methods of differentiating between strain and temperature have been reported and are examined in detail in Section 2.4.4, whilst techniques for multiplexing a number of gratings are examined in Section 2.3.

2.2 Demultiplexing techniques

As shown in the theory presented in the previous sections, Bragg gratings can be used individually as sensors to monitor changes in the strain conditions of the optic fibre. However, in any practical application, (e.g. such as in so-called 'smart structures') a number of points within the region of interest will need to be monitored. Obviously, the more points that can be monitored simultaneously, the better. Bragg gratings are situated within the optical fibre, therefore if they are used singularly, a separate fibre must be used for each grating. An example of this type of spatial demultiplexing is shown below in Figure 2_5:

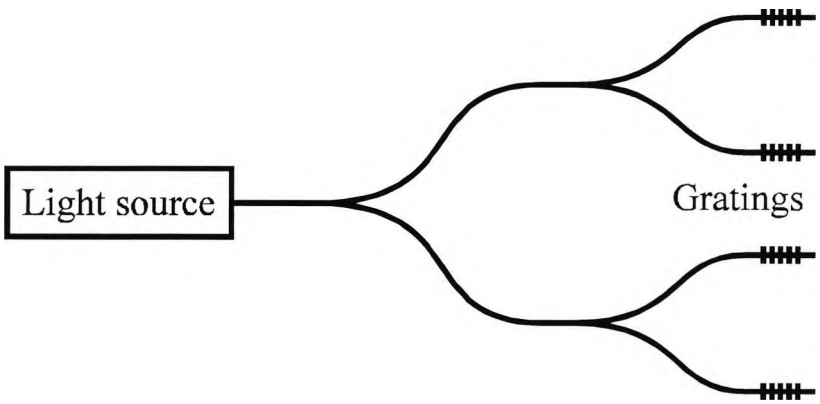

Figure 2_5: An example of spatial demultiplexing.

This diagram is obviously incomplete since no detectors are shown which would further complicate the system. It can be seen that this type of system involves a large number of optical components, and couplers in particular. This will make the final system more complex and expensive than a single fibre 'quasi-distributed' network of sensors such as shown below in Figure 2_6.

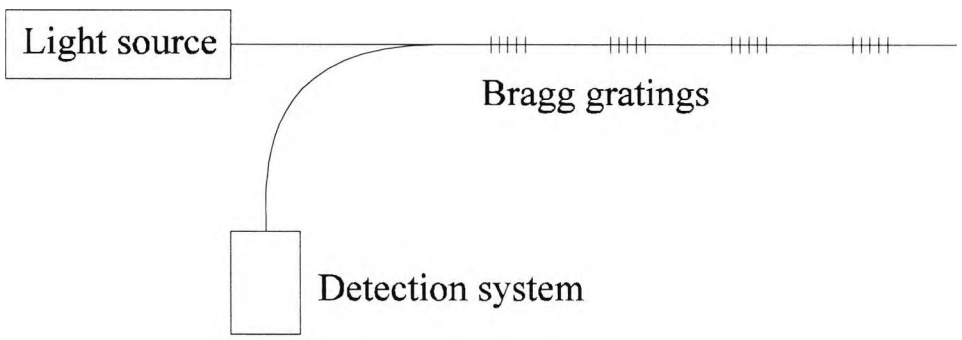

Figure 2_6: An example of a quasi-distributed network of sensors.

These quasi-distributed arrangements are much simpler to manufacture but do present one important problem, i.e. differentiating between the reflected signals from each Bragg grating. It is this problem that the demultiplexing system attempts to solve successfully.

There have been a number of techniques reported to achieve this (reviewed in a number of papers, e.g. A. D. Kersey [30]), however they break down, in broad terms, into two distinct classes. The first class, wavelength division multiplexing, WDM, uses differences between the sensors in the wavelength domain to identify individual gratings. Secondly, time division multiplexing, TDM, uses knowledge of the spatial construction of the sensor network, in order to identify returning signals by the time taken for the source-grating-detector round trip. These two methods are discussed in more detail in the following sections.

2.2.1 WDM theoretical background

The basis of WDM is shown schematically below in Figure 2_7. To operate, such a system relies on the fact that each Bragg grating can be fabricated with a different characteristic Bragg wavelength, λ_B. When the sensors are illuminated with a broadband source, each reflected signal from each grating

will be characterised by a different centre wavelength. In a WDM system, the light source will normally be continuous, therefore, the resultant returned signal from the gratings will be an uninterrupted set of narrowband spectral components, one from each grating in the sensor system.

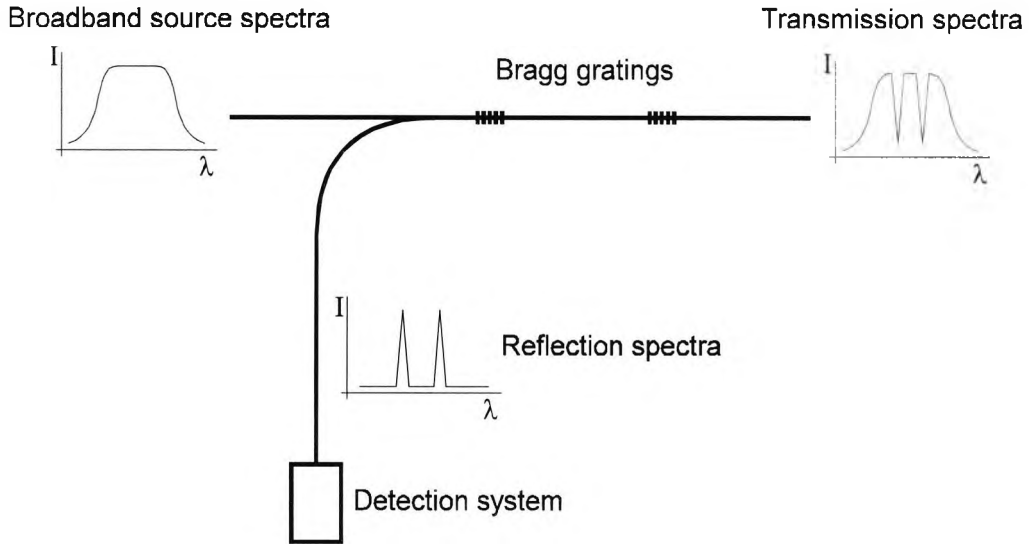

Figure 2_7: An example of a WDM system. The number of gratings depends on the FWHM of the source used.

Before any measurand induced changes in Bragg wavelength can be detected in a single grating, the signal must be separated from the other grating signals. A wavelength filter (such as a Fabry-Perot interferometer, which is discussed in Section 3.4.2) can be used to isolate these reflections and monitor the individual changes in wavelength.

2.2.2 TDM theoretical background

Figure 2_8 illustrates an example of the alternative grating arrangement, a TDM system. The light source is pulsed to produce a short pulse, the duration of which is determined by the spacing between the gratings. This input pulse produces a pulse of reflected light from each of the Bragg gratings used in the sensor array. There will be a time delay between the light source producing a pulse and a pulse reflected from a grating being detected, which is dependent solely on the length of fibre between light source and grating and therefore will be different for each sensor in the network. This fact enables a time domain based system to differentiate between gratings.

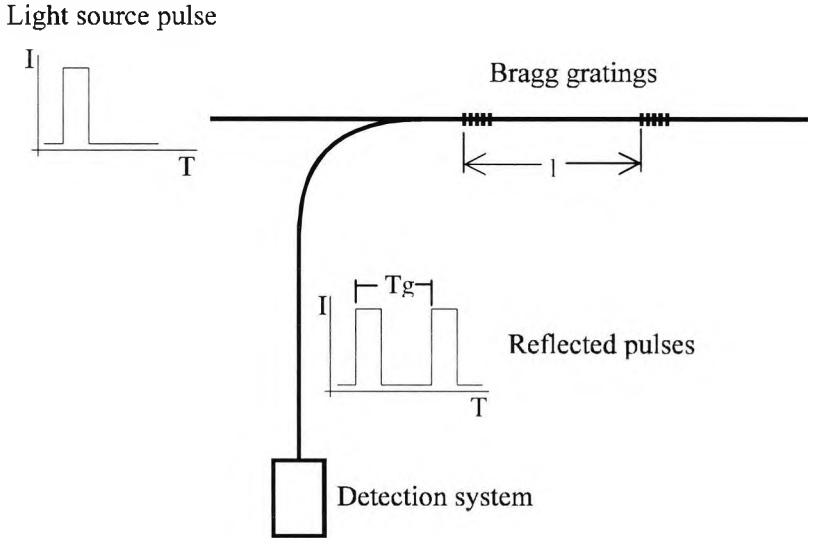

Figure 2_8: An example of a TDM system operation. Reflected signals are separated in time (Tg) due to the distance between gratings (l).

The detection system for a TDM system has to include a method of timing the delay between the laser pulse firing and the returning signals being detected, as well as detecting changes in the wavelength of the gratings.

This system was chosen for development. The reason for a TDM based system, over the apparently easier to implement WDM type, is its potential sensitivity. This sensitivity will be outlined in later Sections of this thesis, but the minimum detectable change of the Bragg wavelength when strained or heated is limited in the WDM system due to the convolution of the Bragg grating reflection spectra and the pass band of the filter used. In TDM systems, no such limitation exists, but the grating spacing is governed by the pulse duration available from the source and the speed at which the associated electrical components can operate.

2.3 Bragg grating computer simulation

To complete the background study of the operation of a Bragg grating a computer simulation was designed. Its purpose was to model numerically the behaviour of a single grating under continuous illumination. The model is based on the propagation method demonstrated by H. H. Lin *et al*, [34]. In order to simplify the model sufficiently so that a numerical approach could be taken, a number of assumptions were made.

The first assumption made was simply to create a 1-dimensional model, i.e. forward and backward propagating light only. This is a reasonable assumption since all the gratings used in this project were written in single mode fibre. Such fibre will have some transverse effects but they will be small enough so that a one-dimensional analysis is a reasonable assumption to make.

Secondly, it was assumed that no light is absorbed or scattered out of the fibre at any point within the gratings. The length of an average grating is about 1cm and since they are written into standard optical fibre, we can expect any loss over this length to be extremely small.

Thirdly, it must be assumed that the gratings are perfectly fabricated, that is, there were no unwanted variations in the strength of grating across the fibre or

along its length. It was also assumed that the changes in refractive index at exactly 90° to the main fibre axis. These are reasonable assumptions for carefully produced gratings, such as those supplied to us for this research.

The basis of the computer model is to consider the gratings as a series of homogeneous layers each having a slightly different refractive index relative to its neighbours. The computer simulation then models the light propagation from one layer to the next, computing the reflections at each boundary. This is shown schematically below in Figure 2_9.

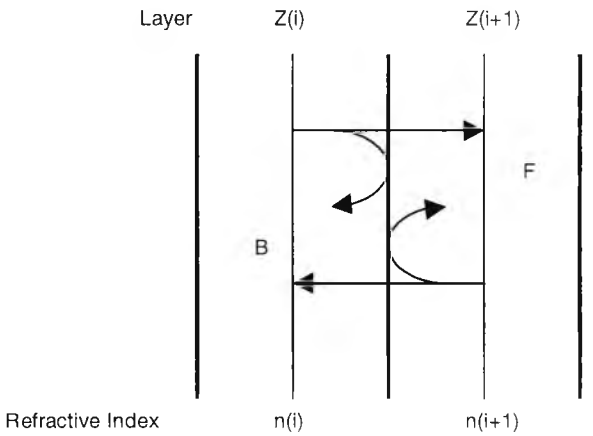

Figure 2_9: The computer models the grating as a series of layers.

The intensity of forward propagating light in light layer Z(i+1) is equal to the light in layer Z(i) (where I is an integer), minus whatever portion of the light is reflected back at the boundary, plus the reflected portion of the backward

travelling wave from Z(i+1). The backward travelling wave in layer Z(i) is equal to the backward travelling wave from Z(i+1), minus whatever portion is reflected at the boundary, plus whatever portion of the forward traveling wave from Z(i) is reflected back. This can expressed as:

$$E_F(i+1) = E_F(i)P(i)P(i+1)T_F(i) + E_B(i+1)P(i+1)^2 R_B(i+1) \qquad (2\_8)$$

For the forward travelling wave and

$$E_B(i) = E_B(i+1)P(i+1)P(i)T_B(i+1) + E_F(i)P(i)^2 R_F(i) \qquad (2\_9)$$

for the backward traveling wave, where $E_F(i)$ and $E_B(i)$ are the amplitudes of the forward and backward traveling waves in the i^{th} layer respectively, P(i) represents the change of phase a wave undergoes when traveling from the center of layer i to the boundary and R_F, R_B, T_F and T_B are the reflection and transmission coefficients for the forward and backward traveling waves.

If the width of a layer is Δz then P(i) given by:

$$P(i) = \exp(-jk_v n_i(\Delta z/2)) \qquad (2\_10)$$

Where n_i is the refractive index of layer i and k_v is the wavenumber.

The values for the reflection and transmission coefficients are derived from the Fresnel equations and the angular dependence of reflection is not involved. Hence:

$$T_F(i) = \frac{2n_{i-1}}{n_{i-1} + n_i} \qquad (2\_11)$$

$$T_B(i) = \frac{2n_{i+1}}{n_{i+1} + n_i} \qquad (2\_12)$$

$$R_F(i) = \frac{n_i - n_{i+1}}{n_i + n_{i+1}} \qquad (2\_13)$$

$$R_B(i) = \frac{n_i - n_{i+1}}{n_i + n_{i-1}} \qquad (2\_14)$$

Where n_i, is the refractive index of the i^{th} layer

Figure 2_10 shows the system output in case of a plane wave propagating through a medium with periodic refractive-index distribution. The length of the medium is ≈50μm and $\Delta n = 0.02$. This was divided into 420 layers.

The refractive index structure was defined as:

$$n(z) = n_o + \Delta n(z) = n_o + \delta n \cos(2kz) \qquad (2\_15)$$

It can be seen that despite the short length of the grating, there is a strong back reflection, due to the high value of Δn. To validate the result of the numerical model, an analytical solution for the case where $\lambda_B = \lambda_{SOURCE}$ was available. The analytical solution for this case (shown in Figure 2_11) is given by the equations below [34]:

$$E_F(z) = \left[\frac{E_{in}}{\cosh(\alpha L)}\right] \cosh[\alpha(L - z)] \exp^{-jkz} \qquad (2\_16)$$

$$E_B(z) = \left[\frac{-jE_{in}}{\cosh(\alpha L)}\right] \sinh[\alpha(L - z)] \exp^{+jkz} \qquad (2\_17)$$

Where L is the total length of the region and

$$\alpha = \frac{k\delta n}{2n_o} \qquad (2\_18)$$

The above analytical solution assumes that E_{in} is the forward propagating wave at the position z=0 and the backward propagating wave is equal to 0 at the position z=L.

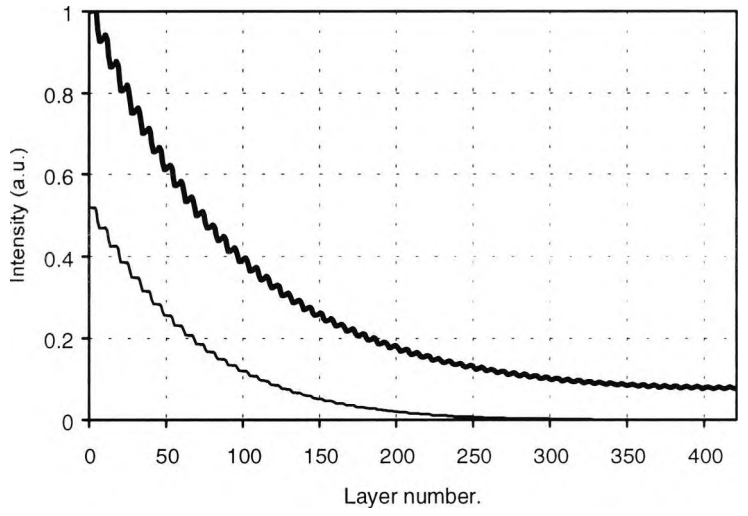

Figure 2_10: Intensity distribution of the forward (bold line) and backward propagating waves through a fibre (Numerical model).

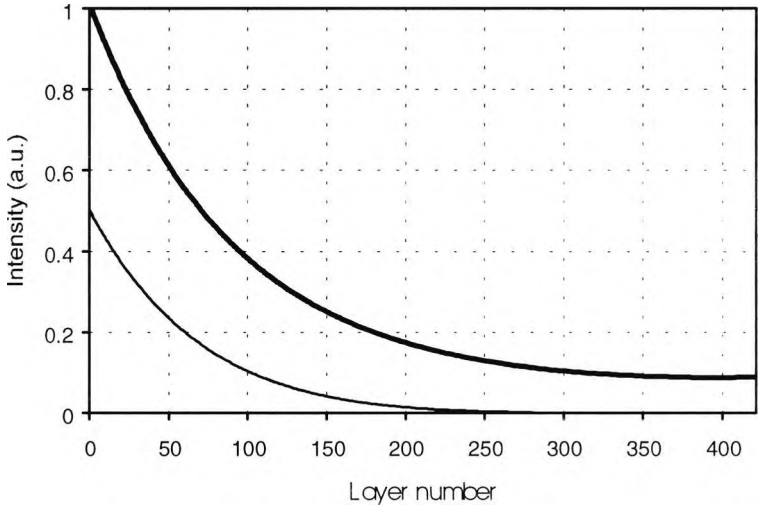

Figure 2_11: Analytical solution, for the both the forward (bold line) and the backward waves, of the case described above.

For both Figure 2_10 and 2_11, intensity is proportional to E^2.

Only one space harmonic is retained in this analytical solution and this accounts for the lack of ripples in the theoretical solution that appear on the numerical solution. The ripples are due to higher order space harmonics of the form exp[-j(2n)kz] where n is an integer. This periodic ripple is connected with the distribution of energy stored between the peaks of the refractive index periodic structure.

The two graphs (of the analytical and the numerical solution) are clearly sufficiently similar, verifying the numerical technique and justifying its use too predict the behaviour and performance of a Bragg grating operating over a range of wavelengths.

By varying the wavelength of the input source considered in the above analysis the graph shown below in Figure 2_12 was calculated showing the spectral response of a grating to such a wavelength. The model assumes that the refractive index perturbation is sinusoidal and has $\Delta n=0.0001$ and $n=1.45$ (typical values for real systems). The period of the grating was set at a value to ensure that the Bragg reflection would occur at a value of 1550nm which is wavelength range used for the sensors in this thesis.

The response shown in the graph is almost what is expected, that is only at values of λ near 1550nm is a strong reflection is shown.

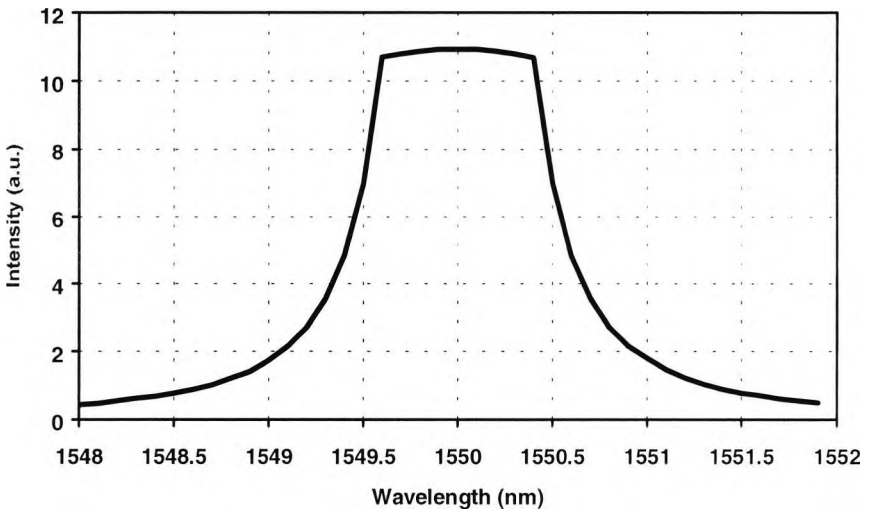

Figure 2_12: Computed graph of wavelength versus intensity.

for a grating length of 250μm.

The resultant grating bandwidth is considerably wider than would be expected from a Bragg grating, and this is due to the limitations placed upon the model in terms of length of the region of the refractive index change. The model consisted of over 2000 layers, nearly the limit that could be handled by the computer simulation available at the time the model was written, but this only gave a total grating length of 250μm. A longer region would give a more narrow bandwidth and a larger reflected signal. This effect can be seen more clearly in the second graph, Figure 2_13, which shows the same grating response but with a grating length of only 100μm, and a resultant greater bandwidth, illustrating the expected trend of narrower bandwidth with grating length increasing.

By increasing the complexity of the model used, the maximum length that could be simulated could be extended, but this would present other problems. This method of modelling the Bragg grating as a series of layers is valid for modelling unusual structures and does demonstrate a process by which the strong back reflections from a Bragg grating are formed. However, modelling the behaviour of a Bragg grating with its associated uniform refractive index perturbation can be achieved with alternative techniques, as shown in the analytical solution for the case where $\lambda=\lambda_B$, above. A second computer model was written, based on the coupling mode equations formulated by Lamb and Garside [31]. This model was used to predict the problems of using two gratings in series that have the same Bragg wavelength and it is discussed in more detail Section 5.1.1.

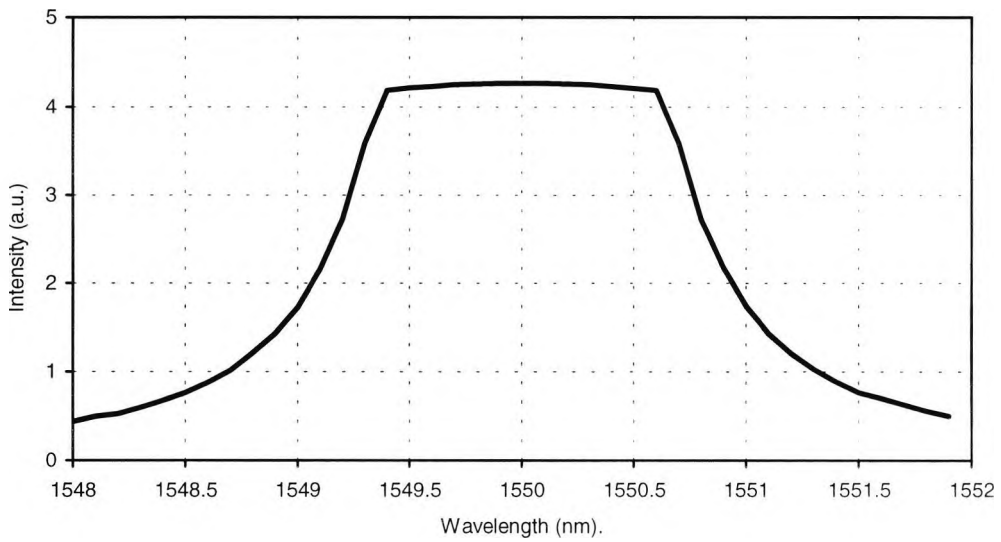

Figure 2_13: Computed graph of wavelength versus intensity.

for gratings length of 155μm.

2.4 Bragg grating literature review

In addition to their increasing utilization in telecommunications, optical fibers are also finding many applications in the field of optical sensing. This has been made more apparent by the recent discovery of the ability to change the refractive index of the core of a standard optic fibre by exposure to UV light. This change in refractive index makes possible a number of structures including wavelength filters such as the Bragg gratings.

Bragg gratings have attracted considerable research interest over recent years, partly due to the nature of optical fibre themselves (i.e. small size, immunity to electromagnetic interference etc.) but mostly because of its ability to act as a wavelength filter. The wavelength that is reflected, as shown earlier, is dependent on the characteristic parameters of the specific device fabricated (such as the period of the gratings and the strength of the refractive index change) and the prevailing conditions (in terms of strain and temperature) of the fibre in question. This fact has meant that a significant portion of the research interest involving Bragg gratings has been directed toward utilizing these devices as sensors for either of these measurands.

In this Section, part of the history of Bragg gratings, including some of these approaches, is reviewed. Two relevant review papers have been published recently (references: [30][43]) and as such are used a sources for some of the following material.

2.4.1 Fabrication

The first permanent grating produced by the action of UV light upon the photosensitive core of a germanosilica fibre was reported by [20]. It was produced by launching the light from an argon ion laser (488nm) directly into the fiber. The 4% reflection from the cleaved end of the fiber set-up a standing wave within the fiber and, after being left for some time, this caused a permanent perturbation of the refractive index of the core of the fibre. The strength of this grating was not particularly strong (10^{-6}) and resulted in a reflection filter at the writing wavelength. This style of grating was known as a *self-organized* grating since they formed without human intervention.

This photosensitivity of fibers remained a little used area of interest for some time after this initial discovery for a number of reasons. Firstly, it was thought only to apply to the particular type of fibre used in the experiment and not too most standard fibre types (this was proved not to be the case by Stone[51] who

demonstrated photosensitivity in a range of germanium doped fibers). Secondly, the method used to fabricate these gratings was inconvenient and finally it only produced gratings with a resonance wavelength in the range of the light source used (i.e. the same as the illuminating UV laser) and not the infrared region used as standard by the telecommunications industry.

Further problems associated with these self-organized gratings are that, due to the small depth of modulation produced, the gratings have to be longer in order to reflect enough power to be detectable. This is obviously unsuitable for localized sensing applications. Also, and perhaps more importantly, because the gratings are written at the same wavelength at which they are used, the gratings evolve with time and their characteristics of operation can change.

However, research interest was increased by a demonstration of a side writing technique by Meltz *et al* (1989) using an interferometric approach. It operated by splitting the incoming beam into two parts (by amplitude) that were then recombined to produce an interference pattern. The fibre was placed within this fringe pattern and the intensity modulation induced a change in refractive index within the core of the fiber with the same period as the fringe pattern. The period of the gratings produced by this method is given by

$$\Lambda = \frac{\lambda_w}{2\sin\theta} \qquad (2\_19)$$

where λ_w, is the UV wavelength and φ is the half-angle between the intersection of the UV beams. Applying this to the standard Bragg grating formula (2_1), the following results

$$\lambda_B = \frac{n\lambda_w}{\sin\varphi} \qquad (2\_20)$$

From the above equation it can be seen that λ_B can be selected by varying λ_w or φ. λ_w is limited to the range of wavelength over which the fibre exhibits photosensitive behaviour. However, there are no restrictions on the value of φ. Therefore, the interferometric method of fabricating gratings allows any value of λ_B to be created by varying φ.

The main disadvantage of this method is that it is sensitive to vibration, and thus small displacements in the position of the mirrors during fabrication can have large effects on the resulting gratings. Using a slightly different approach can solve this, splitting the light by wavefront, rather than amplitude: for instance using a Lloyds interferometer[33] will produce an interference pattern which will

produce gratings in the same way without the same level of vibration sensitivity. The drawback of this type of method is that the length of the grating is limited to the half the width of the UV beam.

This interferometric method of gratings production was improved by J. L. Archambault *et al*[1] who demonstrated Bragg gratings production written by a single excimer laser pulse with a duration of 20ns. The resultant gratings had a FWHM bandwidths of 1.0nm with reflectivities of 65% at 1550nm, and by increasing the length of these gratings, bandwidths of 0.05nm were produced with reflectivities of up to 10%. The same group reported the production of 100% reflectivity Bragg reflectors[2] by increasing the power of the writing laser. These gratings structures are formed by a mechanism in which the core of the fibre fuses producing very large changes in the refractive index of the fibre, of the order ~0.006.

Single pulse production of sufficient power density makes Bragg grating writing possible during optic-fibre drawing[16] . This makes online mass-production of Bragg gratings possible, an important feature for reducing the costs of a final system and has the advantage that it be done before any polymer coating is applied to the fibre which has to be removed for grating production using other methods (Although a method of producing gratings through the polymer jackets

using near-UV light has been developed [50].

Fabrication techniques have been improved to the extent that Bragg gratings are now available commercially. Bragg Photonics Inc., for example, sell gratings at 1550 or 1300nm, with a tolerance of 0.1nm, FWHM = 0.25nm ±0.1nm, and reflectivity = 95%, ±5%.

2.4.2 Wavelength demodulation

It is often the case that the wavelength demodulation component of a complete system is the main deciding factor in achieving the optimum system performance in terms of measurand resolution. It is therefore unsurprising that several techniques for successfully detecting changes in λ_B for a particular sensor have been reported.

One of the earliest Bragg grating specific techniques reported was a ratiometric approach by S. M. Melle *et al* (1992) which was based on the use of broadband filters. Any change in λ_B is detected by comparing the reflected signal transmitted through a filter to that passed through a reference path. This technique offers a limited resolution due to problems associated with the alignment and stability of

the bulk optic filters. An improvement is gained by using a fiber device with a wavelength dependant operation, methods using a WDM coupler have been reported [12][62] and strain resolutions of ~ ±5με were demonstrated.

One of the most popular forms of Bragg grating interrogation is based on the use of a tunable passband filter to track the Bragg signal. A variety of different types of filters have been reported including accousto-optic filters [17][60] and fiber-grating filters [13][21].

The most common form of filter used for this application, however, is based on the use of a Fabry-Perot, FP, interferometer. In essence, the FP acts as a wavelength filter passing only a narrowband of wavelengths depending on the spacing between the two reflecting surfaces in the device. Moving one of the mirrors with a piezo-electric transducer, PZT, enables the filter to scan over a range of wavelengths and the transmitted signal will be a maximum when the passband of the filter matches the λ_B of a grating. Typical characteristics for a FP filter are a free spectral range, FSR, of ~50nm and a bandwidth of ~0.3nm. If the FSR of 50nm is generated via a 16 bit digital-to-analogue conversion produces a theoretical minimum strain resolution of ~0.8ustrain.

The use of a FP filter as part of a WDM system has been expanded with the

inclusion of a pair of optical switches (M. A. Davis *et al*, 1996). The computer controlled switches were used to change between arrays of sensors along different fibre lengths. This combination of spatial and wavelength demultiplexing allowed the FP filter to address 5 sensor arrays each with 12 grating elements for a total of 60 gratings with a single ELED source and detection system. By averaging the results from each sensor 50 times over a 2.5 second period, a resolution of ~±1με was achieved.

Another approach to wavelength discrimination is the use of a fixed bulk optic device that disperses light according to wavelength (e.g. a prism or a diffraction grating). C. G. Askins *et al*[3] reported the use of such a system for use of monitoring the fabrication of gratings during fiber production on a drawing tower. The signal light was dispersed using a diffraction grating into a linear pattern and the result was detected using a linear charge coupled device, CCD. Any changes in wavelength of the signal pattern will be detected as a change in the intensity pattern on the CCD. Gratings spaced by 1nm were resolved using this method and, after some signal processing to determine the center of the wavelength peak, strain resolutions less than 1με were demonstrated. The main advantage of this type of CCD spectrometer over the FP filter is in terms of power. With the CCD the whole the spectra reflected by a grating can be collected, where as the FP filter collects just a small portion of it. The CCD is therefore better when signal

magnitudes are low.

Fourier transform spectroscopy, FTS, is another form of wavelength demodulation. In this case, the signal light is used as the input source of an interferometer in which one arm can be scanned to change the relative OPD. FTS is an efficient technique for the analysis of signals which contain multiple spectral components and therefore is well suited to Bragg grating applications

An example of an FTS system for Bragg grating applications has been reported [14]. The system utilized an all-fiber Michelson configuration with arms 100m in length, one of which was wound around a fiber stretcher producing an OPD of ~30cm. Polarization fading, often a problem with large OPD fiber Michelson interferometers, was avoided by using reflector elements based on Faraday-rotator mirrors. Wavelength resolutions of the order of 0.015nm were reported.

The use of interferometers to detect changes in λ_B, by transposing the change in wavelength into a change of phase of the resulting fringe pattern, has been described by a number of groups (e.g. [26]). The operation of this type of arrangement is described in more detail in a later Section. The theory is based on the fact that the phase of the fringe output from an unbalanced interferometer is dependent upon both the OPD within the interferometer and the wavelength of the

light used. Therefore, if the OPD is scanned with a suitable sawtooth waveform to produce a single sine wave, then any changes of the phase of the sine wave relative to the sawtooth must be due to a change of λ_B.

The phase sensitive interferometric technique is very sensitive to dynamic strains: however, when used for long periods of time, problems can occur due to the drifting in the interferometer. A second problem can be caused by the use of a lock-in amplifier as part of the detection system in an interferometric scheme. The lock-in signal generates a reference signal based on the OPD ramping signal applied to the interferometer and a carrier signal is generated from the interferometer with the use of a bandpass filter. When the amplitude of the ramping signal is set to a level equivalent to the Bragg wavelength, accurate measurement can be obtained. However, the Bragg wavelength will change due to measurand variations and this can cause errors as large as 5% of the total measurement range in single-phase lock-in amplifiers [47].

The inclusion of a second wavelength to act as a reference can improve stability [28] and such a technique has been applied to temperature measurement to permit differential temperature measurement [27]. This was improved upon by S. L. Tsao *et al* [52] who used two gratings with different thermal coefficients to obtain a resolution of 0.01°C with a system immune to frequency drifting in the light

source.

A stabilized interferometric detection system using reference source has been reported [41] designed to make the detection system immune to environmental disturbances such as temperature fluctuations and mechanical vibrations.

2.4.3 Multiplexing techniques

If the wavelength demodulation system is the main factor in determining the strain resolution possible then the multiplexing scheme used can determine the other limiting factors of the final system, e.g. the spatial resolution possible and the number of gratings addressed.

As discussed in earlier Sections, the majority of approaches to multiplexing a number of sensors in series are either wavelength-domain or time-domain based.

Weis *et al* [58] demonstrated a four-element TDM system using gratings in the 1300nm range; this system used a Mach-Zender interferometer to perform the wavelength shift detection and achieved a resolution of $2n\varepsilon/\sqrt{Hz}$ for frequencies greater than 10Hz. The authors expressed the view that for quasi-static variation,

thermal variations would limit resolution.

WDM systems are now becoming available commercially. Micron optics, for example, produces a system capable of multiplexing a maximum of 31 gratings. The specifications state an expected accuracy of ±4με or ±0.5°C for strain and temperature respectively [40]. However, no method is given to differentiate between the two measurands.

A combination of the two approaches can potentially increase the number of sensors addressable in series. The network is arranged with several wavelength-stepped arrays of sensors in series. The arrays are identified in the time-domain and the individual sensors within the array in question are identified in the wavelength-domain. This technique increases the number of sensors usable by reusing spectrum of the light source used. However, it does have some problems (i.e. 'spectral overshadowing' and 'multiple-reflections' both of which are discussed in later Sections). This method has been demonstrated [5] using a 3×3 array of gratings, however only the last grating out of the nine was strained.

Several of the wavelength demodulation schemes discussed in the previous Section, have been successfully employed in a multiplex arrangement. The interferometric detection system in particular has been demonstrated in both

WDM and TDM arrangements. In the case of TDM addressing, a single pulsed source was used to illuminate eight Bragg gratings and wavelength demodulation was achieved with single interferometer [4]. For the WDM arrangement, wavelength filters have been used, to separate the returning signals from the array of grating sensors into individual output channels, after the interferometer. The signal on each output channel is of the interferometric type described above. The system was demonstrated with 4 gratings, spaced 7nm apart, and an interferometer OPD of 0.5cm [6].

Commercial OTDR systems are used for detected the position of faults in optic fibre cables, and typical example (produced by Ando Electric) uses 20ns pulses in 1550nm single-mode fibre. The spatial resolution is 5m.

2.4.4 Temperature / strain discrimination

Potentially the single biggest limitation of using in-fiber Bragg gratings in sensing applications is that they are sensitive to changes in both the strain and temperature conditions of the fiber. This dual behavior can create problem for sensor systems designed to monitor a single measurand, since any changes in the parameter not required (the non-measurand will produce anomalous readings.

For a practical strain sensing system, a second problem associated with changes in temperature is known as thermal-apparent strain. In structural monitoring situations (rather than free fibre applications) the fibre will be attached to a substrate that may have a co-efficient of thermal expansion, α_{sub}, much greater than that of the fiber, α_{fib}.

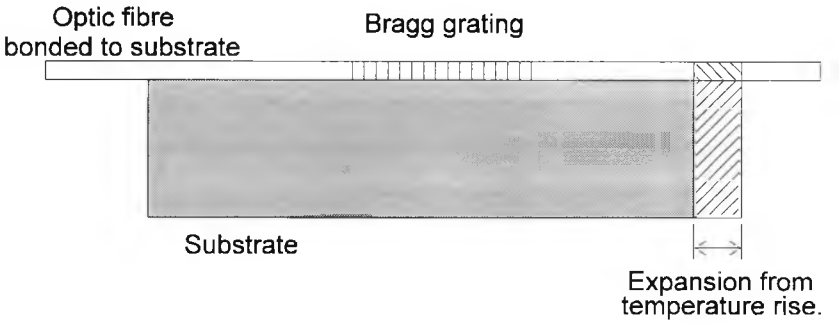

Figure 2_14: Illustration of the thermal strain effect.

A change in temperature, ΔT, will produce a corresponding thermal expansion of the substrate and the fibre will be strained by this expansion. Therefore:

$$\alpha_{fib}\Delta T + \varepsilon_{fib} = \alpha_{sub}\Delta T + \varepsilon_{sub} \qquad (2\_21)$$

where ε_{fib}, and ε_{sub} are the strain of the fiber and substrate respectively. It can be

seen that if the coefficient of expansion and the temperature of the substrate is known then the thermal-apparent strain can be subtracted from the measured value. However, this still presents the problem that both the strain and temperature needs to be measured.

Perhaps the easiest solution to this problem of cross-sensitivity is to use reference gratings in the same vicinity as the sensing array. These reference gratings would be in thermal contact with the substrate but would not respond to local changes in strain. This method is effective, but an ideal solution would use a single fibre to make strain and temperature readings and not require that sections of the fibre are isolated from the local strain effects.

A large number of techniques that attempt to solve this problem have been reported. These are discussed below:

Two Bragg gratings with different values of λ_B can be collocated without seriously degrading the performance of either sensor. As was shown earlier, the response of the gratings to changes in strain and temperature is wavelength dependent (due to the wavelength dependence of the photo-elastic effect and the thermo-optic effect). If the ratio of the responses of the two gratings to strain, $K_{\varepsilon 1}$, $K_{\varepsilon 2}$, are different from the ratio of responses to temperature, K_{T1}, K_{T2}, then the

following matrix equation can be solved.

$$\begin{pmatrix} \Delta\lambda_1 \\ \Delta\lambda_2 \end{pmatrix} = \begin{pmatrix} K_{\varepsilon 1} & K_{T1} \\ K_{\varepsilon 2} & K_{T2} \end{pmatrix} \begin{pmatrix} \varepsilon \\ T \end{pmatrix} \qquad (2\_22)$$

Where $\Delta\lambda_1$ and $\Delta\lambda_2$ are the changes in center wavelength of the sensing elements and caused by the change in either strain, ε, or temperature, T. The ratios of the two sets of coefficients are important because the determinant of the matrix must be non-zero for the equation to be solvable.

Collocating Bragg gratings has been shown to be effective for as many as 7 gratings [43]. Although some loss of quality in the earlier gratings is apparent due to the repeated exposure of the fibre to different intensity patterns of the UV light in order to create subsequent gratings, they are still usable as sensing elements, particularly in case where only two gratings are superimposed.

Xu *et al.* [61] demonstrated, using a pair of collocated gratings centered at 850nm and 1330nm, that the matrix strain coefficients were 6.5% higher and the temperature coefficients were 9.8% lower at 1300nm compared to 850nm. This gives the potential to use collocated gratings at these two wavelengths to simultaneously measure strain and temperature of the optic fiber with resolutions

estimated at ~±5°C and ~±10με. The main drawback of the system demonstrated is that it requires a separate light source and detector for each of the two gratings, these are placed at either end of the fiber. This arrangement would prove difficult to multiplex several of these sensing elements, although different arrangements may be possible.

Another method of using two Bragg gratings in order to discriminate between strain and temperature can be achieved by placing them either side of a splice between differing types of fiber. By splicing together two fibres of differing diameters (135μm and 165μm) [49] with a grating either side of the splice, a temperature-insensitive strain resolution of ~2.6με was demonstrated. This temperature insensitivity is because the two gratings respond in the same way to changes in temperature but, due to the difference in fibre diameters and hence different cross-sectional areas, have very different responses to strain. Hence, any change in the relative wavelength difference is due only to changes in strain. The system used an unbalanced Mach-Zender interferometer as a wavelength shift detection scheme. A similar system, but without the interferometric detection scheme, was reported by S. W. James *et al* [22]. Obviously, this method of splicing together a pair of differing fibers is less than ideal for a practical system where a large number of sensing elements would be required.

Several other systems using two sensing elements, but only one of which is a Bragg grating, have been reported. Systems using other types of fiber gratings in combination with Bragg gratings have been reported. Kanellopoulos *et al* [23] reported simultaneous strain and temperature measurement using a Bragg grating and a polarization-rocking filter in the 800nm range. The system uses the different responses to strain and temperature of the two sensors to operate. If λ_R is the resonance wavelength of the rocking filter then the following characteristics were obtained (for the case of λ_R=798.1nm and λ_B=837.3nm which were the values used),

$$\varepsilon = 1650\Delta\lambda_B + 59.5\Delta\lambda_R \qquad (2\_23)$$

$$\Delta T = -14\lambda_B - 5.41\Delta\lambda_R \qquad (2\_24)$$

The above coefficients are different enough so that the resulting matrix (of the form given in Equation 2_2) will have a non-zero determinant. Therefore, values of strain and temperature can be determined from the above equations and a resolution of $\pm 165\mu\varepsilon$ and $\pm 1.5°C$ was achieved.

Perhaps the most elegant solution to this problem of cross-sensitivity was reported by [37]. A set of three Bragg gratings in series, are arranged in a plane triangle to

form a rosette capable of measuring strain in any direction. If the temperature gradient across the rosette is negligible then all the gratings are at the same temperature. Therefore any temperature change will produce the same thermal-apparent strain in all directions and it can be shown that the temperature effects therefore cancel out. A resolution of ±5.5με for a strain of 1000με and 0.14K/pm for temperature was achieved.

Another type of fiber grating, the long-pitch (or long period) grating, has attracted considerable interest and is discussed in the next Section.

2.4.4.1 Long period (long-pitch) gratings (LPG)

Like Bragg gratings, long period or pitch gratings, LPG, are in-fibre multiple reflection structures that are produced by exposure to UV light causing a periodic change in refractive index. The difference, as the name suggests, is in the pitch of the periodic modulation. The LPG has a pitch that is longer than the coherence length of the light used (typically, grating periods of over 300μm are used and are 1-3cm in length). The LPG operates by coupling light out of the core and into the cladding at specific wavelengths, λ_i, given by the following equation

$$\lambda_i = \left[n_{01} - n_{clad}^{(i)}\right]\Lambda \qquad (2\_25)$$

Where n_{01} is the effective refractive index of the core mode, $n_{clad}^{(i)}$ is the effective index of the i^{th} axially-symmetric cladding mode and Λ is the period of the refractive index variation. The light coupled into the cladding quickly decays and is lost, and therefore the LPG acts, in transmission, as an optical band-reject filter [57].

The LPG is of interest, for sensing applications, due to the linear dependence on the value of Λ of the value of λ_I. In a similar manner to Bragg gratings, any change in strain or temperature can cause large changes in the center wavelength of the rejection band. Also, due to the fact that the power is coupled into cladding modes, the external refractive index and the ratio of the core and cladding refractive indices can also effect the gratings response to external changes.

As a result, different LPG can have very different properties. Reported temperature responses range from –0.20nm/°C up to 0.15nm/°C [7], and strain responses from –0.0007 to 0.0015nm/με. The responses are wavelength dependent, offering the potential to simultaneously evaluate the two measurands by a dual wavelength operation of a single sensor.

However, this single sensor approach will only work provided that the ratio of the responses to strain are different to the responses for temperature (to ensure non-zero determinant for the final matrix as mentioned above). Such systems have been reported [8] the wavelength used were 1248nm and 1634nm and the responses were: 0.00097nm/με, 0.074nm/°C and –0.0039nm/με and -0.03nm/°C respectively. It can be shown that given ideal conditions these values could offer resolutions of ±31με and ±1.5°C. Of course in a real application, noise would be present and the accuracy would be reduced, but the theoretical case illustrates the potential of such a system.

The use of a long-period grating combined with two Bragg gratings in the 1300nm-wavelength range, to form a hybrid dual parameter sensor system, has been demonstrated [63]. The response of the LPG to changes in temperature was shown to be seven times greater than that of the Bragg gratings whilst the response to strain was 50% less. In this arrangement the long pitch grating acts as a wavelength dependent filter, the reflected signals from the Bragg gratings pass through the LPG and thus their intensities are reduced according to the response of the LPG at that wavelength. If a change in strain or temperature is applied, the responses of all the gratings change. By monitoring the change in intensity of the two Bragg gratings, the values of temperature and strain can be calculated. This

system needs to be calibrated with known temperatures and strains over a specific range in order to gauge the response of the LPG/Bragg grating hybrid sensor. Once done, the resolution was reported as ±9με over the calibrated range of 290 to 1270με; and, ±1.5°C over the range 25–50°C.

The final possibility offered by LPG is the construction of a fiber grating that acts as a temperature-independent strain-sensor. This could be achieved by fabricating the grating in a fiber in which the core and cladding refractive indices have been modified to balance the temperature responses. This has yet to be achieved but boron-doping of the core of the fiber [48] has met with partial success with a temperature response of 0.005nm°/C.

2.5 Summary

This Chapter has presented in detail the fabrication and mode of operation of a Bragg grating. The refractive index modulations that form the grating structure can be generated via a holographic technique to give a wide range of behavioral parameters including the Bragg wavelength. In addition, the holographic technique lends itself well to effective mass production.

Simple strain-measurement arrangements using a Bragg grating have been discussed and the essential elements of a full system have been identified. In addition to the grating sensors themselves, these are: a suitable light source and detector, a system for demultiplexing the signals from a series of gratings and a scheme for detecting any changes in the Bragg wavelength of any one of these sensing elements.

Wavelength demodulation is the subject of the next Chapter, and a novel wavelength shift detection scheme using a Wollaston prism is presented. However, due a number of reasons, this scheme was unsuitable for inclusion in the final system, so a range of alternatives are analysed and the final choice, the Michelson interferometer, is presented.

Chapter 3:

Wavelength demodulation

3.1 Introduction to Wollaston prism investigation

Resolving the wavelength encoded back reflections from the Bragg gratings as part of a sensor system is a vital part of any practical device. In this Chapter, the possibility of using a Wollaston prism interferometer in a wavelength demodulation system is investigated. In the following two sections, the Wollaston prism is described and the basic system required for an interferometer based on its action is analysed. Section 3.2 describes a wavelength demodulation system based on a Wollaston prism capable of a wavelength resolution of the order of 0.1nm. This design was altered slightly and shown capable of displacement measurements and this is described in Section 3.3. However, it was decided that although meeting many of the

criteria needed for a successful system it was not an ideal choice due in part to the power considerations necessary, discussed herein, so alternative systems are discussed and the final choice of wavelength demodulation system is analysed in section 3.4.

3.1.1 The Wollaston prism

The Wollaston prism is named after the British chemist and physicist, William Wollaston (1766-1828) who, aside from making a personal fortune from malleable platinum and discovering the elements palladium and rhodium, also contributed to the field of optics by inventing a number of devices. A Wollaston prism itself is made from two wedges of birefringent materials, typically calcite ($CaCO_3$) or quartz (SiO_2), cut and glued together in such a manner that the optic axes of the wedges are perpendicular to each other

As an incident beam enters the first wedge of the prism, the light is split into two rays, an ordinary and an extraordinary ray. These rays travel at different speeds inside the birefringent material. Upon entering the second wedge, due to the perpendicular cut of the optic axes, the situation reverses, that is, the extraordinary ray becomes the ordinary ray and similarly for the second ray. This causes a divergence between the two beams and the beams split.

The net result of this action is that from a single input beam, two orthogonally polarized beams are outputted from the prism. This is shown in Figure 3_1 below.

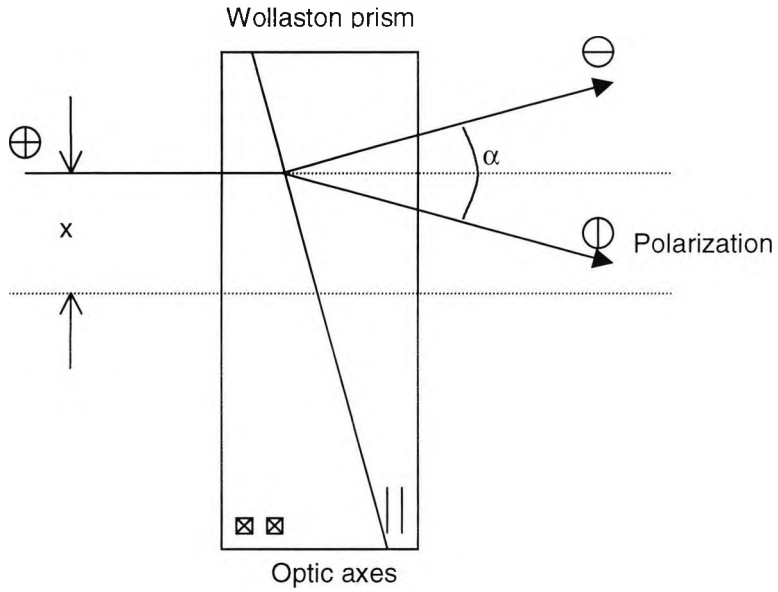

Figure 3_1: Action of a light beam passing through a Wollaston prism, where x is the transverse position of the incident ray and α is the angle between the two emerging rays.

From Figure 3_1, it can be seen that the optical distance a beam travels through the different wedges of birefringent material within the Wollaston prism is dependent on the transverse position of the incident ray across the face of the prism, x. Due to differing cut of the two wedges (with respect to the optic axes), an optical path difference is generated between the two

emergent rays which is proportional to x. This relationship takes the form shown in Equation 3_1 [36].

$$\Delta w = \alpha x \qquad (3\_1)$$

where Δw is the optical path difference between the two emerging rays and α is the angle between them. It can be seen from the above figure that the value of α is itself dependant on the value of the internal angle of the Wollaston prism, θ, and the refractive index of the material from which the prism is constructed. Therefore, Equation 3_1 can be written more accurately in these terms as shown in Equation 3_2 below:

$$\Delta w = 2x[n_e(\lambda) - n_o(\lambda)]\tan(\theta) \qquad (3\_2)$$

where λ is the wavelength of the incident light beam and $n_o(\lambda)$ and $n_e(\lambda)$ are the ordinary and extraordinary refractive indices respectively, which vary slightly for different values of λ. Typical values for n_e and n_o are shown below in Table 3_1:

Crystal	n_o	n_e
Calcite ($CaCO_3$)	1.658	1.486
Quartz (SiO_2)	1.544	1.553
Soduim Nitrate ($NaNO_3$)	1.587	1.336
Zinc Chloride ($ZnCl_2$)	1.687	1.713

Table 3_1: Refractive indices for a range of birefringent crystals at a wavelength of 589.3nm. From Serway (1986).

So, in summary, a Wollaston prism is essentially a polarizing beamsplitter because it passes both orthogonally polarized components. Input light is split into two beams of light with angle α between them and an OPD proportional to the position across the face of the prism.

3.1.2 Using the Wollaston prism in an interferometer

A Wollaston prism can be used as the basis for a polarization interferometer due to the optical path difference produced in the prism. The arrangement for such a system is shown in Figure 3_2 below:

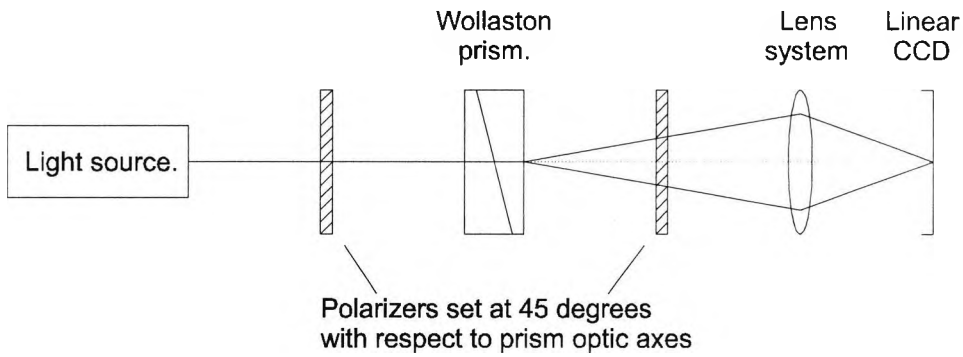

Figure 3_2: Typical arrangement for a Wollaston interferometer

Since the optical path difference produced in the Wollaston prism is dependent on the transverse position of the incident beam across the face of the prism, the fringes produced are spatial in nature and hence a charge coupled device (CCD) can be used to electronically scan the linear fringe pattern produced by the interferometer.

In the arrangement shown above, two polarizers set at 45 degrees (with respect to the Wollaston prism optical axes) are used. The first ensures that the light entering the Wollaston prism contains equal amplitudes of each of the polarization components. The second polarizer acts as an analyser, allowing only a fraction of the orthogonally polarized components through so that the beams at the CCD are polarized in the same direction and hence will interfere.

The other optical component that is often required that is not shown, is a

system for expanding the beam. It is desirable for a large portion of the prisms width to be illuminated at once to ensure that the CCD will scan a range of OPD simultaneously.

The fringe pattern produced has an envelope of the normal "bell shaped" (almost Gaussian) curve with a maximum fringe visibility at the centre of the Wollaston prism, becoming less away from the centre as the optical path difference increases. No fringes are visible away from the centre of the interference pattern where the optical path difference is greater than the coherence length of the light source used. It can be seen, from Equation 3_2, that the exact shape the fringe pattern forms is dependent on the wavelength of the light source used, and therefore any change in the wavelength will produce a corresponding change in the fringe pattern, albeit rather small. It is this small change that enables a Wollaston prism interferometer to decode wavelength-encoded signals.

In the experiments carried out this in research using this kind of experimental arrangement, the output from the CCD was read into a computer via a digital storage adapter, DSA, which converts the analogue signal from the CCD into an eight-bit digital signal. Once in the computer, signal processing (e.g. in the form of a Fourier transformation analysis to recover frequency data) can be used to calculate the frequency of the fringes.

This type of system has a number of advantages over other interferometers (e.g. a Michelson or a Mach-Zender) in that the lack of any mechanical movement greatly reduces the sensitivity to vibration noise. In the context of research of this thesis, its biggest disadvantage is that it is a bulk optic device and as such is not readily suitable for inclusion in a fiber-optic based system. However, for the application as a method detecting changes in wavelength of fiber optic based sensors, this would not present a great problem since the fiber would only provide the input light source and would not be integral to the detection system.

As the above analysis demonstrates, the Wollaston prism interferometer can be used as a simple spectrometer. The input source is made to interfere with itself generating an interference pattern in the usual way. The frequency of the fringes produced will depend on the characteristic parameter of the Wollaston and the wavelength of the light used. Hence if the wavelength of the light were to change then the frequency of the fringes would change. The resolution reported for such a device is about ~3.92nm over a range of 500nm (Manufacture's data, 1995). This level of accuracy is not sufficient for the application in mind using the Bragg grating system. However, the addition of a second wavelength greatly improves the quality of the system by producing a combined interference pattern that responds to changes in wavelength of the signal source with much greater sensitivity. This is discussed in more detail in Section 3.2.

3.2 Wavelength change determination using a Wollaston prism interferometer

Reflected light from a Bragg grating contains measurand information that is wavelength encoded, requiring an effective system for detecting any change in wavelength. In this Section, an examination of the suitability and sensitivity of a Wollaston prism interferometer for this purpose is presented.

Due to reasons that will be highlighted later in this chapter, the Wollaston prism configuration was not used in the final system. Section 3.4 will discuss the system that was used and why it was better suited to the application in question.

3.2.1 Introduction

Fourier-transform spectrometers with an electronic scanning system via a linear CCD have been previously reported. The lack of any moving parts enables the device to be vibration insensitive and compact configurations are possible since no mechanical scanning is necessary. However, in many of these systems, the width and number of the pixels in the CCD fix the resolution. Consequently, small changes in the signal wavelength cannot be detected.

The inclusion of a second light source of a known wavelength to act as a reference enables a far higher accuracy to be achieved. In this scheme, the signal and reference light sources are analysed with a Wollaston interferometer, the output of which becomes the superposition of the two sets of interference patterns produced by the two different wavelengths.

The two superimposed interference patterns form a *beat pattern* that is characterised by a modulated wavelength, λ_m, and a combined wavelength, λ_a. The modulated wavelength is defined as the period of the envelope of the beat pattern and the combined wavelength is defined as the period of the fringes within the beat pattern and is equal to the average fringe width of the two fringe patterns.

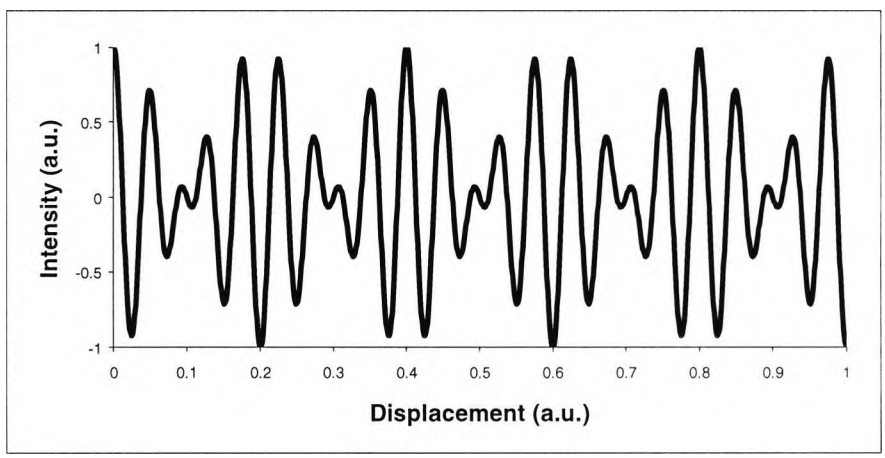

Figure 3_3: An example *beat pattern*. The fringe width (λ_a) is 0.05 and the modulation (λ_m) is 0.4.

Any change in the wavelength of signal source will produce a relatively large change in the modulated wavelength. Hence, with the use of suitable filtering

techniques, much smaller changes can be detected than would otherwise be possible.

3.2.2 Theoretical background

The experimental arrangement used in this work is shown schematically below in Figure 3_4, and consists of a Wollaston prism interferometer used in a dual-source configuration. The first source acts as a reference and operates at a known wavelength, λ_1, while the second source is the signal from which any changes in wavelength, λ_2, are to be detected.

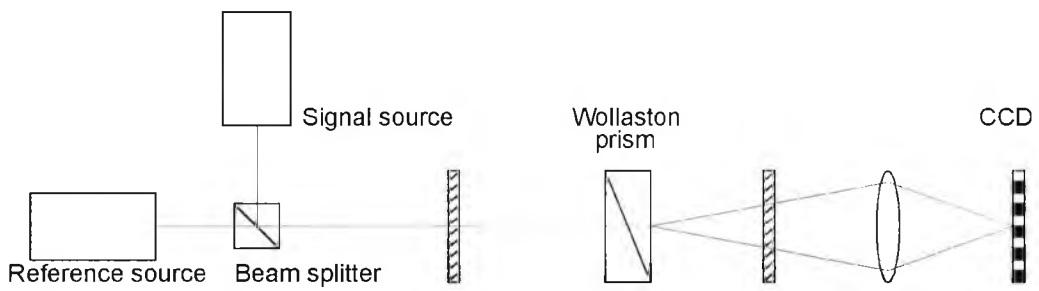

Figure 3_4: Arrangement for dual source wavelength-decoding using Wollaston prism interferometer.

Both beams are linearly polarized at a direction of 45° with respect to the Wollaston prism optic axis and they are each then divided, by this prism, into two separate beams with orthogonal polarizations. These components are then recombined to form an interference pattern, which is then imaged onto a CCD

via suitable lenses, and a polarizer again set at 45° with respect to the optic axis of the prism. The second polarizer is used to ensure that the two components have the same polarization to optimise fringe visibility.

The fringe pattern produced on the CCD by this arrangement is a combination of the fringe patterns produced by each individual light source. The effective optical path difference between the two components of each wavelength, $\Delta w_1(x)$ and $\Delta w_2(x)$ respectively are

$$\Delta w_1(x) = 2x\left[n_e(\lambda_1) - n_o(\lambda_1)\right]\tan(\theta)$$

$$\Delta w_2(x) = 2x\left[n_e(\lambda_2) - n_o(\lambda_2)\right]\tan(\theta) \qquad (3\_3)$$

where x is the transverse distance from the centre of the prism across, $n_e(\lambda)$ and $n_o(\lambda)$ are the ordinary and extraordinary refractive indices of the prism at wavelength λ and θ is the internal angle of the prism used.

Therefore, the intensity formed at the CCD is given by Equation 3_4 below:

$$I(x)=\frac{1}{2}\left\{\begin{array}{l} I_{01}(x)\left[2+\exp\left(-\left(\frac{4(n_e(\lambda_1)-n_o(\lambda_1))\tan(\theta)\Delta w_1(x)}{L_{c1}}\right)^2\right)\cos\left(\frac{2\pi\Delta w_1(x)}{\lambda_1}\right)\right]+ \\ I_{02}(x)\left[2+\exp\left(-\left(\frac{4(n_e(\lambda_2)-n_o(\lambda_2))\tan(\theta)\Delta w_2(x)}{L_{c2}}\right)^2\right)\cos\left(\frac{2\pi\Delta w_2(x)}{\lambda_2}\right)\right] \end{array}\right\}$$

(3_4)

where I_{01} and I_{02} are the spatial intensity distributions produced by the signal beam and reference beam. If it is assumed that these are the same, i.e.

$$I_O(x)=I_{01}(x)=I_{02}(x) \qquad (3\_5)$$

and the coherence lengths are approximately the same, i.e.

$$L_C=L_{C1}=L_{C2} \qquad (3\_6)$$

then Equation (3_4) becomes

$$I(x)=\frac{1}{2}I_o(x)\left\{4+\exp\left[-\left(\frac{8x(n_e(\lambda_1)-n_o(\lambda_1))^2\tan^2(\theta)}{L_c}\right)^2\right]\right\}\cos\left(\frac{4\pi x}{\lambda_m}\right)\cos\left(\frac{4\pi x}{\lambda_a}\right)$$

(3_7)

Where λ_m is the modulated wavelength and λ_a is the combined wavelength

and are given by:

$$\lambda_m = \frac{\lambda_1\lambda_2}{\{[n_e(\lambda_1) - n_o(\lambda_1)\lambda_2] - [n_e(\lambda_2) - n_o(\lambda_2)\lambda_1]\}\tan(\theta)} \qquad (3\_8)$$

$$\lambda_n = \frac{\lambda_1\lambda_2}{\{[n_e(\lambda_1) - n_o(\lambda_1)\lambda_2] + [n_e(\lambda_2) - n_o(\lambda_2)\lambda_1]\}\tan(\theta)} \qquad (3\_9)$$

From the above Equations, it can be seen that any changes in the wavelength of either of the two sources will produce a large change (relative to the wavelength of either source) in the pattern produced by the system. An example of the magnitude of the change tat can be achieved is shown in Figure 3_5. With one source acting as a reference, the wavelength of which was assumed not too change throughout the course of experiments, any change in the pattern will therefore be due to the signal source. So, in operation, by measuring the modulated wavelength of the final pattern any changes in the signal wavelength can be detected.

The accuracy and range of any changes in the wavelength of the signal source which can be measured depends on a number of factors, but the main conditions are the resolution of the CCD and the difference between the wavelengths of the two sources.

3.2.2.1 Computer-based simulation

A computer-based simulation of the system used in the experiments outlined below was written to validate the results obtained experimentally. The simulation was based on the equations given in the theoretical discussion above.

The variation of the modulated wavelength as a function of the signal wavelength change can be obtained from the computer simulation using reference and signal wavelength of 671 and 785nm respectively. The result is shown in the graph below.

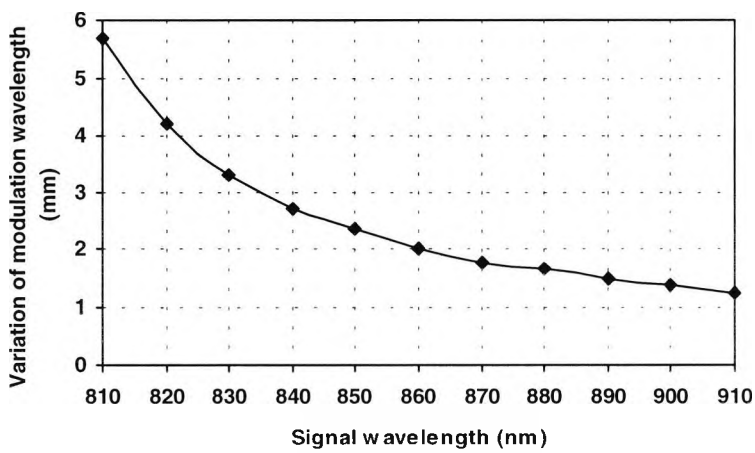

Figure 3_5: Variation of the modulated wavelength of the combined interference pattern as a function of signal wavelength change.

These results, shown in Figure 3_5, indicate that the average variation of the modulated wavelength is about 10^4 times larger than that of the signal wavelength. Hence, by measuring the change of modulated wavelength a very small corresponding change in the signal wavelength can be determined. For example, a total change of 2μm in λ_M represents a signal wavelength variation of 0.01nm (for wavelength around 825nm) or 0.1nm around 870nm. Obviously, the measurable range of the system is limited due to the size of CCD, whilst the resolution is limited by the size of the individual CCD elements.

3.2.3 Experimental method

For the experiment a Wollaston prism with an internal angle of 0.5 degrees was used (which has a width of ~1cm). The CCD (manufactured by Hamamatsu) had 1024 pixels with a centre-to-centre spacing of 24μm. The reference and signal sources of light were generated using LED at 785nm and 810nm (L_C= 50μm and 135μm respectively).

The wavelength of the signal LED was altered by varying the driving current, over a short range this provides a linear variation of wavelength. The wavelength of the reference source was assumed to remain constant over the

period of time the experiments were carried out.

The output from the CCD was read into a computer via a digital storage adapter. The resulting data consisted of a large amount of noise produced by the pulse nature of the CCD. This noise was removed by using a fast Fourier transform algorithm to transpose the signal into the frequency domain. The high and low frequency noise can then be removed by windowing on the frequencies of interest (a Hanning window was used).

Figure 3_6, below shows a resulting interferogram obtained experimentally after the noise has been removed in this manner. The fringes are at the combined wavelength and the modulated wavelength is clearly visible as the longer envelope pattern. The combined wavelength (and hence the fringes) can be removed in the same manner that the CCD pulse noise was removed above, this leaves the pattern shown in Figure 3_7.

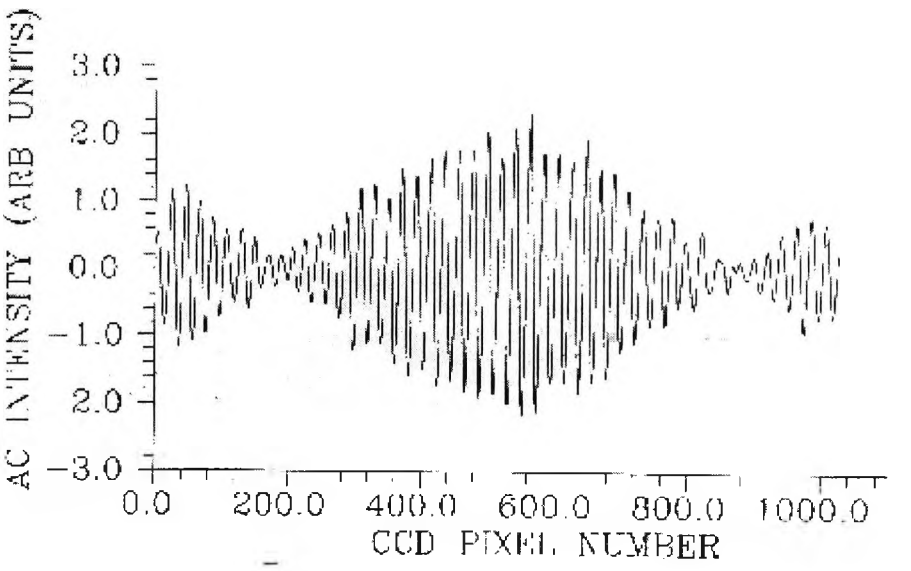

Figure 3_6: Example of an experimentally obtained interferogram.

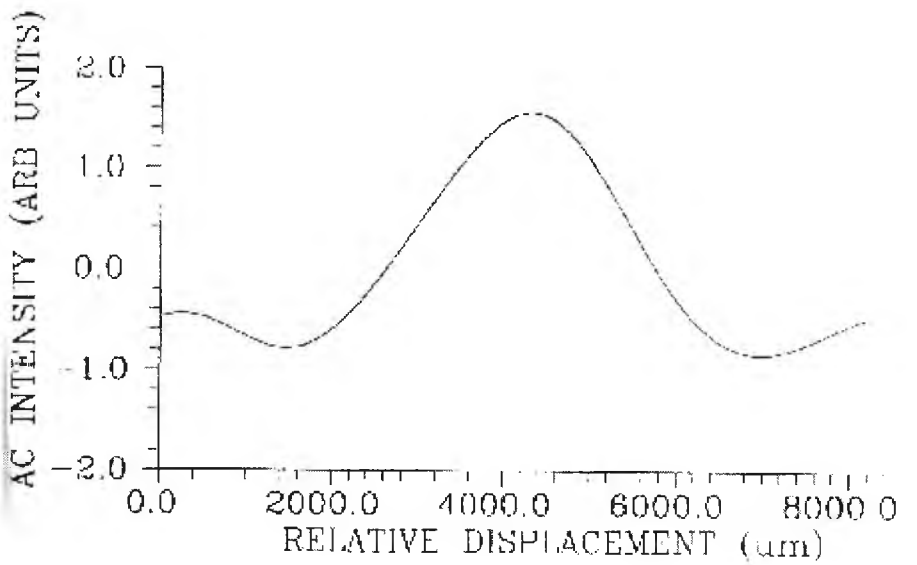

Figure 3_7: Interferogram after signal processing to obtain modulation wavelength for signal shown in Figure 3_7.

Once the interferogram shown in the above graph has been obtained, the modulation wavelength is calculated by determining the average distance between successive peaks (or troughs) of this curve.

3.3.4 Results and discussion

The results from both theory (solid line) and experiment (points) are shown below in Figure 3_8 as a graph of variation of signal wavelength as function of modulated wavelength. Due to the limitation of the tuneable wavelength range of the LED used in this work, the results obtained from the experiment could only be compared with theory over a range of 1.5nm where a resolution of 0.01nm was obtained.

In essence, recording interference fringes generated by the reference and signal wavelength sequentially and then combining the two in the computer using software could derive the modulated wavelength. The proposed scheme has a number of advantages, such as self-calibration for each measurement. Further, the measurement of the fringes produced, is essentially an intensity-based operation and therefore any changes in the detected intensity over time will not effect the accuracy of the measurements.

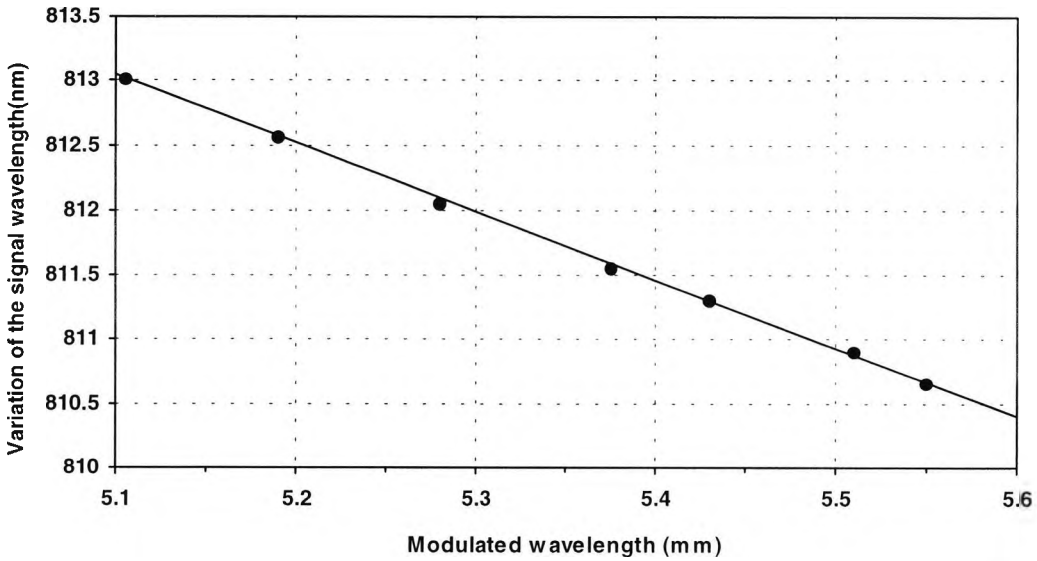

Figure 3_8: Graph of modulated wavelength against signal wavelength variation for theoretical (solid line) and experimental results (points)

3.3 Displacement measurement interferometer

Displacement measurement is a related area to strain measurement, and it is ideally suited to implementation using optical sensing techniques. An efficient system would have a similar range of possible areas of applications.

The Wollaston prism interferometer is combined with a Michelson interferometer, in a dual interferometer arrangement, to measure the displacement of one of the mirrors of the Michelson. The system operates without the use of any polarizers external to the Wollaston interferometers.

As mentioned in the previous section, polarization interferometers (such as the Wollaston interferometer) operate by splitting incident light by polarization and introducing an optical path difference (OPD) between the two orthogonal components of the input beam, which are then recombined to produce fringes after passing through an analyser (a polarizing element set at 45 degrees). The spatial nature of the output from these systems means that a charge-coupled-device (CCD) array can be used to scan the interference pattern generated, electronically, thereby reducing the susceptibility of the system to noise from moving parts which may vibrate in the more familiar mechanical scanning system, often used.

Dual interferometers operate by using two connected interferometers, the first

being employed as a sensor to detect the changes in the measurand and the second to monitor the changes in the optical output from the first. Such a system has a number of advantages over single interferometer devices including increased range as well as enabling remote sensing via an optical fibre link. Systems similar to dual interferometers using a Wollaston prism have been previously discussed [54][55]. These systems have sensing interferometers that introduce an optical path difference between the orthogonal components of the beam before it passes into the Wollaston prism, causing the pattern produced to shift relative to the centre fringe packet.

The system described herein utilises a dual interferometer arrangement consisting of a conventional Michelson as the sensing interferometer, i.e. that directly experiences the influence of the measurand, and a Wollaston prism as a receiving interferometer. Although the Michelson splits light by amplitude and not polarization, output fringes on the Wollaston prism (which are imaged onto a CCD) can be produced without the use of correcting polarizers either within the Michelson itself or between it and the Wollaston prism. Such fringes are shown to consist of two fringe packets, a centre stationary packet produced by the Wollaston prism, which is independent of any variation in the Michelson, and a second, which because it is produced by the Wollaston and Michelson acting in concert, shifts across the CCD in sympathy with any variation of optical path difference in the Michelson.

3.3.1 Principle of method

The experimental arrangement used in this work is shown in Figure 3_9. It comprises a standard Michelson interferometer coupled to a Wollaston polarisation interferometer via an open-air path.

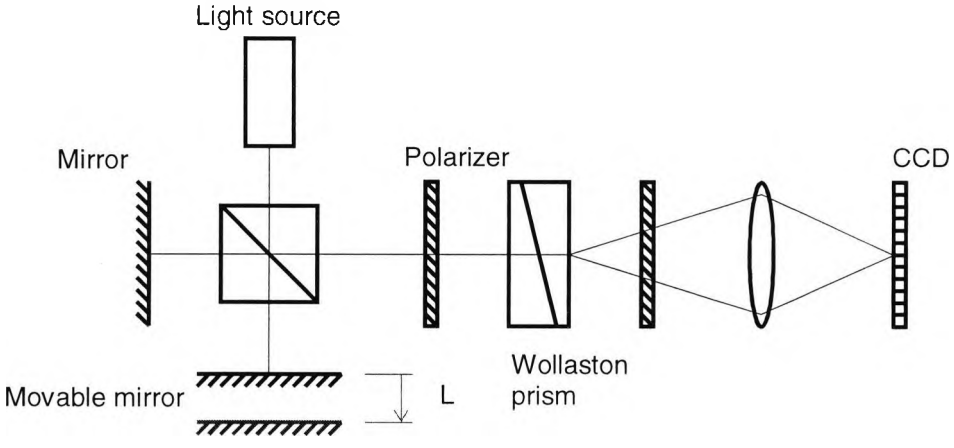

Figure 3_9: Experimental arrangement for displacement measurement system.

If good alignment and flat normal mirrors are assumed, then the output from the Michelson can be thought, in simple terms, as having resulted from two coherent, parallel, plane sources separated by a distance, L. The optical path difference (Δm) between these two beams is therefore 2L. If one of the mirrors is attached to a surface whose displacement is to be measured, the changes in Δm can then be related directly to that displacement.

As mentioned above a Wollaston prism interferometer operates by splitting an

incident light beam by polarisation producing two orthogonally polarised output beams. These beams have an OPD between them dependant on the transverse distance from the centre of the Wollaston prism of the incident beam. Therefore using an analysing polariser and recombining the two outputs, an interference pattern can be produced. If used as a single interferometer the output is the familiar bell shaped curve, the centre of which (i.e. the maximum of the interference pattern) will correspond to the centre of the Wollaston prism.

With the Michelson preceding however, the Wollaston interferometer can be thought of as having two collinear, coherent inputs, out of corresponding to an OPD, Δm. Since the Michelson splits the input source by amplitude and not polarisation, both output beams will contain equal parts of each polarisation.

Both input beams therefore are split into two orthogonally polarised output beams by the Wollaston prism and an OPD (Δw) is introduced between them. Therefore the output from the Wollaston prism consists of four beams one ordinary ray and one extraordinary ray for each of the input beams. They will be out of phase, with respect to each other, by Δm and Δw respectively. This is shown schematically in Figure 3_10.

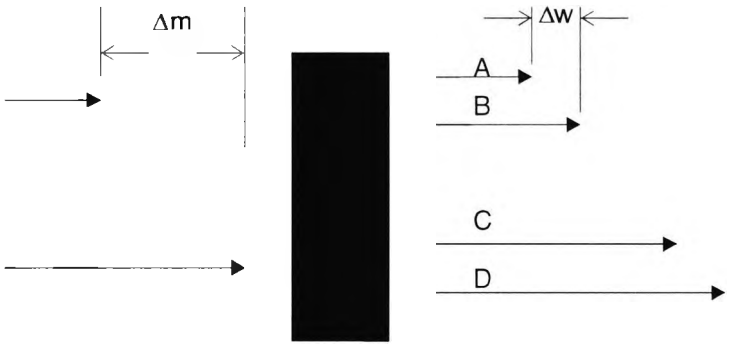

Figure 3_10: Schematic of Wollaston output beams, colinear beams separated for clarity.

The OPD from the Michelson, Δm, will be constant across the Wollaston prism, and will only vary if the Michelson imbalance changes, whereas Δw will vary only across the width of the Wollaston prism itself. The combination of these two OPDs causes the final interference pattern.

The two extraordinary beams (shown in the figure as A and C) are from differing arms of Michelson and therefore will only interfere and produce fringes if the value of Δm is less than the coherence length of the source used (L_C). The same situation is true for the two ordinary beams (B and D). If Δm is less than L_C, then the resultant interference pattern from all the beams will be almost impossible to detect due to the Michelson fringes which will occur right across the CCD. It is therefore important that the system is used beyond this point, hence a low-coherence length light source is used.

The beams A and B are from the same arm of the Michelson and will interfere and produce fringes if the value Δw is less than L_c. The OPD produced by the Wollaston prism, Δw, between the extraordinary and the ordinary beams, across the Wollaston prism is given by equation 3_1 above.

Thus the fringes caused by A and B will occur in the centre region of the output of the Wollaston prism. The same analysis holds true for beams C and D.

The beams B and C, shown in Figure 3_10, are from differing Michelson arms but are also separated by the Wollaston (i.e. one is an ordinary beam the other is an extraordinary beam). Consequently these beams may interfere depending on the values of Δw and Δm. If a position across the Wollaston exists such that $\Delta w = \Delta m$, then fringes will occur at that position. This is the basic premise under which the system operates. The beams A and D will have an OPD greater than Δm and therefore will not produce interference fringes.

So, in the case where $\Delta m > L_c$ and Δm does not equal 0, the interference pattern on the Wollaston prism (which is imaged onto a CCD) consists of a central fringe packet and a secondary fringe packet displaced away from the central packet. The central fringe packet itself is produced at the centre of the

Wollaston prism, with a width proportional to L_c, and will not move.

The displacement of the secondary fringe packet from the central fringe packet depends solely on Δm. Therefore the distance between the two fringe packets is directly related to the mirror displacement. In addition, since the central fringe packet will occur in the same place every time, the need for calibration before each reading is reduced. Of course, if the imaging optics has changed then some calibration will be needed.

Obtaining the optimum resolution achievable with the two packets gives an estimate of the smallest theoretical displacement detectable. Since the width of the fringe packets is dependent on the coherence length of the source used, it may be expected that smaller values of L_c will lead to smaller detectable displacements.

Assuming that the minimum separation between the two fringe packets that can be detected occurs when the full width half maximum (FWHM) points just overlap, thus when the separation between the two peaks is given by L_c. This occurs when $\Delta w = \Delta m$, and $\Delta m = 2L$. Thus under these conditions, the minimum detectable displacement from the balance position is approximately $L_c/2$. Of course, a much smaller relative displacement could be detected, in which case the centre fringe of the side fringe packet could be tracked and a

displacement of a half a fringe width would be detectable.

The maximum absolute displacement that can be measured depends on the physical size of the CCD and on the degree of magnification (M) used. Taking this magnification factor into account, the distance between neighbouring maxima in the fringe pattern, x_f, on the CCD is given by:

$$x_f = \left(\frac{\lambda}{\alpha}\right) M \qquad (3\_10)$$

For light of wavelength, λ. Therefore the number of fringes visible on the CCD, n, is given by:

$$n = \frac{CCD_{width}}{x_f} \qquad (3\_11)$$

Where CCDwidth is the physical with of the CCD used. The relationship between n and the OPD is given by:

$$n = \frac{OPD}{\lambda} \qquad (3\_12)$$

where at the peak of the second fringe packet the OPD = Δm and in turn, Δm = 2L. Thus

$$L = \frac{\alpha\, CCD_{width}}{2M} \qquad (3\_13)$$

This theoretical limit for the value of L is very difficult to achieve in practice, since to do so assumes that the centre fringe for both fringe packets would be at the extreme ends of the CCD to utilize its full length. However, in doing so this would make identification as the centre fringe, in the presence of any noise, difficult, since only half the fringe packet would be visible. A trade off between fringe visibility and measurement range is evident since smaller imaging magnifications or larger of values of α both would increase the range but also reduce the final size of the fringes produced.

3.3.2 Computer Simulation of system

A simple computer model was devised in order to develop an understanding of the system performance and to compare its output with the experimental results. This involved simulating the fringe pattern resulting from the Wollaston prism where the intensity distribution output from an interferometer of this type is given by:

$$I_o = I_I \exp\left[-\left(\frac{2\Delta}{L_c}\right)^2\right]\cos\left(\frac{2\pi\Delta}{\lambda}\right) \qquad (3\_14)$$

where I_O is resultant intensity, I_I is the input light intensity and Δ is the OPD between the interferometer output beams. If Int_{AB} is the intensity distribution for the output beams A and B then the output from the whole system may be given by:

$$I_{Tot} = Int_{AB} + Int_{AC} + Int_{AD} + Int_{BC} + Int_{BD} + Int_{CD} \qquad (3\_15)$$

where I_{tot} is the total intensity distribution.

This basic equation can be used to give a reliable model of the output from the Wollaston system. Better results can be obtained by computing α (used to calculate, Δ, in Equation 3_14 from the internal angle of the Wollaston prism used, since this cannot vary with wavelength which α does. This is done using the following relationship:

$$\alpha = 2.(n_e - n_o).\tan(\theta) \qquad (3\_16)$$

In the experimental work detailed below, the Wollaston prism used was such

that α=0.5° when λ= 600nm. This value was also used in the computer simulation.

An example output of the kind of fringe pattern produced by the experimental arrangement used is shown in Figure 3_11 as a graph of deviation from the centre of the Wollaston prism against intensity. The graph was produced using a computer simulation based on the analysis described above. The different fringe packets are clearly visible on the figure which shows a full fringe envelope pattern with Δm=100μm, α=0.5° and λ= 825nm.

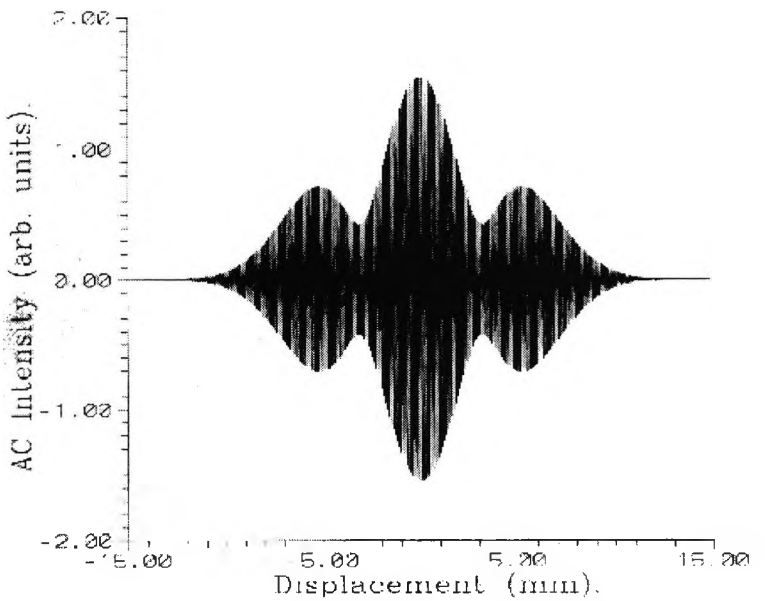

Figure 3_11: Typical output from computer simulation of Wollaston prism diplacement measurement system.

3.3.3 Experimental Results

An experiment was performed to compare the results of the above simulation using the arrangement shown in Figure 3_9. The source used for the experiment was a superluminescent diode with λ=825nm and L_C=30μm. The Wollaston prism employed was manufactured from quartz with α=0.5° at λ= 600nm.. The output fringe pattern was recorded using a CCD with 1024 pixels with a centre-to-centre spacing of 24μm, connected directly to a PC via an analogue-to-digital conversion card.

The magnification used in the imaging system can be calculated simply by comparing the final fringe width (13 CCD pixels were visible per fringe) and the actual fringe width (calculated using Equation 3_10 with M=1). The final displacement from the central fringe of the secondary fringe packet was measured on the CCD and scaled down to account for this magnification.

The results from an experiment are shown in a graph of the Michelson offset (the amount by which the monitored mirror is displaced from the balance position) against fringe displacement (the measured distance between the centre fringes of the centre and side fringe packets) in Figure 3_12. The experimental data points are shown on the graph along with a straight line representing the theoretical result from the computer simulation.

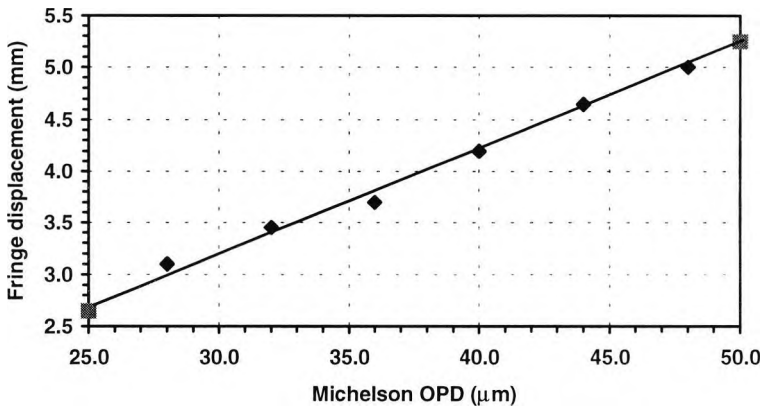

Figure 3_12: Graph of experimental results (points)

and computer simulation(solid line).

It can be seen that the experimental result shows a good linear relationship between the Michelson offset and the fringe displacement and that the data agrees with the simulation. It may be seen that the graph show the clear relationship between the OPD produced in the Michelson interferometer and the fringe displacement.

The accuracy of the experimental result obtained, was limited to due to the accuracy of the movement of the Michelson interferometer (or rather, the movement of the displaced mirror with the interferometer), which was monitored with a calibrated mechanical micrometer. Also, the light source used had a spectral bandwidth of 23nm (FWHM) and this range of input wavelengths will have affected the results obtained to some degree, since α is dependent on wavelength, and a monochromatic light source was assumed in

the simulation.

3.3.4 Discussion of displacement measurement system

The system has no moving parts other than the displacement of the mirror itself and being a dual interferometer, remote sensing via an optic fibre link would be feasible. It would be possible to manufacture a remote sensing head as a genuinely small device since only the elements making up the Michelson interferometer would be required within it. A Michelson interferometer consists of a beam splitter and two mirrors (one of which could be physically attached to the beam splitter). The final dimensions would, of course, depend on the application but a sensing head less than 2cm square would be feasible.

All fibre Michelson interferometers, where the two arms are made entirely of optic fibre would also be usable. This would require a different method of generating a measurand dependant OPD compared to the open air version shown above, and the most probable solution would be to stretch the optic fibre in one arm of the interferometer.

The results obtained from the arrangement shown represent absolute measurements, and the distance between the central and side fringe packets is directly proportional to the optical path difference imbalance in the two arms

of the Michelson. Possible areas of measurement application are varied since any desired effect that could produce an optical path imbalance could be measured.

An obvious extension of this work is to apply some of the previously reported techniques of dual wavelength interferometry using dual sources such as that described in the wavelength demodulation system in Section 3.2. With the inclusion of a second light source at a slightly different wavelength, the final interference pattern would be the addition of the output from the two sources, and would display a fringe beating effect. This would improve the system stability (because any small change in the wavelength of either of the light sources would change the fringe-beating pattern and therefore could be detected and accounted for) and make the identifying of the centre fringe much easier.

3.4 WDM system used in experimental arrangement

A variety of physical measurands may be transposed to a phase modulation of a light wave by the use of a suitable interferometer. This type of system produces a fringe pattern that either will be temporal (e.g. from a Michelson) or spatially based (e.g. from a Wollaston). In either case, fractional changes in the phase of a single fringe can be detected, corresponding to a high-resolution detection of the measurand itself.

Accurate detection of any changes of Bragg wavelength in the signals reflected back from the gratings in this type of system is obviously crucial to its success and in this section the scheme chosen and developed is examined. In Section 3.4.1 the main reasons for not choosing a scheme based on the previously presented Wollaston prism interferometer are given. Section 3.4.2 examines some of the other possible systems that could have been chosen and in Section 3.4.3 the final choice, the Michelson interferometer, is considered and analyzed.

3.4.1 Practical difficulties in implementing Wollaston prism interferometric system

As presented in Section 3.2, the Wollaston prism interferometer combined with a suitable reference source can be used to detect changes in wavelength

with an impressive level of sensitivity. A resolution of 0.01nm in wavelength terms equates to a strain resolution of ~8μstrain in an extended Bragg grating which would be sufficient for measurements for a number of civil engineering applications. However, the Wollaston approach does suffer from a number of problems that make it unsuitable for the applications considered.

The first, and most important consideration, is the difficulty in using a CCD detector in conjunction with this type of system where high-speed operation is important. Linear detection devices like CCD suffer from a time delay as the accumulated charge on each detection cell is read out in a serial fashion, as shown schematically in Figure 3_13

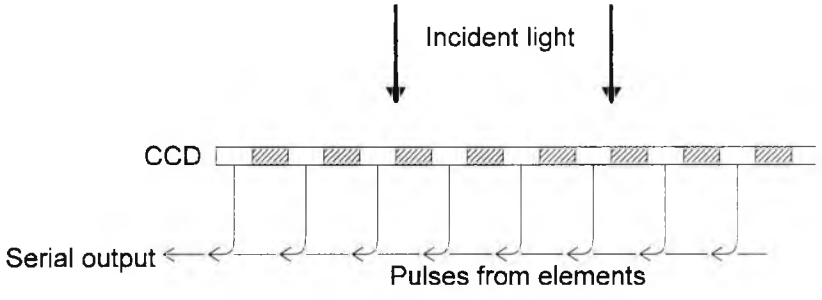

Figure 3_13: Schematic of CCD output sequence

In a time based demultiplexing system, the time taken for the signal processing scheme to process the detected signal from a single grating governs the distance by which two gratings can be separated, since at no time can the returned signals overlap. Therefore, any delays in the signal detection would

mean that the resolution of the grating spacing in the sensor system is reduced.

There are two delays incurred in the use of a CCD, the data read-out time and the integration time. The first is the time taken to read out the signal once it has been detected. In the CCD used in the Wollaston experiments presented previously, the maximum clock frequency usable was 3MHz and 6 clock periods were required to read the signal from a single detection element. Therefore, the complete range of 1024 elements would take over 340μs, far too long to be produced simply by the optical distance (at maximum a few tens of meters for an effective sensor system) in the fibre between two gratings.

The above time gap ignores the second time gap which is produced by the need of the CCD for an integration time period. This presents the second difficulty with implementing the Wollaston prism interferometer, namely the power available from the source. The CCD operates by charge accumulation, where the output signal obtained is proportional to the amount of light exposure (light intensity × accumulation time), and therefore it is important to use a bright source if a fast integration time is desired. With the sources available, and the desire to use ultimately a compact (but comparatively low power) ELED this was seen as a presenting a further obstacle to an effective system.

Moreover, the optical signals received back from the gratings will be weak

and unpolarized. If a Wollaston interferometer arrangement were to be used effectively, then the pulses would pass through two polarizing elements set at 45° with respect to the optical axes of the prism that would reduce the power in the signal further. Based on the above, it is for these reasons that the Wollaston prism was not chosen as the wavelength demodulation scheme in the final system.

3.4.2 Analysis of other possible choices for a wavelength demodulation scheme

There are a number of possible alternative schemes that can be employed to decode the wavelength-encoded signals. One of the most popular solutions is a wavelength filter based on a Fabry-Perot interferometer [29]. The basic arrangement for a Fabry-Perot is shown below in Figure 3_14.

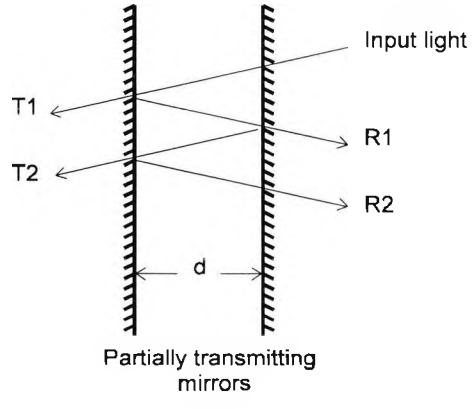

Figure 3_14: Schematic of a Fabry-Perot interferometer.

A Fabry-Perot interferometer usually consists of two plane, mirrored surfaces,

one of which is only partially reflecting to allow light transmission. These two mirrors form an optical cavity and multiple reflections inside this cavity produce an interference pattern dependent on both the mirror separation, d, and the wavelength of the light source, λ. The characteristic equation governing the intensity of the output, I_o, from the Fabry-Perot interferometer is well known and given by [36]:

$$I_o = \frac{a^2 T^2}{(1-R)^2} \frac{1}{1+\left(4R/(1-R)^2\right)\sin(\delta/2)} \qquad (3\_17)$$

where

$$\delta = \frac{2\pi}{\lambda}\left(2d\cos(\theta)\right) \qquad (3\_18)$$

where a is the input light intensity, R and T are the reflection and transmission coefficients of the mirrors, θ is the incident angle of the light and δ is the phase difference between two successive output beams.

For the case under consideration, it is assumed that the angle θ will be 0° and that the light input will be due to the reflections from the Bragg grating. The output from the detector for a particular value of d is the sum of the output intensities for all values of λ, i.e.

$$S = \int I_o(\delta, R)d\lambda \qquad (3\_19)$$

Where S is the signal at the photodetector, and I_o is intensity output from the Fabry-Perot given by Equation 3_17 above.

The system output is, therefore, a convolution of the finesse of the micro-filter spectral response and the Bragg grating bandwidth. This presents severe conflicts in system design since a higher finesse will change not only the resolution attainable, but also the total spectral response available.

To estimate the accuracy to which the Bragg wavelength can be determined using a Fabry-Perot etalon, in the presence of the inevitable noise, a computer simulation using the above equations was written. The technique employed is shown below in Figures 3_15 and 3_16, where in both Figures, the solid line is the signal produced by the system in the absence of noise while the dotted lines are the upper and lower values that could be detected allowing for the presence of noise.

It can be seen that the peak of the curve (and hence the root of the differentiated curve), could lie between X1 and X2. When differentiated, this will result in an error range in the location of the root, as shown schematically

in Figure 3_16.

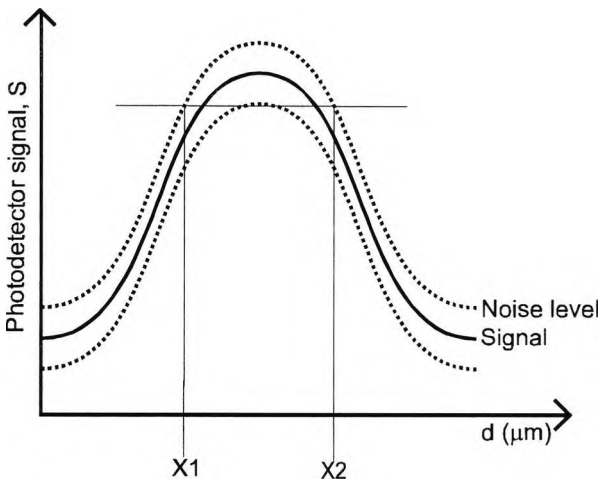

Figure 3_15: Graph of S against d, illustrating that the noise limits the accuracy to (X1-X2)

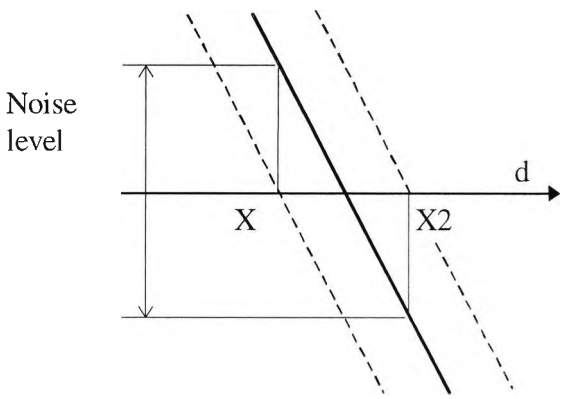

Figure 3_16: Close up of differential curve at root

From this error range, an associated signal to noise ratio, SNR, in the output can be calculated by knowing the gradient at the root and the values of X1 and

X2.

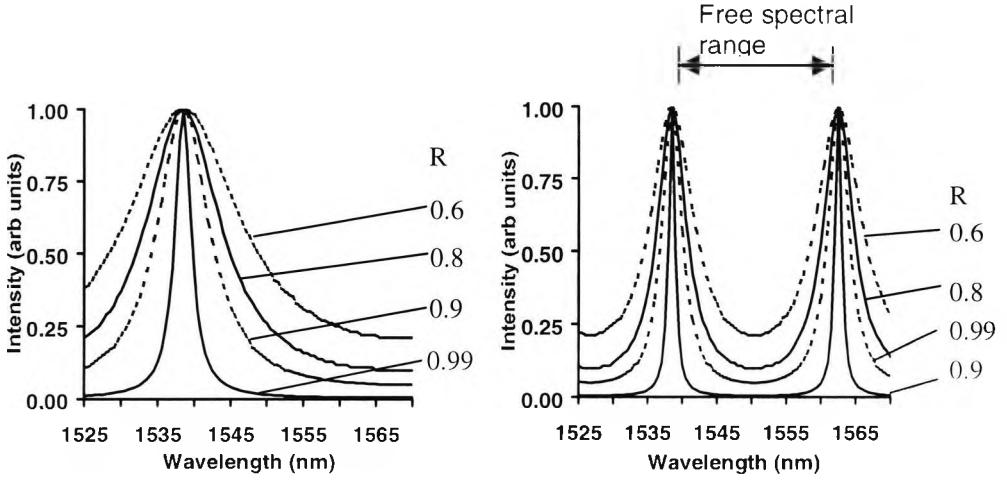

Figures 3_17 & 3_18: Typical outputs from Fabry-Perot. Graph on the left is for 20μm and on the right is d=50μm.

Convolution results of the output functions for two gratings, combined with those of the Fabry-Perot micro-filters shown in Figure 3_17 and 3_18, are presented where the first grating has a value of λ_B = 1540nm and the second has a value of λ_B=1550nm. As is shown, in Figures 3_19(a)-(d) below, the linewidth and in particular the free spectral range of the micro-filter, change the output spectral response of the system as a whole. This will have a marked effect on the resolution possible in the presence of noise and on the possible multiplexing potential of the system.

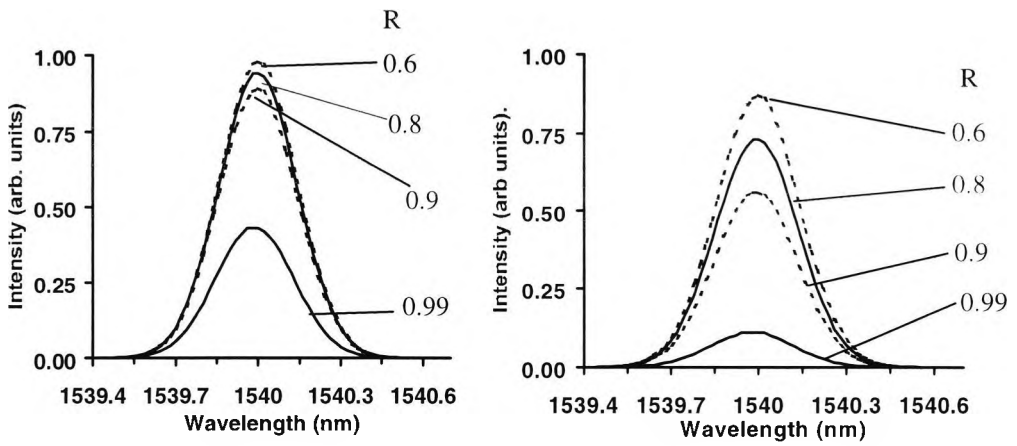

Figure 3_19(a) and (b). λ_B=1540nm with the above microfilters, (a) is combined with the micro-filter in Figure 3_14 and (b) with that shown in Figure 3_17.

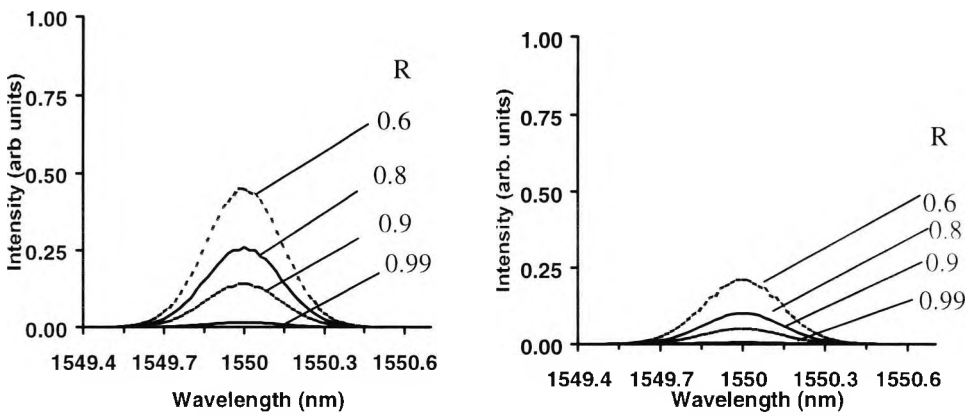

Figure 3_19(c) and (d). λ_B=1550nm with the above micro-filters, (a) is combined with the micro-filter in Figure 3_14 and (b) with that shown in Figure 3_17.

These graphs show how the performance of the system varies as the Fabry-Perot mirror separation, d, (and therefore the free spectral range) changes, such as is required to optimize the design of a practical system of this type.

Calculations are undertaken to show the effects of noise and are shown below

are for different simulated noise levels (N), namely 0.1%, 1% and 10% of the detected signal, illustrating the root range, X2-X1, the noise level and the SNR for the system.

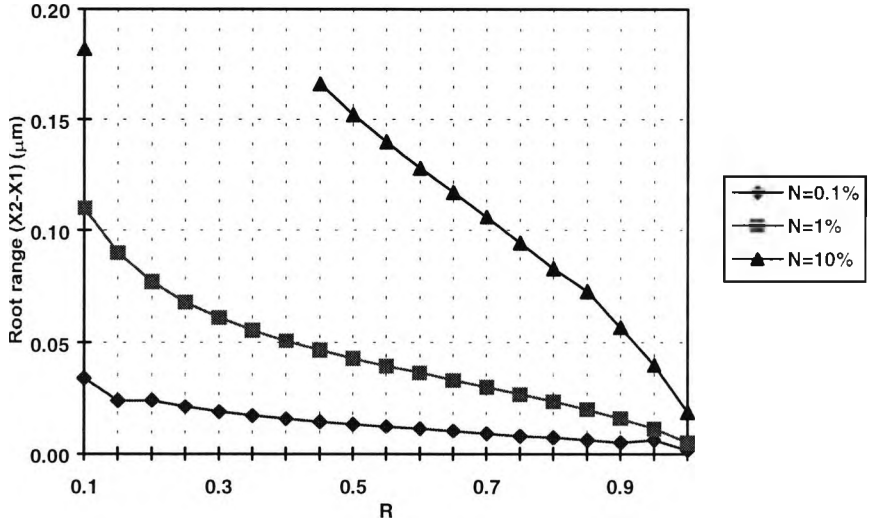

Figure 3_20: X2-X1 against Reflectivity, R.

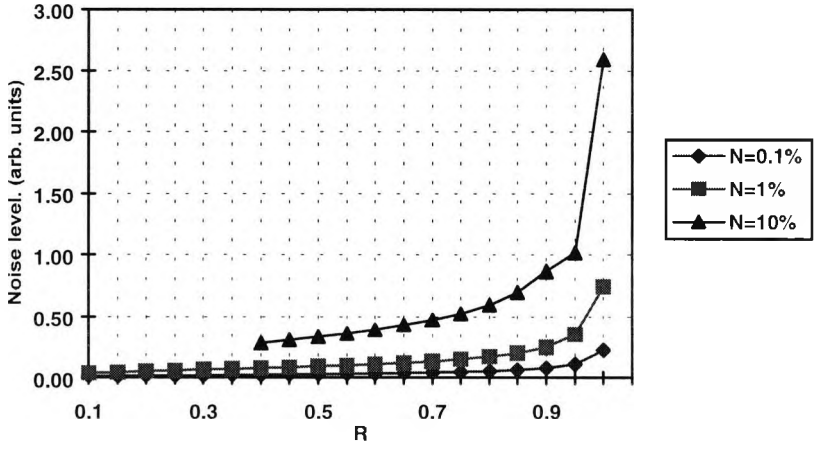

Figure 3_21: Noise at root against reflectivity, R.

Figure 3_20 shows that as the reflectivity of the microfilter increases, the resolution limit of the peak decreases resulting in a lower error in the identifying of the peak of the detected signal. It can also be seen that at lower noise levels, the choice of micro-filter makes very little difference whilst at the higher noise levels the ambiguity in the position of the root is much more marked for lower values of reflectivity. However, in Figure 3_21, it is shown that the noise level at the root of the differentiated curve increases as the reflectivity, and hence the finesse, increases. These two effects operate simultaneously and can be expressed in the graph of signal to noise (SNR) versus reflectivity (R) shown below.

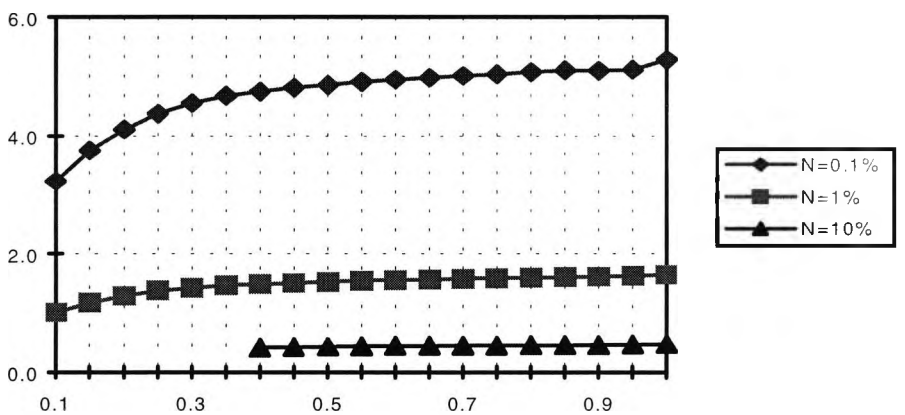

Figure 3_22: Signal to noise as a function of reflectivity, R.

Figure 3_22 illustrates the result of the combination of the noise and the resolution limit.

There are two main sources of noise in a system the effects of which are

simulated in this section. Firstly, photodetector induced noise (e.g. shot noise will be present) and secondly there is an uncertainty as a result of the fact that the value of d cannot be known exactly and thus it will induce some ambiguity in the measurements.

The main sources of errors in this simulation will come from the numerical integration and differentiation of the curves. It is not thought that these errors will have a significant effect upon the results presented. It is worth noting however that differentiation followed by root hunting is not the only method that could be used to search for the wavelength peak. Some form of curve fitting routine may have produced better results, since by this method some of the effects of the modelled noise could be eliminated.

It can be seen that Fabry-Perot interferometer-based filters with a high finesse are not necessarily the best design for this particular application. It is true that there is less ambiguity in the peak detection, but this is balanced by a higher noise value in the determination of λ_B. This will have an influence on the optimal design of a grating based sensor system

3.4.3 Analysis of the scheme chosen, the Michelson interferometer

Invented by the German born American physicist Albert A. Michelson (1852-1931), the Michelson interferometer consists of a beamsplitter and two mirrors. The arrangement is shown below in Figure 3_23.

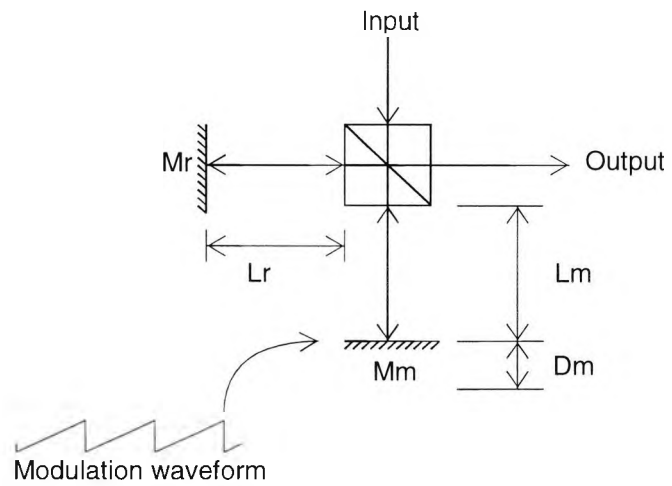

Figure 3_23: Schematic of a Michelson interferometer arrangement.

One beam reaches the detector via the stationary mirror Mr, therefore being designated the reference beam. The second beam reaches the detector via the second mirror, Mm. This mirror is adjustable thereby changing the optical path difference between the two beams. The relative phase of the beams at the detector will therefore depend on the difference between the two optical paths. Thus, any changes in the position of Mm can be detected as a change of phase of the combined signal at the detector. It can be shown that the phase output from the interferometer is of the form:

$$S = A\cos(\omega_0 t + \Delta\varphi) \qquad (3\_20)$$

where ω_0 is the scanning angular frequency of the interferometer, $\Delta\varphi$ is the phase shift of the interferometer fringes. The relationship between the wavelength variation of the reflected signal from the grating and the phase shift output at the interferometer is given by the transfer function for a Michelson interferometer, which is:

$$\Phi = \frac{4\pi L}{\lambda} \qquad (3\_21)$$

where Φ is the phase of the output beam from the Michelson interferometer and L is the interferometer optical path difference, OPD, and is equal to twice the distance Dm shown on Figure 3_23. However, from the above equation, it can also be seen that the phase of the output is also related to the wavelength of the input source and it is this fact that makes this type of interferometric sensing, arising from changes in wavelength possible.

If the back-reflection from a Bragg grating is used as the input light beam then the corresponding change in phase of the output for a given change of Bragg wavelength is given by:

$$\Delta\Phi = \left(\frac{4\pi L}{\lambda_B^2}\right)\Delta\lambda_B \qquad (3\_22)$$

Therefore, the sensitivity of the phase change to changes in Bragg wavelength is dependent upon the arm imbalance of interferometer. In operation, the Michelson interferometer is repeatedly scanned across a given OPD range with a sawtooth waveform, producing a sinusoidal temporal fringe pattern in the usual familiar manner. The number of fringes produced in a single OPD sweep is dependent on the amplitude of the waveform used, where the optimum position being reached when exactly one fringe is produced per OPD sweep which will occur when the OPD is modulated by $\lambda/2$. The measurand-induced change in wavelength can then detected as a change of phase of this fringe pattern.

The phase response to the applied strain may then be determined. The strain responsivity (i.e. fractional Bragg wavelength change, $\Delta\lambda_B/\lambda_B$) is numerically a factor of 0.74 of the corresponding applied strain, $\Delta\varepsilon$ [64]. This is due to the change in refractive index caused by the strain-optic effect. Therefore:

$$\Delta\Phi \approx 0.74\frac{4\pi L\Delta\varepsilon}{\lambda_B} \qquad (3\_23)$$

It can be seen that the phase sensitivity of the system increases linearly with

the OPD of the interferometer, and it is for this reason that the processing interferometer is kept unbalanced.

The value of the OPD is very important because it can change the phase shift ratio ($\Delta\varphi/\Delta\lambda$), which is related to the resolution achievable from the system. The larger the OPD, the higher the resolution that may be obtained. However, increasing the OPD will decrease the fringe visibility of the interferometer and the signal-to-noise ratio of the signal [64]. This limit is introduced by the coherence length of the light source used, where for a Bragg grating reflection, the coherence length required is related to the Bragg grating parameters by

$$L_C = \frac{\lambda_B^2}{\Delta\lambda_{Bandwidth}} \qquad (3\_24)$$

For a grating at 1550nm with a bandwidth of 0.2nm this gives L_C of ~12mm. Thus, the choice of OPD should be balanced to reflect both requirements of achieving a satisfactory fringe visibility and phase shift ratio.

For an OPD of 10mm, the corresponding phase range is ~620 radians for a 10% elongation or 100 fringes. If the phase change is 0.01 of a fringe, then this gives 10,000 resolution points or 1μstrain resolution.

3.5 Summary

Chapter 3 has presented a novel wavelength shift detection scheme that utilized a Wollaston prism interferometer. The use of a second light source to act as a reference wavelength enables a resolution of ~0.01nm to be achieved. However, the Wollaston approach was shown to be unsuitable due to problems concerning the CCD detector. These problems are likely to be partially solved in the future, as new versions of CCD that operate faster and with smaller elements, become available. At such time, the Wollaston prism approach could then be reconsidered.

As an alternative, an interferometric approach using a Michelson interferometer was presented that has the potential for a high level of accuracy by transposing the wavelength shift into a change of phase of the interferometric output.

Once the reflections from the Bragg gratings have passed through the Michelson interferometer, a demultiplexing system is required to sort the different signals into separate channels for processing. Chapter 4 examines the demultiplexing system developed, which uses a series of electrical switches to separate the signals from different gratings.

Chapter 4:

Optical time domain reflectrometry (OTDR) using Bragg gratings

In this Chapter, the OTDR system that has been developed is presented. Section 4.1 will introduce the theory by which OTDR operates, Section 4.2 will examine the various components of the system in detail. In Sections 4.4, 4.5 and 4.6 results are presented that demonstrate the system working as expected. Section 4.7 draws conclusions about the systems potential and introduces the work presented in Chapter 5 concerning possible further work.

4.1 Introduction to optical time domain reflectrometry

The use of a single Bragg grating as a strain or temperature sensor requires a system similar to that outlined below in Figure 4_1. With this type of system, the grating is illuminated continuously by a broadband source and the light

reflected back along the fibre is converted to an electrical signal by a suitable detector. Any measurand induced change in wavelength of the detected signal is calculated using a suitable scheme, such as was described in the previous chapter.

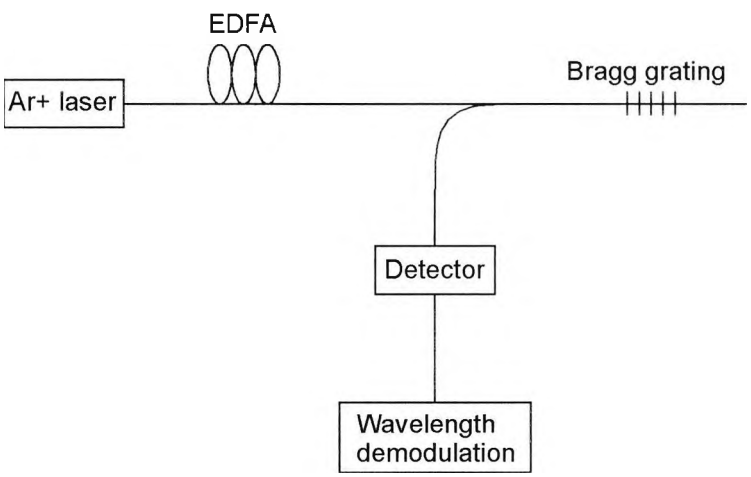

Figure 4_1: Basic Bragg grating sensor system arrangement using an erbium doped fibre amplifier (EDFA).

The system shown in Figure 4_1 above uses a erbium doped fibre amplifier as a light source. However, any sufficiently powerful broadband light source can be used provided it operates at the Bragg wavelength of the grating used. Monochromatic light sources are unsuitable since the Bragg wavelength of the grating will change when under strain and if the new Bragg wavelength is outside the spectral envelope of the source then no light will be received by the detection system.

However, this type of system suffers from a number of problems. A portion of the back reflections will strike the light source which may interfere with its output (depending on the light source used), however this can be solved by including an optical isolator in between the light source and coupler. The two main problems of the system, however, are the cross-sensitivity between temperature and strain as mentioned in earlier Sections, and the obvious limitation of only using one grating.

Various methods of differentiating between temperature and strain effects (both of which will change λ_B) have been reported as have been discussed in Section 2.4.4 above. In the strain measurement experiments carried out during the course of this work, the temperature was assumed to be constant throughout, therefore any change in λ_B will be due to changes in the strain conditions. In a practical situation one of the approaches outlined in the literature review would be employed.

Optical time domain reflectrometry is the proposed method by which the problem of demultiplexing a series of gratings can be solved. The basic system for an OTDR based arrangement is shown below in Figure 4_2.

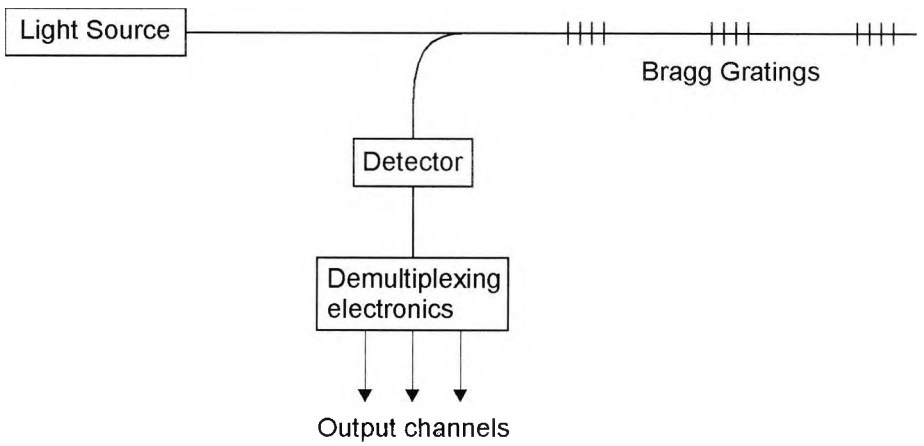

Figure 4_2: Basic optical time domain reflectrometry (OTDR) arrangement.

The broadband light source is chosen to ensure that its spectral envelope will cover all the Bragg wavelengths of the gratings used. It is modulated either directly from a light source driver or externally via an optical modulator to produce a series of pulses that are incident on a series of Bragg gratings via a coupler. The distance between successive gratings defines the maximum width of these pulses (if the pulse is too long then reflections from successive gratings will overlap). The number of gratings defines the time gap between the pulses produced by the light source. The reflected pulse from the last grating before must be detected before the reflected pulse from first grating on the next pulse can be detected.

This will produce a series of reflected pulses (one from each grating), for each incident light pulse. The time interval between pulses is directly proportional

to the distance between successive gratings. Therefore by timing the gap between the light source emitting a pulse and the time a reflected pulse is detected, and knowing the gap between the gratings, the returned signal from individual gratings can be identified.

After the pulses have been detected and converted to an electrical signal (with any necessary amplification), the signal from individual gratings must be sorted into separate channels for processing. If the sensing elements are not too far apart, then the pulses will be too fast to be read directly into a computer and sorted by suitable software analysis. For example, if the gratings are 20m apart, then the reflected pulses would be ~100ns apart, too fast for most PC based analogue-to-digital conversion). Therefore, this sorting must be done at a hardware level.

The method chosen to do this was to create a binary tree using two pole switches. By synchronizing the timing of the switch operations with the arrival of the pulses, the various outputs from the binary tree will be open for the arrival of a pulse from a single grating. This approach gives a final system arrangement shown the Figure 4_3 below.

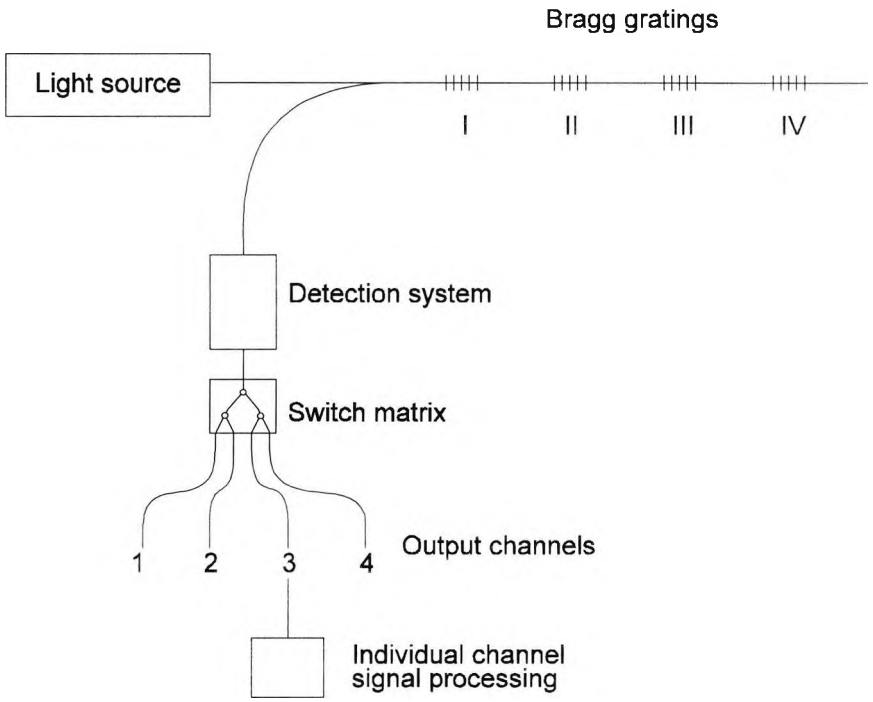

Figure 4_3: System schematic showing output channels.

The individual components of the system outlined above will be discussed in more detail in the next section.

A similar tree arrangement to demultiplex the sensors into separate channels has been demonstrated [35]. However, in this case the tree was in the optical domain and constructed from optic fibre couplers with each sensor on a different fibre. The main drawback of the system as reported is the complexity of the network which requires, for x sensors, (x-1) fiber couplers and x/2 detectors. It is obvious that including the tree arrangement after the optical pulses have been converted into electrical signals requires a much simpler optical network.

4.2. Examination of various components of the system

The electronic demultiplexing system proposed herein is based on the basic OTDR arrangement as outlined above in Section 4.1 combined with the interferometric demodulation system outlined in Section 3.4. In the following section the various elements of the system will be examined in more detail.

4.2.1 Erbium doped fibre amplifier light source

The light source chosen for this type of system has to fulfil two main criteria, namely power and bandwidth. The bandwidth of the source used is important because this is the ultimate factor that limits how many gratings can be used in series on the single fibre (assuming that the gratings used are fabricated such that each operates at a different Bragg wavelength). This limitation is assumed because each grating will reflect a large proportion of the light at a particular wavelength (i.e. the Bragg wavelength for that grating) and hence following gratings further down the fibre cannot use that wavelength.

The alternative case, where $\lambda_{B1} = \lambda_{B2}$ is possible and systems involving both WDM and TDM have been reported that use gratings at the same wavelength

in series [5]. However, this does present two problems (namely spectral overshadowing and multiple reflections) and these are discussed as further work in Sections 5.1.1 and 5.1.2 respectively.

Given that the Bragg wavelengths for individual gratings are going to change, as the strain conditions of the fibre changes, it is necessary to separate the grating spectrally by a value in the region of 2nm.

The other light source criteria is power, high power sources are preferable because the reflected signal from a Bragg grating will have a very narrow linewidth and therefore may only have 1% of the power incident on the grating. Detecting the reflected signal (especially when the incident light is pulsed) can, therefore, be tricky with low power light sources.

The light source chosen to fit these criteria was an Argon ion laser (λ=514nm) pumping an 8m section of erbium doped florescent source (doped to 500ppm) EDFS. This arrangement has the advantages of having a reasonably wide bandwidth and high power (1-10mW). The main drawback, however, is that neither the EDFS, nor the Argon ion laser are suited to being modulated. An alternative system for pulsing the light was therefore necessary which would modulate the light external to the source itself. The modulation system used is shown below in Figure 4_4.

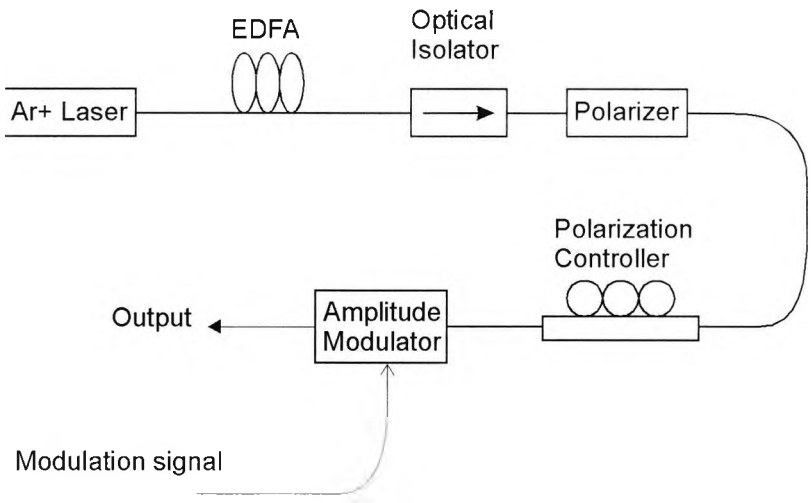

Figure 4_4: Laser modulation system used.

The optical isolator stops any unwanted back reflections from the rest of system returning to the EDFS.

The optical amplitude modulator (manufactured by GEC-Marconi) pulses the light according to the input received from the electronic demultiplexing system outlined in the next section. The commercial amplitude modulator used operates (in simple terms) by using a Mach-Zender interferometric architecture. Input light is split into two parts and these propagate through the device via separate paths. The electrical control signal changes the local refractive index, via the electro-optic effect, in such a way so that one beam is retarded by up to a wavelength whilst the second is advanced by the same amount. The two beams are then recombined at the output and transmitted back into the fibre if

they are in phase, and lost as high-order interference modes if not.

The amplitude modulator is polarization dependent and hence a polarizer and a polarization controller are needed to ensure the amplitude modulators optimum performance. The polarizer controller consists of a length of single mode fibre wound around three loops, these loops are free to rotate slightly, changing the angle between them. This causes the fibre to twist and hence the polarization orientation of the light relative to the fibre axis is changed.

If the modulator does not perform correctly (which maybe caused by an incorrect signal voltage or if the polarization of the input light is misaligned) some light would pass through the modulator during the off period of the desired light source modulation. If this does occur the Bragg gratings will be continuously illuminated which will produce a large amount of crosstalk between the separate channels.

4.2.2 Electronic demultiplexing system

It is obvious from what has been discussed so far that in any system based on OTDR it is important that the returning pulses from the Bragg gratings are synchronised with the operation of the demultiplexing system. To ensure this an electronic control system was devised based largely on FAST TTL logic chips.

In the system shown schematically in Figure 4_5, a clock pulse in generated and all the operations are synchronised with it.

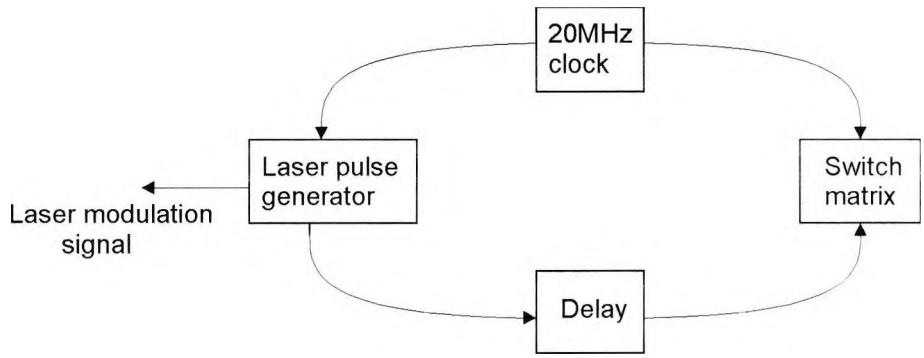

Figure 4_5: Schematic of the demultiplexing system.

It can be seen from the above figure that the electronic system breaks down into a number of separate parts, each of which is described below. Many of these circuits use Pal (Programmable Array Logic) integrated circuits and these are outlined below.

Pals contain a series of AND gates, NOT gates and D type latches interconnected with user programmable links. A Pal program is written (using a computer program called Palasm) which defines the inputs and outputs that the device will have and also defines the relationship between them using a number of Boolean logic equations. This program is written onto the integrated circuit using a suitable programmer.

The main advantage in using these devices is that the program a Pal is running can be changed simply by overwriting it with a new version. This flexibility can be used so that the specifications of the circuit can be changed without having to rebuild the whole. The main disadvantage lies in the propagation delay (≈8ns) which occurs due to the signal having to pass through a number of logic gates. However, any delay that does occur will be constant and therefore can be allowed for within the laser-go pulse delay system.

4.2.2.1 External electronic clock

This produces a square wave at 20MHz using a TTL compatible quartz crystal oscillator module (manufactured by AEL crystals). The output signal was gated through a TTL Schmitt trigger. This ensures the output signal has sufficient power to drive the necessary inputs (TTL outputs generally have sufficient power to be connected to ten TTL inputs) and the Schmitt trigger ensures fast rising and falling edges. This clock signal is sent to all the other components in the scheme and is used to synchronise all the other systems. This clock module defines the speed at which the whole system will run and therefore the spatial resolution at which the gratings can be placed and still be demultiplexed successfully. If we assume that a single output channel will be open for one complete clock period (i.e. the time gap between successive rising edges of the clock signal), then the spatial resolution will be equal to the round trip covered

in that time, i.e.:

$$Sg = \frac{\left[\frac{c}{1.45}\right]\left[\frac{1}{Clock_{freq}}\right]}{2} \approx 5m \qquad (4\_1)$$

Where Sg is the distance between successive gratings, c is the speed of light in a vacuum and $Clock_{freq}$ is the frequency of the electrical clock.

4.2.2.2 The GaAs switch controls

The GaAs switches used to separate the signals from the gratings into individual channels are controlled electronically and therefore require an input control voltage to determine which of the two output channels is open. This control signal is generated by the following method.

In the binary tree arrangement, each of the eight output channels is given its own unique binary code based on the route through the tree. This is shown below, in Figure 4_6:

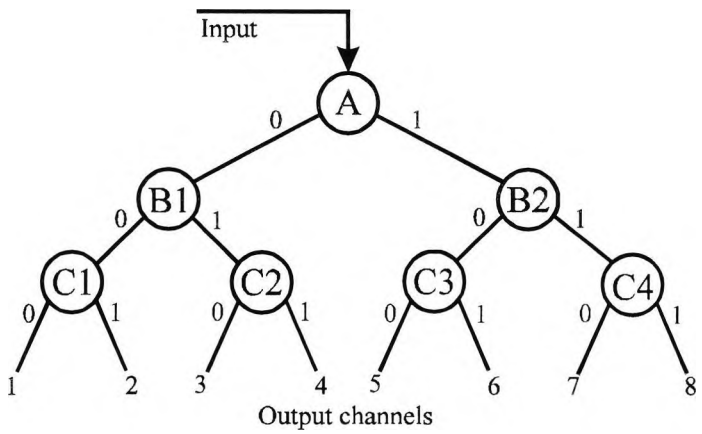

Figure 4_6: Schematic of the switch matrix

Therefore, the basis of the control signal generation is a 4-bit counter (74F163) which steps through the eight channels from 0000 to 0111. The input to the counter is the external clock signal after it has been gated with the 'READY' signal (RC) from Pal 1 and the 'LASER_GO' signal (LSG) from the laser go pulse generation board. This gating process, using two D type latches (74F74) and an AND gate (74F08) produces an internal clock signal which consists of a square wave which continues while the RC signal from Pal 1 is high. The Pal is programmed to change RC from high to low at a binary signal of 1000 so that the internal clock produced looks like the trace shown in Figure 4_7 which shows the timings of the main sections of the electronics system.

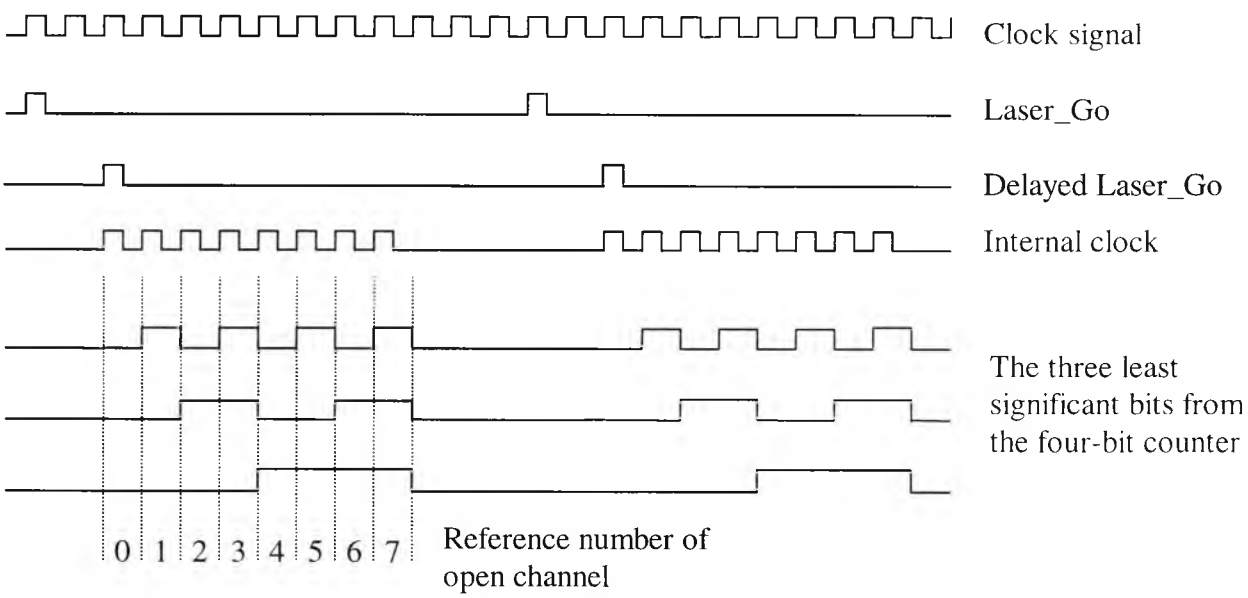

Figure 4_7: Timing diagram of electronic demultiplexing system. A pulse of light is emitted at the first 'Laser_Go' pulse. The switch matrix starts operations on the second (delayed) pulse.

The internal clock has one pulse per output channel (and, therefore, per grating). This signal is then used as the count input for the counter. The output from the 74F163 is therefore a 4-bit binary signal that steps from 0000 to 0111 in time with the external clock. This signal is placed onto a latch (74F374) to improve the stability of the system.

Once the counter has stepped through all the channels and RC is low, the system then waits until the next 'LASER_GO' signal is received when the counter having been reset to 0000 starts again. Usually, it is desirable that the delay between the 0111 channel closing and the 0000 channel opening is the same as the delay between successive channels in the middle of the sequence.

However, with the system outlined above this need not be the case and if larger delays were needed (e.g. to allow other parts of a larger system enough time to reset fully or if accurate triggering is required) then this could be produced using the laser go pulse generator board outlined in the next section.

The electronic GaAs switches require two complimentary signals with voltages of 0V and -5V so the TTL signal produced by the above method have to be converted to this format before it can be passed to the switches themselves. This is done using a digitally controlled analogue switch (74HCT4053).

A 74HCT4053 is a triple, two pole switch and in this arrangement is used 'backwards' (i.e. 2 inputs, 1 output). Two of the three switches are required for each pair of control signals. To produce the complimentary pairs required the inputs are tied -5V or 0V in opposite ways. The TTL signal (from the counter) opens one of the input too output routes within the 74HCT4053, therefore the outputs are set at -5v or 0V depending on the state of the TTL signal.

4.2.2.3 Laser_Go pulse generation

To ensure that all the various components of the electronic system start at the same time, a single pulse is used as a 'GO' signal. This pulse is passed to the

light source modulator, instructing it to fire, and to the electronic control system generation, via a delay, instructing the system to begin operations. The pulse is based on the external clock and is generated by a counter (74F163 was used again) that counts pulses from the clock and when it reaches a certain value it will reset and produce a single pulse.

A delay is necessary between the time the laser pulses and the time the switch control circuitry begins its operations, to allow for the time taken by the pulse of light to travel along the fibre, reflect back from the Bragg grating and return to the detector.

Using the control mechanism described above, the system is arranged so that one channel opens as the previous channel closes, also there is no delay between the last channels closing and the first reopening for the next laser pulse reflection. This means that the delay required by the system will never be greater than 50ns since all that is needed is to synchronise the arrival of a pulse at the detector with the opening of a channel, which will close as the pulse ends. Of course, this may mean that the returning pulse from the first grating emerges from the, say, third channel. However, determining which channel is which is a minor system calibration and providing the clock frequency remains stable then the pulse from this grating will always emerge from the third channel.

There are a number of ways that delays of this magnitude can be incorporated into the system. Delay-line chips are readily available which can provide delays up to 100ns in increments of 5ns. However, the simplest method is to insert a length of optical fibre between the light source modulator and the Bragg gratings of a suitable length such that the light pulse will be delayed by the appropriate amount. This method has been used in these experiments.

4.2.3 Detector and high frequency amplifier

Throughout the duration of the project, two different types of optical detector were used, a PIN photodiode and an avalanche photodiode, APD. A comparison of these different types of detectors is shown below:

Parameter	PIN-110	PIN-415	APD-110	APD-415	Units
Transimpedance	47	5.6	47	5.6	kΩ
Responsivity	40	4.5	275	50	KV/W
Bandwidth	140	450	140	450	MHz
Spectral noise volts	40	15	50	25	nV/√Hz
NEP	1.0	3.0	0.18	0.5	pW/√Hz
Sensitivity	-4.2	-34	-48	-42	dBm

Table 4_1: Specifications of various photodiodes
(typical values from manufacturers notes).

Definition of terms. (from Melles Griot handbook).

Responsivity($\Re$) is the ratio of the photocurrent generated for each watt of incident light. Depends directly on the quantum efficiency (η), (probability of an incident photon generating a charge).

$$\Re = \frac{\eta\lambda}{1.24\times10^{-6}} \qquad \text{(in A/W)} \qquad (4\_2)$$

Noise Equivalent Power (NEP) is the incident light level which produces a photocurrent equal to noise level. The signal to noise ratio (SNR) maybe computed by taking the ratio of the incident optical power to the photodiode NEP.

$$NEP_{rms} = \frac{i_{rms}}{\Re} \qquad (4\_3)$$

where

$$i_{rms} = \sqrt{\left(\int_{f1}^{f2}\left(i_1^2(f)+i_2^2(f)+\ldots+i_n^2(f)\right)df\right)} \qquad (4\_4)$$

The NEP is a function of the photodiodes responsivity, the noise of the photodiode and the associated circuit, and the frequency bandwidth over which the noise is measured. It is therefore regarded as a good figure of merit.

The 4 photodiodes outlined in Table 4_1 above differ in a number of ways, the two 110's have larger transimpedences but lower bandwidths than the 415's. The higher transimpedence of the two 110 photodiodes affects the responsivity generating a correspondingly larger output current for a given incident power. Obviously, the 110-APD with the extra gain and the higher transimpedence has the highest responsivity by a large margin. However, it is worth noting that the responsivity of the APD-415 is larger than either of the two pin diodes even with the higher bandwidth.

However, noise must also be considered, the two APDs have a far lower NEP which, as mentioned above, is an important parameter.

Bandwidth is, of course, an important consideration the lower bandwidth devices may have trouble producing a good output (fast rising edges, etc) for a signal that is pulsed at 20MHz and faster signals would produce more problems. So from an applications viewpoint, and in particular in case of future advancements that may increase the speed, the higher bandwidth devices are to be preferred. However, a bandwidth of 140MHz is adequate for this system in its current format.

For any practical system, cost is an issue that deserves some consideration. All other things being equal, the cheaper solution is to be preferred. Pin diodes are considerably cheaper than their APD counterparts, however given the improved output signal and in particular the improvements in the NEP that the APD provides, some justification for the cost can be made. It is also worth noting that the difference in price between PIN and APD detectors is reducing, as APDs become cheaper. The photodiode chosen for this application was the APD-110 for the reasons outlined above.

4.2.4 Test results from prototype switch array

The initial demultiplexing system developed used a matrix of seven, two pole switches in binary tree arrangement. Before an improved version was installed (see next Section) some initial results were taken using this system and are shown below in Figure 4_8. These show the outputs on two channels when a single grating is used.

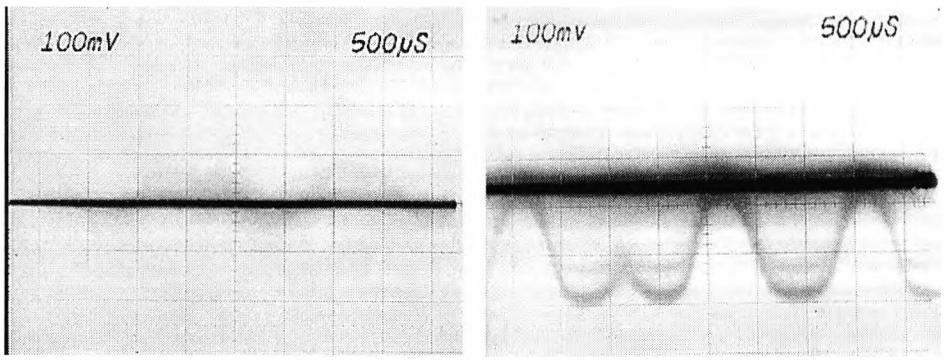

Figure 4_8(a) and (b) : Oscilloscope photographs from two different channels. (Time and vertical scales as shown)

Figure 4_8 shows the output signal from two different channels of the switch matrix (neither has had any filtering). The time-scale used is such that the individual pulses cannot be seen, however, the interference fringes (produced by the Michelson interferometer) are seen in Figure 4_8(b), but not in (a). The output signal demonstrated in (b) consists of light that has been reflected back from the Bragg grating and as such carries measurand information in the form

of its phase. As mentioned, above the signal consists of a series of pulses with a sine wave as an overall envelope pattern. Once the signals have been demultiplexed, the pulses are no longer required so this signal would then be filtered (using a bandpass filter centered on the frequency of the fringes) to make phase change detection easier.

The output signal from this system suffered from two problems however. Firstly, the crosstalk was too high (sometimes as much as 20% of the signal was detected on the wrong channels). The second problem was that the amount of noise produced by the switch matrix was too high for practical operation. In an effort to correct this problem, a four channel switch control board was printed by Queensgate Instruments (Previous boards were manufactured within City University) to higher production standards than were achievable at the University.

4.2.5 Test results from four-channel system

The four-channel system uses exactly the same method of operation (in terms of control logic etc.) as the eight-channel device. The four-channel system was tested using a single grating system (i.e. one Bragg grating, Michelson

interferometer and APD) and the output signals from the four channels are shown below in Figure 4_9 in the form of oscilloscope photographs.

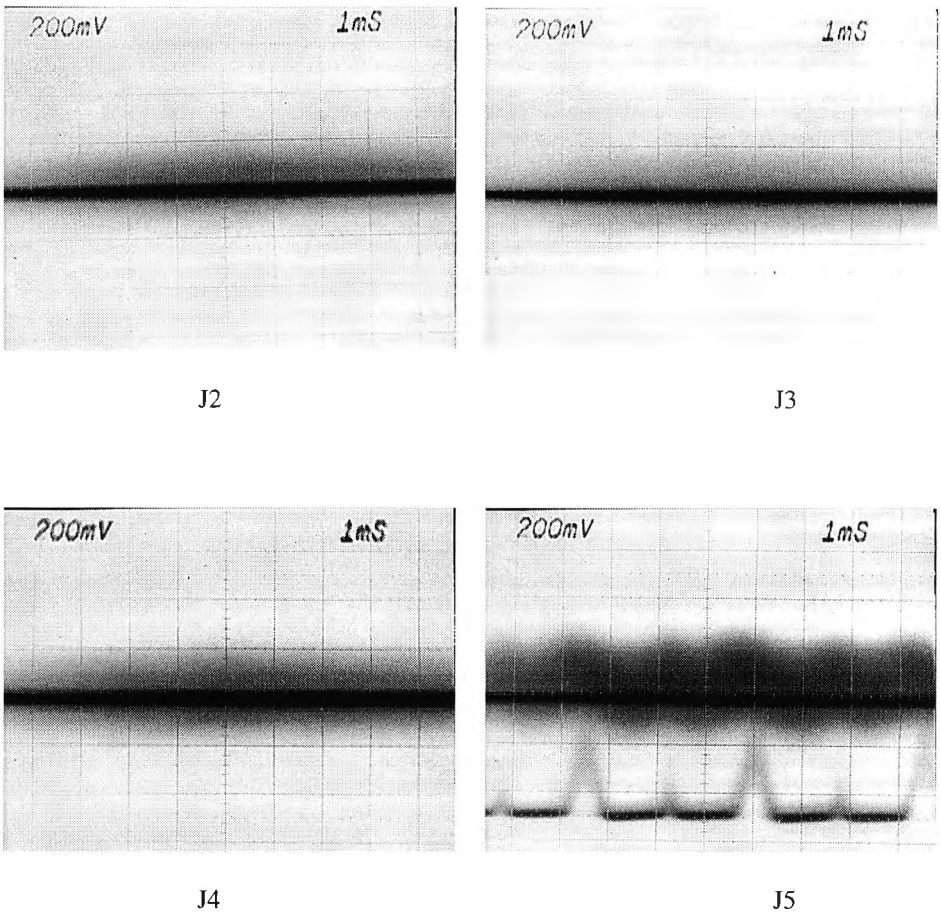

Figure 4_9: Oscilloscope photographs output signal from the four channels J2 - J5.

(Time and vertical scales as shown)

If the system worked perfectly, all the Michelson fringes would appear at only one channel whilst the other three channels would have a "zero" signal level. The above pictures show that the system developed works satisfactorily to

achieve a clear visual distinction between active and inactive channels. To convert this result into a useable signal, the output from J5 would have to be bandpass filtered at the fringe frequency (a value of around 300Hz was typically used for this work). Any phase shift can then be monitored directly using a system like that described earlier.

As further confirmation of the systems ability to demultiplex signal successfully, the oscilloscope traces below show a series of pulses for the case where two gratings are demultiplexed. The distance between the two gratings was just over 10 meters, as is clear from the pulse propagation times in the system.

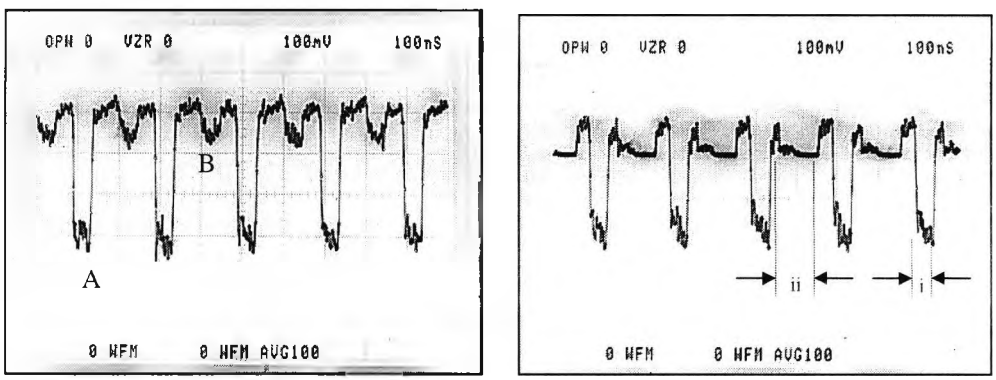

(A) (B)

Figure 4_10: Oscilloscope photographs showing (A) output directly from APD, and, (B) output after it has passed through switch matrix.

Figure 4_10(A) shows the signal detected by the APD, with the returning pulses from two gratings visible (the difference in intensity arises because the light source had a lower power at the wavelength at which the second grating

operated). A typical pulse from each grating is marked 'A' and 'B' as an example. Figure 4_10(B) shows the output from a single channel, and it is clear that the signal due to the smaller pulse has been removed from this trace. On the Figure (B), the region marked 'i' is the pulse from the grating, and 'ii' is the period when this route is closed and is therefore at ground. The small gap in between the channel opening and the pulse, which appears to be a positive going pulse and/or noise, is caused by the AC coupling of the amplifier and does not contribute to the overall noise level significantly.

These figures show conclusively that the proposed system can demultiplex the returned signal from a series of gratings successfully.

4.2.5 Frequency domain results

By replacing the Michelson interferometer with a wavelength-filter (in this case a filter based on a Fabry-Perot interferometer) information on the level of crosstalk can be gained. The following graphs show results from a system test, whereby the signals from two Bragg gratings separated by a 10m length of fibre were passed through a Fabry-Perot filter. The filter was ramped so that the OPD range scanned though included both gratings. The signals were detected using the APD and a commercial bandpass filter was used to remove

the excess high-frequency noise caused by the pulses. The results were then displayed and printed out using a signal analyser.

Figure 4_11 below, shows the combined signals from both gratings, both of which can be clearly seen. The sawtooth OPD ramp signal is also shown. This combined signal was demultiplexed using the switch matrix outlined in previous section, and the signals from different gratings appear at different outputs, as shown in the following graphs.

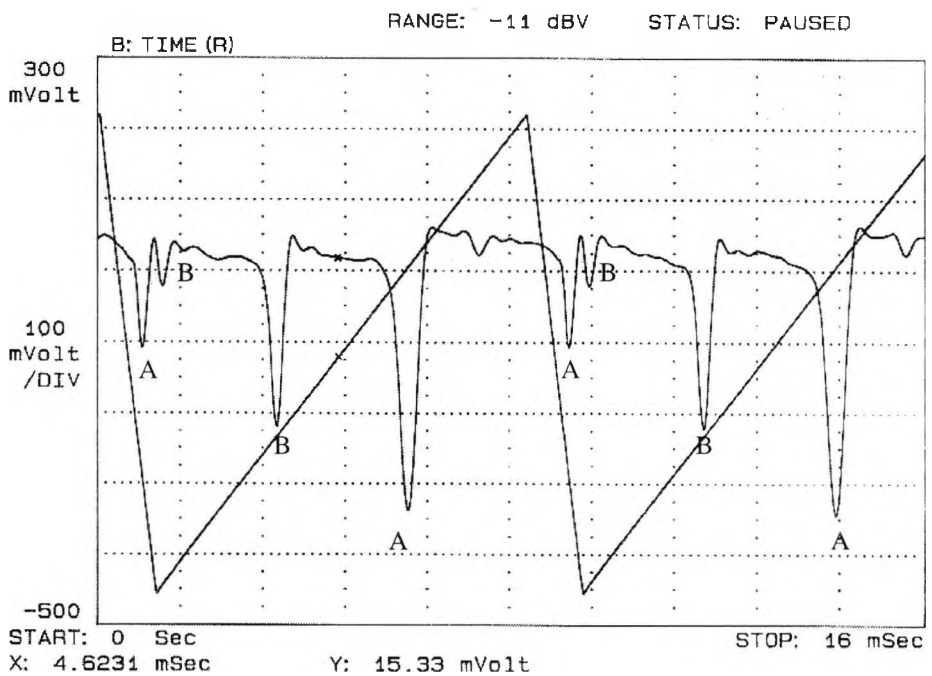

Figure 4_11: Combined output containing signals from both gratings (A & B). Sawtooth signal used as OPD ramp for the filter is also shown. (Vertical and horizontal scales as shown).

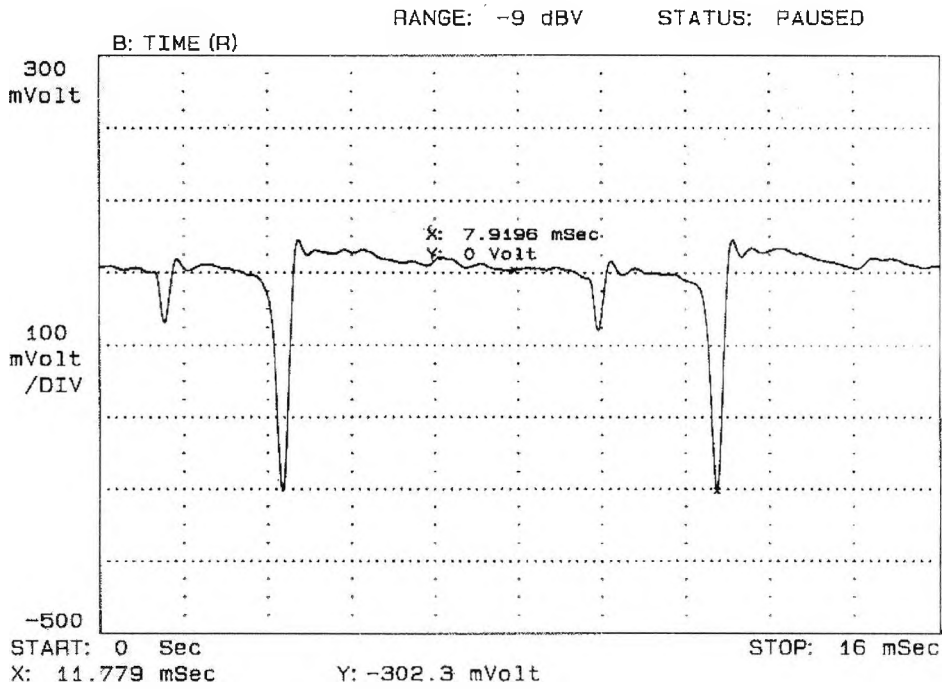

Figure 4_12: Output channel for the first grating.

Figures 4_12, and 4_13 show that the signal from the gratings has been successfully demultiplexed. If a significant level of crosstalk, caused by the electronic demultiplexing system had been present, between the two channels, then a peak at both Bragg wavelengths would be visible. It is obvious that any crosstalk present is below the background noise level present within the system.

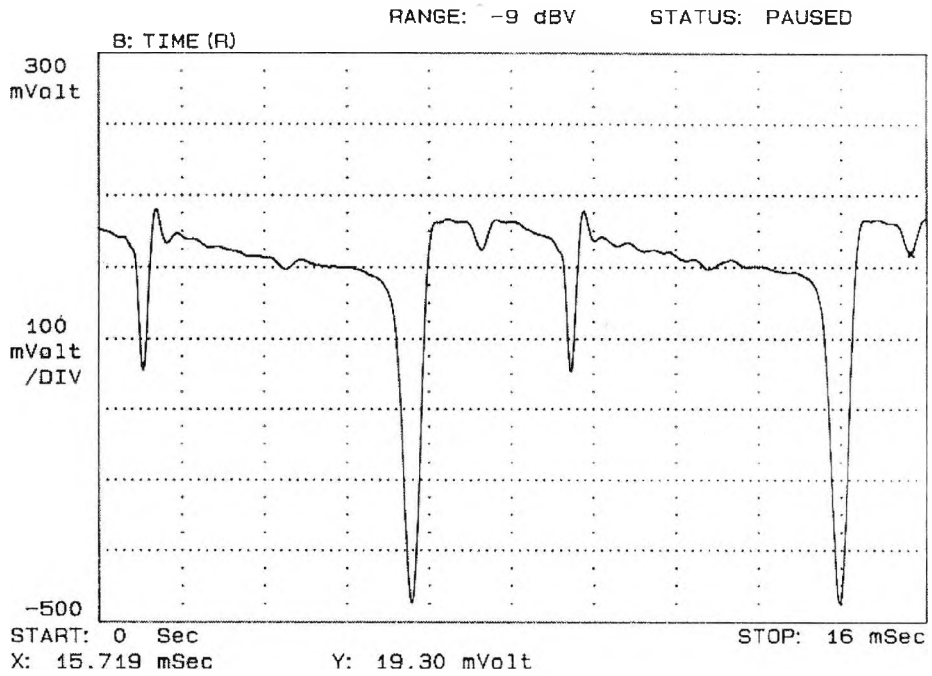

Figure 4_13: Output channel for the second grating.

4.3 Signal to noise ratio (SNR) achieved by the system

The frequency domain results presented as Figures 4_11, 4_12, and 4_13 in Section 4.2.5 can be used to estimate the SNR achieved by the system. Figures of this nature are usually given as decibels, which are defined as:

$$\mathrm{SNR} = 20\log_{10}\left(\frac{\mathrm{S}}{\mathrm{N}}\right) \qquad (4\_5)$$

where S and N are the signal and noise levels respectively (in volts). From Figure 4_11 this gives a SNR of ~-20dB. An estimation of the level of crosstalk between the two channels can be calculated by comparing the magnitude of the grating signal present in the channel, with the magnitude of the signal at the wavelength of the other grating. From Figures 4_12 and 4_13, the level of crosstalk is of the order ~-30dB, and therefore can be considered less than the noise level present.

The change of intensity of the signals between Figure 4_10 and the respective signals in Figure 4_11 and 4_12 is due to the way in which the signals were combined (both channel outputs had to be connected to the same filter).

4.4 OPD sensitivity testing

To determine the performance of the detection and signal processing scheme ultimately chosen, an experiment was carried out using a single grating under strain. The grating was attached to the underside of a brass beam (300×20×2mm), which was supported at both ends by metal pillars. In this arrangement, a weight placed on top of the beam will strain the beam, and therefore the grating, in a predictable and reproducible way.

In this experiment the sensitivity of the system to changing the optical path difference, OPD, of the interferometer was tested using the system shown below in Figure 4_14.

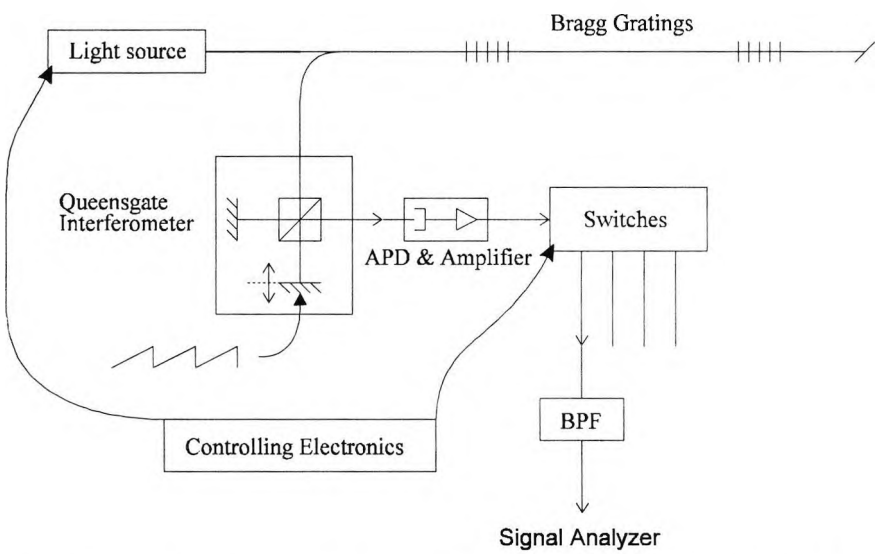

Figure 4_14: Diagram of complete system used in this experiment.

(APD = Avalanche photodiode and BPF = Band-pass filter)

The light source was modulated to produce 50ns pulses with a 1:4 mark-space ratio. The reflections from the gratings were passed through the Michelson interferometer before being detected by the avalanche photodiode. The interferometer was ramped with a sawtooth waveform to modulate the OPD (a frequency of ~330Hz was used). The switch matrix was in place and only the signal from one of the output channels was used as the input for the bandpass filter as would be the case in a practical arrangement. The bandpass filter, BPF, was a commercial device set up such that the center of the pass band matched the OPD modulation frequency with a bandwidth of ~50Hz. The BPF removes noise caused by 50Hz mains and the high frequency noise from the signal pulses. After the BPF the signal is reduced to a sine wave, the phase of which is dependant on the wavelength of the light returning from the Bragg gratings, as has been explained in previous sections.

The phase change was recorded using a digital signal analyser that was triggered using the TTL output of the function generator. The fringe movement caused by the change of strain state (weight on - weight off) was measured by following by the peak of the fringe and converting this to a phase change. This was repeated for a range of OPD values of the Michelson interferometer.

As can be seen from Figure 4_14, the light source (in this case an ELED) is modulated using a signal from the switch control electronics. The demultiplexed signal was then filtered using a band-pass filter to extract the fundamental frequency of the interference fringe pattern (equal to the frequency of the ramp modulation of the Michelson interferometer). The results are shown as a graph of increasing OPD against phase difference, on Figure 4.15.

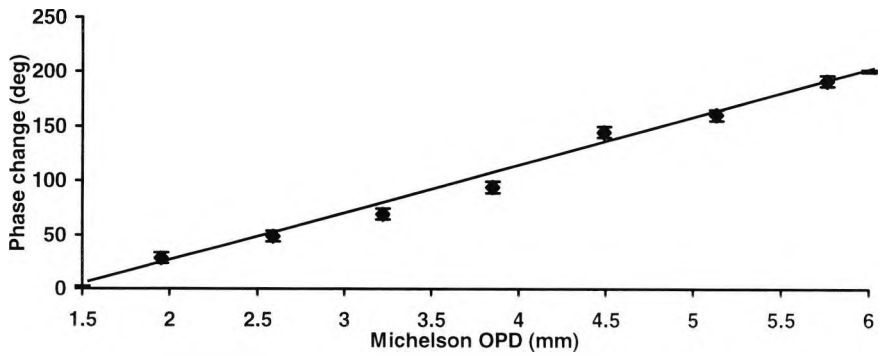

Figure 4.15: Graph of optical path difference against phase difference.

The linear response of this graph shows that the system is working as expected, i.e., changes in the state of strain of the brass beam can be detected with a pulsed illumination and after demodulation using the GaAs switches. The sensitivity of the system can be improved by increasing the OPD of the interferometer.

At higher values of OPD the fringe visibility will be reduced due to the coherence length of the input light source where, a reduced fringe visibility will adversely effect the signal-to-noise ratio of the system because the noise

inherent in the system will remain. The reflected light from a grating will have a coherence length of the order ~12mm (for a spectral bandwidth of 0.2nm and λ_B=1550nm), so this measurement could be extended beyond the region shown.

4.5. Strain measurements using demultiplexed sensors

To characterise the system, strain and temperature measurements were taken using the time-domain demultiplexing approach combined with the Michelson interferometric phase detection scheme outlined in previous sections.

For demonstration purposes the experiments used two gratings in series separated by a 10meter length of fibre. The Bragg wavelength of the gratings used were 1529m and 1531nm respectively. The 1529nm wavelength grating was strained, whilst the 1531nm was kept free.

The system used is shown above as Figure 4_14, where the broadband source used was an ELED, producing ~100μW of output power at a centre wavelength of 1526nm with a ~70nm spectral width, when the supply current was 100mA.

The decision to change the light source to the ELED from the EDFS that was used for the earlier work was made for a number of reasons. The ELED is considerably

easier to use, since it can be modulated directly using a suitable driver without the need for the external modulator. It is smaller and cheaper, making it a more suitable choice for a practical system. The disadvantages with these devices are that they are considerably lower power, and the maximum speed of modulation is less. The final decision to swap light sources was, in a sense, forced when the external modulator broke.

The light was coupled into and out of the optic fibre via fibre-pigtails attached the light source and the detector respectively. The fibre used for this experiment (and all experiments in this presented in this work) was standard 1550nm single-mode fibre (9 / 125μm).

The integer period (2π) of phase shift was recorded by a bi-directional hardware counter. The +1 or -1 counting pulse was produced by a logic circuit in which the value of the original sine wave signal and a corresponding 90° phase shifted cosine signal were used to create the counting pulse at the crossing point of integer period.

The grating under test was attached to two ends of the test bench: one fixed, while the other could move along a slide when a driving micrometer was rotated. Thus a known level of strain was produced by stretching the fibre, and hence the grating, directly. The second grating was kept free of tension to use as a reference.

The results are shown below in Figure 4_16.

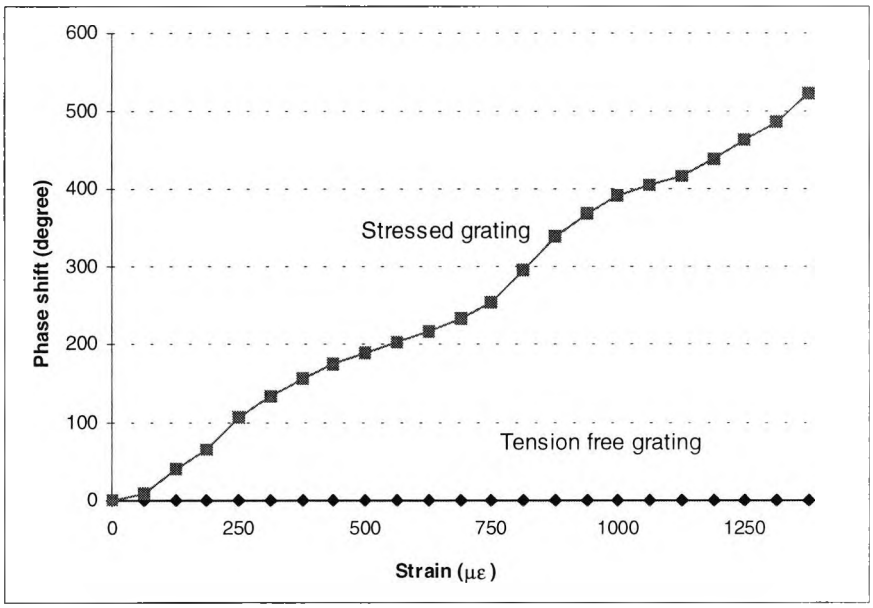

Figure 4_16: Phase shift for two gratings when a strain is applied to the first.

It is clear from Figure 4_16 that the level of crosstalk between the channels is very low because the phase of the free grating shows no change as a result of the changes in the first. From the experimental results, it can be calculated that approximately 2.65μstrain corresponds to one degree of phase shift, or, the phase shift responsivity to strain ($\Delta\varphi/\Delta\varepsilon$) is about 0.37 °/με. This corresponds to wavelength shifts of 1.59×10^{-3}nm/με for the 1529nm wavelength grating used.

In ideal conditions, the above graph would be linear, the slight deviation is due to the mechanical movement of the micrometer used to apply strain. This can be removed by calibrating with a more stable system.

4.6 Temperature measurements using demultiplexed sensors

Bragg gratings are responsive to temperature as well as strain and therefore can be used as temperature sensors. To show the systems possible use in such an application a similar experiment to the above strain measurement was carried out using a water bath to change the temperature of the fibre. Figure 4_17 shows the effect of temperature on the same grating used in the strain test (1529nm wavelength) when it was heated from room temperature to 75°C. Compared with the strain-phase graph, the temperature-phase curve in Figure 4_17 shows a similar linear response. The responsivity of temperature to phase shift is about 2.8° per °C, which corresponds to wavelength shifts of 1.19×10^{-2} nm/°C for the 1529nm wavelength grating.

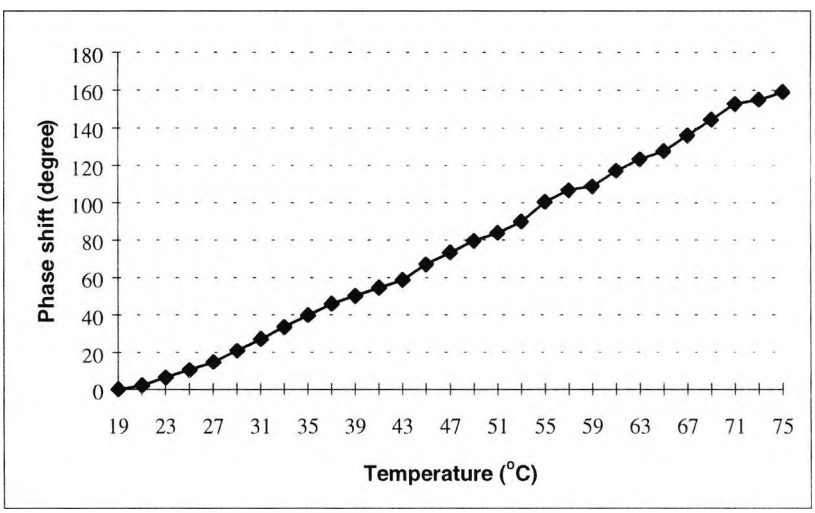

Figure 4_17 Phase shift response to changes in temperature from the room temperature to 75 (°C) in a water bath.

Results from the temperature experiments similar to that shown above would be probably needed even for sensors system used purely for detecting strain. This would be necessary for calibration purposes. The method of strain / temperature discrimination by using two colocated Bragg gratings, would be an example of when this information would be needed.

4.7 Summary

In this Chapter the concept of TDM has been introduced and applied to the problem of demultiplexing a series of Bragg gratings. A time-domain based sensor system has been developed that utilizes a series of GaAs switches to separate the signal pulses for analysis. The electronic control system synchronises laser pulses with the switch operation so that the arrival of the reflected pulses coincides with the correct channel.

The system has been evaluated and is capable of multiplexing a number of sensors with a SNR of the order of 20dB, with negligible channel crosstalk. When combined with the interferometric wavelength shift detection, a strain sensitivity of 1.59×10^{-3}nm/μm and a temperature sensitivity of 1.119×10^{-2}nm/°C was demonstrated.

In the final Chapter these results are discussed along with avenues for future work and problem that may be associated with expanding the system.

Chapter 5:

Discussion of results

The results presented above in Chapter 4 demonstrate that the TDM approach, when combined with interferometric demodulation, can be successfully applied to this type of application. The system is capable of detecting the measurand-encoded changes in wavelength from individual Bragg gratings sensing elements and demultiplexing a number of gratings successfully. However, some problems have been encountered that still have to be overcome to produce an optimum sensing system.

In Section 5.1 two of these limitations will be examined and possible solutions will proposed. Improvements to the system that could be made by the addition of new equipment and component devices that have become available during the lifetime of the project will be outlined in Section 5.2. Section 5.3 will review the results of the work presented in light of the aim and objectives stated earlier.

5.1 System inherent noise sources

5.1.1 Spectral overshadowing

In order to increase the number of sensors that can be used along a single optical fibre, it is necessary to fabricate the gratings in such a manner that the centre wavelengths are not spaced too far apart. However, set them too close and some spectral overlapping will occur. (The major limiting factor placed upon the number of sensors usable will be the bandwidth of the light source used). Indeed, systems using gratings with the same Bragg wavelength repeatedly along a single fibre have been reported [5].

This type of system (such as that presented in [5]) does present one obvious complication. That is, more than one grating will operate at a particular wavelength, either as the result of fabrication, or from a change in measurand changing the centre wavelength of one sensor to match another.

The work presented in this section attempts to characterize the effect of the situation where two gratings with similar Bragg wavelengths are placed in series along a single fibre.

5.1.1.1 Spectral overshadowing computer simulation

The computer model of the wavelength dependent reflectivity of the Bragg grating used in the simulation was based on the coupled mode theory demonstrated by Lam and Garside[31]. The result of this approach can be summarized as the following equation:

$$R(L,\lambda) = \frac{\Omega^2 \sinh^2(SL)}{\Delta\beta^2 \sinh(SL) + S^2 \cosh^2(SL)} \qquad \text{for } \Omega^2 > \Delta\beta^2 \qquad (5\_1)$$

$$R(L,\lambda) = \frac{\Omega^2 \sin^2(QL)}{\Delta\beta^2 - \Omega^2 \cos^2(QL)} \qquad \text{for } \Omega^2 < \Delta\beta^2$$

where R(L, λ) is the grating reflectance as a function of wavelength and grating length; λ is the wavelength; L is the grating length; Ω is the coupling coefficient; β is the eigen propagation constant; Λ is the perturbation period; $\Delta\Omega = \beta - (\pi / \Lambda)$; $S = (\Omega^2 - \Delta\beta^2)^{1/2}$; $Q = (\Delta\beta^2 - \Omega^2)^{1/2}$.

This equation can be used to plot the reflectivity of the gratings, where a typical example is shown below.

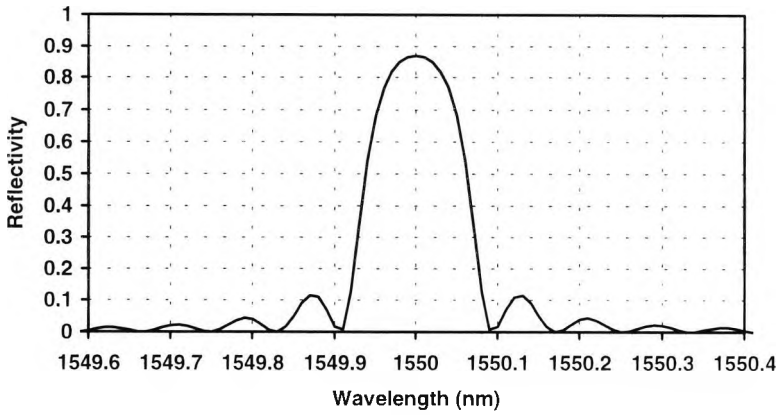

Figure 5_1: Typical output from the model for a single grating.

For the case where two gratings are placed in series, two effects change the detected signal from the second grating compared to the typical curve, above. Firstly, the intensity of light that reaches the second grating from the source will be reduced by the amount that is reflected by the first. Secondly, a portion of the light reflected by the second grating is reflected back away from the detector by the first grating. Due to the nature of the Bragg gratings behavior, both these effects will be wavelength dependent.

Knowing the reflectivity of the grating at a particular wavelength (from the above equation), it is obvious that the simulation can be formalized as:

$$\mathrm{Int}_1(\lambda) = \mathrm{Int}_o R_1$$

$$\mathrm{Int}_2(\lambda) = \mathrm{Int}_o T_1^2 R_2$$

$$\mathrm{Int}_3(\lambda) = \mathrm{Int}_o T_1^2 R_1 R_2^2 \qquad (5\_2)$$

where Int_1 and Int_2 are the computed intensities from the first and second gratings respectively, Int_o is the input intensity from the light source and R_1, R_2, T_1 and T_2 are the reflection and transmission coefficients of the first and second gratings respectively where

$$T_n = 1 - R_n \qquad (5\_3)$$

If the Bragg wavelengths of the two gratings are close together then multiple reflections between them will cause signal interference effects and thus noise at this wavelength, this is explained further in the next section. These harmonics will be small compared to the main detected signal from the gratings and for the simulation results presented herein only the first harmonic, Int_3, is considered.

The light source is assumed to have a bandwidth sufficiently wide enough so that the two gratings will be illuminated equally, this is valid since most practical light sources will have a bandwidth at least 30nm compared to the bandwidth of the Bragg gratings reflection which will be about 0.2nm. The distance between the two gratings is assumed to be greater than the coherence length of the light source used, again this is valid when the bandwidth of the source used is considered.

The effect of this interaction on the signal received from the second grating is shown on Figures 5_2 and 5_3 below for two different grating strengths.

In a WDM system the wavelength separation is such that the two reflection spectra will not overlap at any time, in a TDM this overlapping is ignored since the two signals can be separated in the time domain.

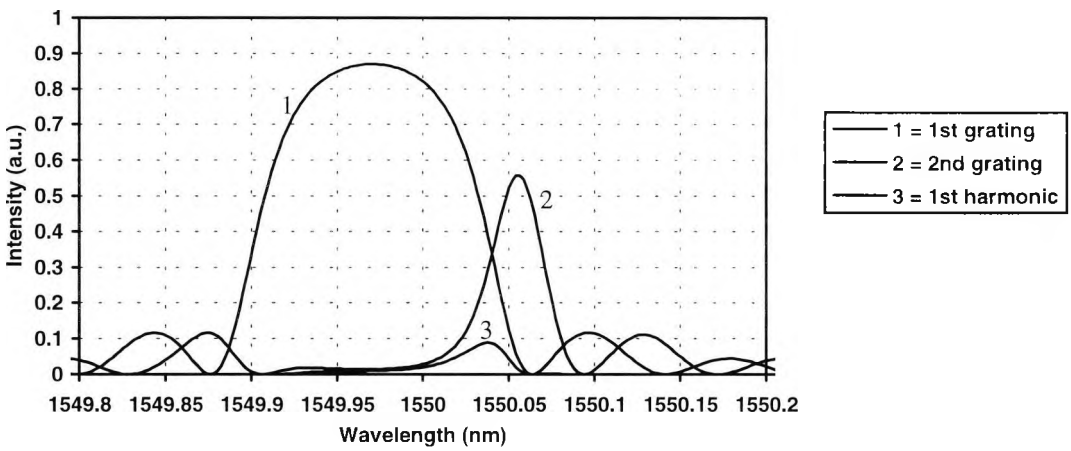

Figure 5_2: Graph of the individual responses from 2 gratings and the first harmonic.

Figure 5_2 shows wavelength spectra for two gratings (Δn = 0.0001 & L=1.0cm, which gives a reflectivity ≈85% which can be seen in curve 1), λ_B = 1549.7 for the first grating and 1550nm for the second.

The spectral output from the first grating is exactly as would be expected, however the spectrum from the second grating has been greatly deformed. It can be seen that curve from the second gratings has considerably less power

within it (the remainder has been reflected back by the first grating), and the centre of the wavelength curve has moved away from 1550nm.

The reduced amplitude of the second curve will have a negative effect on the system performance in terms of signal to noise, however the movement of the center of the curve is a more important source of noise in this type of system. It can be seen in the above graph, that the peak of the second grating has shifted by over 50pm simply by the presence of the first. This will be detected as crosstalk between the two channels and will limit the strain resolution achievable.

This problem can be partially rectified by using gratings with lower reflectivity. A reasonable arrangement was modeled using weaker gratings (which would be produced where Δn = 0.00003 & 0.000045, largest first, which gives a maximum reflectivity of 20% for the first grating and 40% for the second).

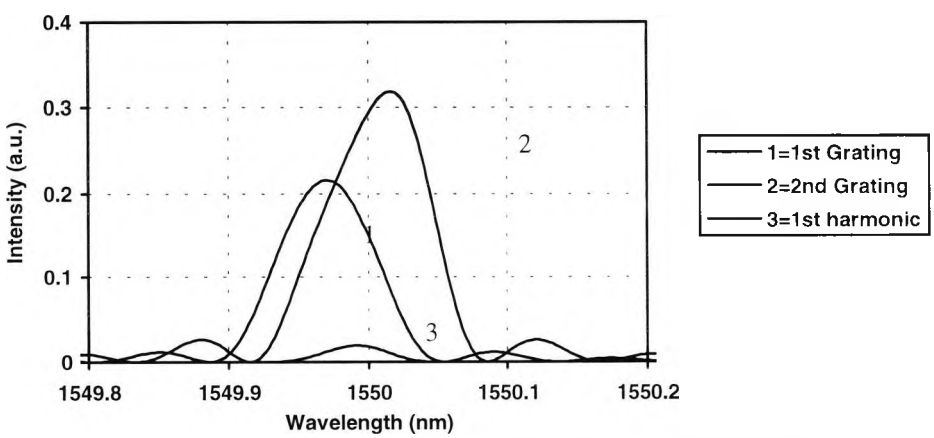

Figure 5_3: The same situation as Figure 5_2, but with weaker gratings.

Even with the weaker gratings, the deviation from the expected value of the peak of the second gratings is present. The magnitude of this deviation can be plotted as a function of the Bragg wavelength of the first grating; this is shown below in Figure 5_4.

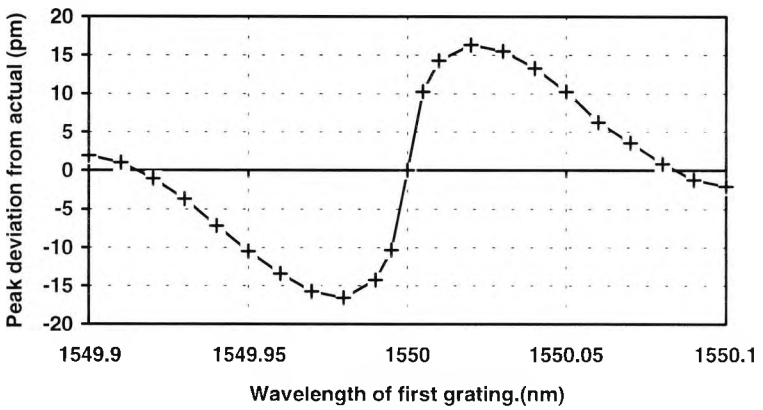

Figure 5_4: Deviation from expected value of wavelength peak against Bragg wavelength of first grating.

The shape of the curve shown in Figure 5_4 remains the same for different gratings strengths but the magnitude changes. For example, with reflectivities of 85% for both gratings gives a maximum deviation of just under 50pm. For comparison, a typical value of strain sensitivity that has been reported, using a Bragg grating system, would be ≈1.0 pm/μstrain.

This deviation would be received as crosstalk between the two gratings, since any change in the Bragg wavelength of the first grating would produce a small change in the second.

The method used in the simulation, for finding the peak of the wavelength curve, was to numerically differentiate it and then search for the zero-crossover. In practice, other techniques (such curve fitting) are equally valid and could bring a somewhat different result.

Other than using low reflectivity gratings, there appears to be no simple way by which this problem can be overcome. For systems where accuracy is important, the problem will have to be minimized by using gratings that have a very small bandwidth which will enable the gratings to be reasonably close together spectrally without interfering with each other.

The fabrication of gratings with bandwidths as low as 0.029nm have been reported [45]. These were fabricated by scanning the phase mask used along the fibre and thus producing a grating length of the order of 50mm. This phase mask scanning means that the depth of modulation of the refractive index is not as strong as other methods but this is compensated by the increased length. The final reflectivity produced was of the order of 70%. Presumably, though this is not explicit, a similar grating could be made with a reduced reflectivity and a similar (if not better) bandwidth.

5.1.2 Multiple reflections between gratings

A second problem that would be caused by placing gratings that operate at the same wavelength in series is that of multiple reflections. Obviously only those reflections that reach the detector will contribute to the noise level. The use of a time-domain based multiplexing system will eliminate most of these unwanted reflections because most will have traveled different path lengths to that of the signal being analyzed and hence will arrive at the detector at different times.

However, not all the noise will be eliminated by this, some reflections will have traveled via routes that are the same length as the grating signal. Therefore these signals will arrive at the detector simultaneously. This will increase the noise detected for a particular channel. This situation is illustrated in Figure 5_5 below:

This type of noise is similar to that described for a series of Fabry-Perot sensing elements [25]. If first-order multiple reflections, MR_1, are defined as those that are reflected 3 times and return to the detector at the same time as the signal from the sensor in question then it is clear that for sensor number p (where the sensors are numbered from 0 to P-1. P therefore being the total number of sensors):

$$MR_1 = \sum_{i=0}^{n-1} i = (p-1)+(p-2)+\ldots+1 \qquad (5\_5)$$

Which can be rewritten as

$$MR_1 = \frac{p(p-1)}{2} \qquad (5\_6)$$

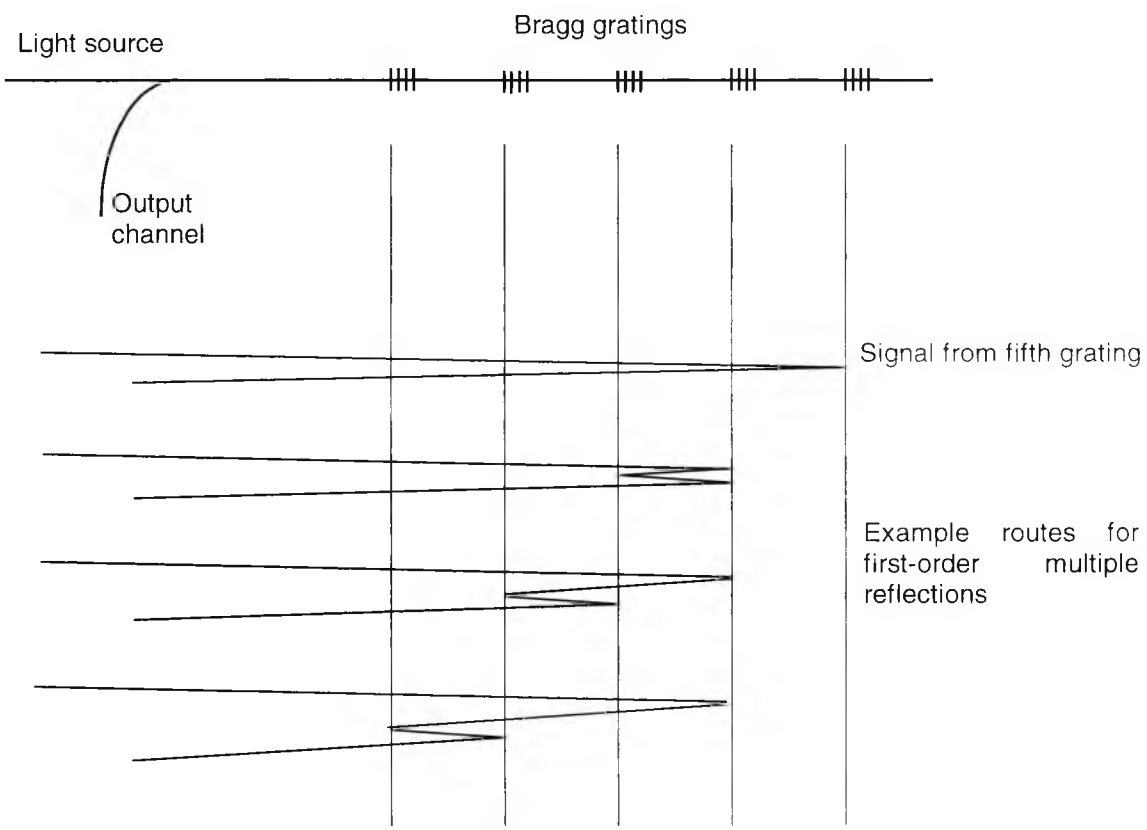

Figure 5_5: Three example routes (from a total of six) for first order multiple reflections for grating number four.

It is obvious that from this Equation 5_5 that this problem becomes more severe as for higher values of p, as the graph below demonstrates.

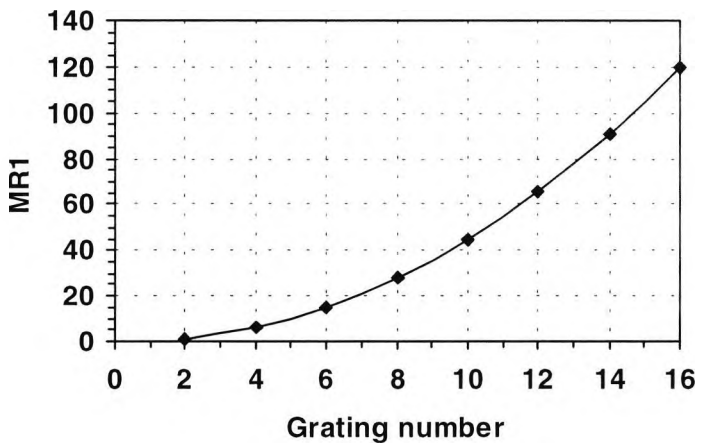

Figure 5_6: Number of first-order crosstalk pulses received for each sensor.

The strength of these crosstalk pulses is dependent on the reflection coefficients of the gratings used. If the all gratings have a reflection coefficient of R, then each crosstalk pulse will be a factor $R^2/(1-R)^2$ weaker than the primary signal pulse. Therefore, if a series of gratings are used with similar Bragg wavelengths, it is important to make them weak to avoid the signal being swamped by noise caused by these multiple reflections.

The situation can be improved slightly by staggering the values of R such that the

first gratings have a low reflection coefficient (e.g. 10%) with successive gratings getting progressively stronger (15%, 20% etc). This will mean that the signal will be reflected from a stronger grating than the multiple reflected noise pulse.

In the above referenced paper [25], it was also noted that this type of noise (i.e. that which is produced by multiple reflections) would continue after the last signal pulse has been received. A delay between successive light source pulses to allow for this maybe needed to compensate.

5.2 Possible improvements to the demultiplexing system

In many ways, the optical strain sensor system developed and demonstrated in the above Sections can only be considered a prototype version. It has proved the theory and the results taken have demonstrated that it could be used as the basis for a practicable system for a strain measurement application.

However, as with any prototype system, a number of improvements could now be attempted to increase the system overall effectiveness. These improvements stem

from two main sources, new or alternative equipment now available and improvements in either strain or spatial resolution of the sensors themselves. These two areas will be discussed in the following sections.

5.2.1 Improvements in resolution

To improve the spatial resolution of the sensors, it will be necessary to run the controlling electronics at a higher speed because the returning signals from the gratings will be closer together.

The majority of the electrical components used in the system were chosen for the their ability to operate at higher speeds than was used in the experimental demonstrations outlined above. FAST TTL, which formed the basis of much of the controlling system, can typically operate at frequencies in excess of 100MHz, whilst the GaAs switches are specified with a top rating of 1GHz. This is not true for all the components used however. There will be three main areas where increasing the speed of operation may prove problematic. These are: the detector and high-frequency amplifier, the switch control signal generation and the light source driver.

The detector and the associated amplifier need a bandwidth that is high enough to detect the pulses returning from the gratings and amplify the signal enough so that the rest of the signal processing can operate. A typical 'rule of thumb' to ensure fast enough rise times would be to design a system with a frequency response approximately 10× higher than the frequency of the arriving pulses. Trans-impedance amplifications in excess of 10^7 are often needed and constructing devices of this nature with a high bandwidth is not a trivial task. Low-noise, high-bandwidth devices are available but these generally have a low gain level, therefore the only solution would be to place a number of such devices in series.

The timing of the switch control signal can be generated using TTL, however the GaAs switches require control signals to be of the form 0v / -5v. The manufacture's application notes for the switches list three methods of performing this conversion. The first, the scheme chosen for this project, uses HCT4053, TTL compatible CMOS switches with a rated top frequency of 160MHz. The second method uses the manufacture's custom built driver IC, this has a top speed of 40MHz (which seems odd considering it's driving a 1GHz rated switch!) and as such does not seem to be an ideal choice. The third is to float the switch at +5v with respect the rest of the system, the TTL pulses will then appear to the switches to be 0v / -5v albeit in the opposite sense. The main problem with this approach is

that the ground signal for the switches will be a +5v presumably from a power supply unit and will therefore, not be as stable as a good earth connection.

To improve the spatial resolution of the sensors it will be necessary to produce shorter pulses of light. High frequency laser diodes are available, but these devices can present problems. Diodes have a 'turn on' or threshold voltage that is above 0v (typically 0.7v), so to avoid a lag time, drivers are run with a bias voltage that is just below this threshold. However, this can mean that the light is not completely turned off during the 'off' period of the desired light modulation, which can cause a substantial noise signal that would be detected as crosstalk.

5.2.2 New equipment

During the lifetime of this project, a number of potentially useful pieces of equipment have become more readily available. Of these, the most interesting include different types of switches and more powerful light sources.

A super-luminescent diode, SLD, is now available with a center wavelength of 1550nm. It has a rated optical power output of up to 1mW. This extra power will enable weaker gratings to be used (which will reduce the noise sources outlined in

Section 5.1); alternatively less amplification will be needed after the detector which will reduce the amount of noise contributed to final system from the amplifier.

Erbium-doped fiber amplifiers light sources are now available as packaged devices that include a pumping laser and an optical modulator as integral components. These devices have a large power output and a spectral bandwidth of the order ~100nm, larger than can be expected from laser diode. Larger bandwidth light sources have the advantage that more sensors can be placed in series without the need to use the same Bragg wavelength more than once. However, at present this device does have the disadvantage of being rather costly in comparison to the SLD mentioned above.

GaAs switches are becoming more popular and various configurations that can be used to create different switch matrix topologies are available. A 1-input, 4-output switch could reduce the number of switches needed for a set number of output channels.

5.3 Discussion of aims and objectives

The aims and objectives of this project were outlined in Section 1.3. They

consisted essentially of an investigation into the suitability of Bragg gratings as strain sensors and the development of a system capable of accurate strain measurements using a series of Bragg gratings as a quasi-distributed network of sensors. With this is mind, it can be seen that the work presented achieves these aims.

The Wollaston prism based wavelength demodulation system achieves an adequate wavelength resolution (0.01nm equivalent to a strain resolution of ~8μm). The arrangement developed uses a second light source as a reference wavelength which reduces the need for calibration. The nature of the Wollaston prism would enable a relatively small device to be constructed with no moving parts. This system is limited however, by the quality of the CCD used both in terms of speed of operation and element size. The speed of operation limits sensor spatial resolution achievable, whilst the element size determines the smallest wavelength change resolvable. When better CCD detectors are available, this arrangement will be worth reconsidering.

The demultiplexing system enables a number of gratings to be used as sensing elements when placed in series. The SNR achieved was of the order of 20dB and the crosstalk between output channels was less than the noise level. Using an

interferometric wavelength-shift detection system based on a Michelson interferometer allows a measurement sensitivity of 1.59×10^{-3}nm/μm and 1.119×10^{-2}nm/°C.

The sensitivity figures given above suggest the main problem with the system as it stands will be cross-sensitivity. As mentioned in earlier sections, there is no way of differentiating between changes in wavelength due to strain and those due to temperature. The method used in the strain experiments in this work was to simply to assume the temperature remained constant, for all the gratings, for the duration of the experiment. For laboratory work, this is a valid assumption, however for a 'real' system a more stable arrangement is required. The literature review in Chapter 2 highlighted some of the methods that have been reported which attempt to solve this problem, the most practical of which generally requires additional sensors. In a situation where gratings are attached to a substrate, the changes in strain of which is to be monitored, a second grating can be attached in the same area but in a manner such that it does not experience the changes in the strain conditions of the substrate. This second grating acts as a temperature reference and can be in series with the former. The TDM system presented would be suitable to demultiplex the signals from each and the calculation of the actual strain conditions can then be carried out.

The system was designed to be as flexible as possible to allow for future expansions and/or improvements and Chapter 5 has discussed some of the methods by which this could be achieved. One of the potential advantages of a TDM system is the possibility of using Bragg gratings at the same wavelength and the problems associated with this have been examined in detail.

Publications by the author relevant to the thesis

X.Q. Jiang, J. Kemp, Y.N. Ning, A.W.Palmer, K.T.V. Grattan,"Accurate wavelength determination in a Wollaston prism interferometer for sensor applications", IEEE Photonics Technology Letters, 1996, Vol 8, No 8, pp1055-1057.

X.Q.Jiang, J. Kemp, Y.N. Ning, A.W. Palmer, and K.T.V. Grattan,"Self-reference scheme for wavelength measurement using a Wollaston interferometer", Proceedings of the Applied Optics Divisional Conference of The Institute of Physics, Reading 1996, pp403-406.

X.Q. Jiang, J. Kemp, Y.N. Ning, A.W. Palmer, K.T.V. Grattan, "High-accuracy wavelength-change measurement system based on a Wollaston interferometer, incorporating a self-referencing scheme.", Applied Optics, 1997, Vol 36, No 21, pp4907-4912.

J. Kemp, X.Q. Jiang, Y.N.Ning, A.W. Palmer, K.T.V. Grattan, "Dual interferometric displacement measurement system, incorporating a Wollaston interferometer", Proceedings of the Society of Photo-optical Instrumentation Engineers (SPIE), 1997, Vol 3000, Chp 23, pp82-89.

J. Kemp, X.Q. Jiang, Y.N. Ning, A.W. Palmer, K.T.V. Grattan, "A displacement measurement system, utilizing a Wollaston interferometer", Optics and laser technology, 30, 1998, pp71-75.

J.Kemp, R.Ashoori, A.W.Palmer, K.T.V.Grattan, A.Meldrum and L.Li, "Optical time domain demultiplexing of Bragg gratings sensors using fast GaAs switches", Submitted, Eurosensors XII Conference, Southampton, September 1998. To be published by Institute of Physics Publishing, Bristol, UK, 1998.

J.Kemp, R.Ashoori, A.W.Palmer, K.T.V.Grattan, A.Meldrum and L.Li, "Microfilter convolution effects in Bragg grating sensor demodulation", Proceedings of the Applied Optics Divisional Conference of The Institute of Physics, Brighton 1998, pp187-190, Pub: Institute 0f Physics Publishing, Bristol, UK, 1998.

S. Xiao, J. Kemp, K.T.V. Grattan and A.W. Palmer, "Time-domain multiplexing for a four Bragg grating sensor system with phase-sensitive detection using a lock-in amplifier", Optics Communications, Submitted.

Reference list and Bibliography

1. J.-L. Archambault, L. Reekie and P. St. J. Russel, "High reflectivity and narrow bandwidth fiber gratings written by a single excimer pulse", Electronics Letters, Vol. 29, No.1, p28, 1993.

2. J.-L. Archambault, L. Reekie and P. St. J. Russell, "100% reflectivity Bragg reflectors produced in optical fibres by single excimer laser pulses", Electronics Letters, 29(5), 453-5, 1993a.

3. C. G. Askins, M. A. Putnam, G. M. Williams and E. J. Freibele, "Stepped-wavelength optical fiber Bragg grating arrays fabricated in line on a draw tower", Optics Letters, Vol. 19, p147, 1994.

4. T. A. Berkoff and A. D. Kersey, "Eight element time-division multiplexed fiber grating sensor array with integrated-optic wavelength discriminator", in Proc SPIE 1994 2nd European Conf. Smart Struct. Materials, Glasgow, Scotland, Oct. 1994, Vol. 2361, p350.

5. T. A. Berkoff *et al*, "Hybrid time and wavelength division multiplexed fiber grating array", in Proc. SPIE, Vol. SPIE-2444, p288, 1995

6. T. A. Berkoff and A. D. Kersey, "Fiber Bragg grating array sensor system using a bandpass wavelength division multiplexer and interferometric detection", IEEE Photonics Technology Letters, Vol. 8, P1522, Nov. 1996.

7. V. Bhatia and A. M. Vengsarkar, "Optical fiber long-period grating sensors", Optics Letters, Vol. 21, p 692, 1996.

8. V. Bhatia, K. A. Murphy, R. O. Claus and A. M. Vengsarkar, "Simultaneous measurment systems employing long-period grating sensors", on Conf. Proc. Fiber Sensors-11 (OFS-11), Sapporo, Japan, p702, 1996a.

9. F. Bilodeau, B. Malo, J. Albert, D. C. Johnson and K. O. Hill, Optics Letters, Vol. 18, p953, 1993.

10. Camlibel, D. A. Pinnow and F. W. Dabby, Applied Physics Letters, Vol.26, p185, 1975.

11. B. Culshaw and J. Dakin (Editors), "Optical fiber sensors: Principles and components", Artech House, 1998

12. M. A. Davis and A. D. Kersey, "All fiber Bragg grating strain sensor demodulation technique using a wavelength division coupler", Electronics Letters, Vol. 30, p75, 1994.

13. M. A. Davis and A. D. Kersey, "Matched filter interrogation technique for fiber Bragg arrays", Electronics Letters, Vol. 31, p822, 1995.

14. M. A. Davies and A. D. Kersey, "Application of a fiber Fourier transform spectrometer to the detection of wavelength-encoded signals from Bragg grating sensors", Jnl of Lightwave Technology, Vol. 13, No. 7, p1289, 1995a.

15. M. A. Davis, D. G. Bellemore and M. A. Putnam and A. D. Kersey, "Intorrogation of 60 fiber Bragg grating sensors with μstrain resolution capabilty", Electronics Letters, Vol. 32, p1393, 1996.

16. L. Dong, J. L. Archambault, L. Reekie, P. St. J. Russel and D. N. Payne, "Single pulse Bragg gratings written during Fibre drawing", Electronics Letters, Vol. 29, No. 17, p1577, 1993.

17. J. R. Dunphy *et al*, "Instrumentation development in support of fiber grating sensor arrays", in Proc. SPIE Distributed and multiplexed fiber optic sensors, Boston MA, Sept 1993, Vol. 2071, p2.

18. E. J. Friebele, C. G. Askins, M. E. Gingerich and K. J. Long, Nucl. Instrum, Methods Phys. Res. B, Vol. 1, p355, 1984.

19. K. T. V. Grattan and B. T. Meggitt (Editors), "Optical fiber sensor technology", Published by Chapman & Hall, 1995.

20. K. O. Hill, Y. Fujii, D. C. Johnson and B. S. Kawasaki, Applied Physics Letters, Vol. 32, p647, 1978.

21. D. A. Jackson *et al*, "Simple multiplexing scheme for a fiber optic grating sensor network", Optics letters, Vol. 18, p1193, 1993.

22. S. W. James, M. L. Dockney and R. P Tatum, "Simultaneous independent temperature and strain measurement using in fibre Bragg grating sensors", Electronics. Letters, 32(12), 1996, pp1133-1134.

23. S. E. Kanellopoulos, V. A. Handerek, A. J. Rogers, "Simultaneous strain and temperature sensing with photogenerated in-fibre gratings", Optics Letters, 20(3), p333-5, 1995.

24. P. J. Kaiser, Jnl Optical Society of America, Vol. 64, p475, 1974.

25. A. D. Kersey and A. Dandridge, "Analysis of intrinsic crosstalk in tapped-serial and Fabry-Perot interferometric fiber sensor arrays", SPIE Vol. 985, Fiber Optic and Laser Sensors, p113, 1988.

26. A. D. Kersey, T. A. Berkoff and W. W. Morey, "High resolution fiber Bragg grating based strain sensor with interferometric wavelength shift detection", Electronics Letters, Vol. 28, p236, 1992.

27. A. D. Kersey and T. A. Berkoff, "Fiber optic Bragg grating differential temperature sensor", IEEE Photonics Technology Letters, Vol. 4, p1183, 1993.

28. A. D. Kersey, T. A. Berkoff and W. W. Morey, "Fiber optic Bragg sensor with drift compensated high resolution interferometric wavelength shift detection", Optics Letters, p72, 1993

29. D. Kersey, T. A. Berkoff and W. W. Morey, "Multiplexed fibre Bragg grating strain-sensor system with a fibre Fabry-Perot wavelength filter", Optics Letters, 18(6), pp1370-2, 1993

30. A. D. Kersey, M. A. Davis, H. J. Patrick, M. LeBlanc, K. P. Koo, C. G. Askins, M. A. Putnam and E. J. Friebele, "Fiber grating sensors", Jnl Lightwave Tech., 15(8), pp1442-1463, 1997.

31. D.K.W. Lam and B.K. Garside, "Characterization of single-mode optical fiber filters", Applied Optics, Vol. 20, No 3, February 1981.

32. P. J. Lemaire, R. M. Atkins, V. Mizrahi and W. A. Reed, Electronics Letters, Vol. 29, p1191, 1993.

33. H. G. Limberger, P. Y. Fonjallaz, P. Lambelet, Salathe, Ch. Zimmer and H. H. Gilgen, Proc. SPIE 2044, p272, 1973

34. H. H. Lin and A. Korpel, "Heuristic scalar paraxial beam propagation method taking into account continuous reflections", Jnl Opt. Sco. Am. B, 8(4), p849-857, 1991.

35. A.B. Lobo Ribeiro, Y.J. Rao, L. Zhang, I. Bennion and D.A. Jackson, "Time-and-spatial-multiplexing tree topology for fibre-optic Bragg-grating sensors with interferometric wavelength-shift detection", Applied Optics, Vol. 35, No. 13, May 1996.

36. R.S. Longhurst, "Geometrical and Physical Optics", Longmans, 1957

37. S.Magne, S.Rougeault, M.Vilela and P.Ferdinand,"State-of-strain evaluation with fiber Bragg grating rosettes: application to discrimination between strain and temperatures effect in fiber sensors."Applied Optics, 36(36), 1997, pp9437-9447.

38. S. M. Melle, K. Liu and R. M. Measures, "A passive wavelength demodulation system for guided wave Bragg sensors", IEEE Photon Technology Letters, Vol. 4, pp516, 1992.

39. G. Meltz, W. W. Morey and W. H. Glenn, "Formation of Bragg gratings in optical fibers by a transverse holographic", Optics Letters, Vol. 14, No. 15, p823, 1989.

40. "Miniature Fourier Transform Spectrometer", Manufacturer's Data, Photonex, 1995.

41. Y. N. Ning, W. J. Shi, K. T. V. Grattan, A. W. Palmer and B. T. Meggitt, "Interferometric detection scheme for measuring wavelength shift using a stabilized interferometer with an additional reference wavelength", Optics Comms., Vol. 138, p27, 1997.

42. Orthonos, "Fiber Bragg gratings", Rev. Sci. Instrum., 68(12), pp4309-4341, 1997.

43. Othonos, X. Lee, R. M. Measures, "Superimposed multiple Bragg gratings", Electronics Letters 30(23), 1972-4, 1994

44. J. Rogers, "Optical methods for measurement of voltage and current at high voltage and current at high voltage", Opt. Laser Technol., 273, 1977

45. H.N. Rourke, S.R Baker, K.C. Byron, R.S. Baulcomb, S.M. Ojha and S. Clements, "Fabrication and characterization of long, narrowband fibre gratings by phase mask scanning", Electronics Letters, Vol.30, No. 16, 1994.

46. R.A. Serway, "Physics for scientists & engineers", Saunder College Publishing, 1986.

47. W. J. Shi, Y. N. Ning, K. T. V. Grattan and A. W. Palmer, "The wavelength-measurement error induced by using interferometric detections schemes for fiber-grating sensors", Meas. Sci. Technol., Vol. 8, p217, 1997.

48. K. Shima, K, Himeno, T. Sakai, S. Okude, A. Wada and R. Yamauchi, "A novel temperature-insensitive long-period fiber grating using a born-codoped-germanosilicate-core fiber", Tech. Dig. Cong. Opt. Fiber Commun, Dallas, TX, p347, 1997.

49. M. Song, B. Lee, S. B. Lee and S. S. Choi, 'Interferometric temperature-insensitive strain measurement with different-diameter fiber Bragg gratings', Optics Letters, 22(11), 1997, pp790-792.

50. D. S. Starodubov, V. Grubsky and J. Feinberg, "Bragg gratings fabrication in fibers by near-UV light", in Proc 12th Int. Conf. on Optical Fiber Sensors, Williamsburg, Virginia, October, 1997.

51. J. Stone, Jnl Applied Physics, Vol. 62, p4371, 1987

52. S.-L. Tsao and J. Wu, "Highly accurate temperature sensor using two Fiber Bragg gratings", IEEE Jnl of Selected Topics in Quantum Electronics, Vol 2, No. 4, 1996.

53. E. Udd (Editor), "Fiber optic smart structures", John Wiley & Sons, 1995.

54. Urbanczyk, K. Pietraszkiewicz, W.A. Wozniak, 'Novel bi-functional systems for measuring the refractive index profile and residual-stress birefringence in optical fibres and preforms', Optical Engineering, Vol.31, No.3, 1992, pp491-499.

55. Valera and J.D.C. Jones, 'Vibration analysis by modulated time averaged speckle shearing interferometry', Measurement Science & Technology, 1995, Vol.6, No.7, pp965-970.

56. V. Vali and R. W. Shorthill, "Fiber ring interferometers", Applied Optics, Vol. 15, p1009, 1976.

57. M. Vengsarkar, P. J. Lemaire, J. B. Judkins, V. Bhatia, T. Erdogan and J. E. Sipe, "Long-period fiber gratings as band-rejection filters", Jnl of Lightwave Technology, Vol. 14, p58, 1996.

58. R. S. Weir, A. D. Kersey and T. A. Berkoff, "A four element fiber grating sensor array with phase-sensitive detection", IEEE Photonics Technology Letters, Vol. 6, No.12, p1469, 1994.

59. D. L. Williams, B. J. Ainslie, R. Kashyap, G. D. Maxwell, J. R. Armitage, R. J. Campbell and R. Wyatt, Proc. SPIE, Vol. 2044, p55, 1993.

60. M. G. Xu *et al*, "Novel interrogation system for fiber Bragg grating sensors using an accousto-optic tunable filter", Electronics letters, Vol. 29, p1510, 1993.

61. M. G. Xu *et al*, "Discrimination between strain and temperature effects using dual wavelength fiber grating sensors", Electronics Letters, Vol. 30, p1085, 1994.

62. Q. Zhang *et al*, "Use of highly overcoupled couplers to detect shifts in Bragg wavelength", Electronics letters, Vol. 31, p480, 1995.

63. H. J. Patrick, G. M Williams, A. D. Kersey, J. R. Pedrazzani and A. M. Vengsarkar, "Hybrid fiber Bragg grating/ long period fiber grating sensor for strain/temperature discrimination", IEEE Photonics Technology Letters, p1223-1225, 1996.

64. B. T. Meggit. "Optical fibre Bragg grating sensors", Report for DTI Link OGSMS project partners. Unpublished.